

**The Search for Extrasolar Planets  
and the Characterization of Variable Stars with the  
Tautenburg Exoplanet Search Telescope**

Dissertation  
zur Erlangung des akademischen Grades

doctor rerum naturalium (Dr. rer. nat.)

vorgelegt dem Rat der Physikalisch-Astronomischen Fakultät  
der Friedrich Schiller Universität Jena

von Diplom Physiker Philipp Eigmüller  
geboren am 10.12.1979 in Berlin

**Gutachter**

- 1.
- 2.
- 3.

**Tag der Disputation:**

## Zusammenfassung

Seit der Entdeckung des ersten Exoplaneten 1990 ist die Zahl der bekannten Planeten außerhalb unseres Sonnensystems auf über 500 gestiegen. Ein Großteil der entdeckten Planeten umkreist ihren Mutterstern mit Umlaufzeiten kürzer als zehn Tage. Diese kurzen Umlaufzeiten und die damit verbundene hohe Wahrscheinlichkeit einer Bedeckung des Zentralsterns erlaubt die Entdeckung dieser Planeten mithilfe der Transitsuche. 1999 wurde der erste Transitplanet gefunden. Die Nachfolgeuntersuchungen erlaubten ein sehr viel genaueres Bild von dem Planeten zu gewinnen, als es für Exoplaneten möglich war, die mit anderen Methoden entdeckt wurden. In der Folge begannen mehrere Forschungsgruppen, mit Kleinteleskopen gezielt nach solchen Transitplaneten zu suchen. Den bisherigen Höhepunkt dieser Forschungsarbeit bilden zwei Satellitenmissionen, *CoRoT* unter Führung der CNES, und *Kepler* finanziert von der NASA.

Die Thüringer Landessternwarte (TLS) beteiligt sich schon seit langem wissenschaftlich an der Planetensuche. Mit dem 2-m Teleskop werden Radialgeschwindigkeits Messungen an hellen Sternen unternommen. Zusätzlich wird die CoRoT-Mission seit ihrem Start im Dezember 2006 mit photometrischen Nachfolgebeobachtungen unterstützt. 2007 wurde im Rahmen dieser Arbeit das Tautenburg Exoplanet Search Telescope (TEST) an der TLS in den automatischen Betrieb genommen. Das TEST hat das Ziel, große Gasplaneten mit geringen Umlaufzeiten, sogenannte "hot Jupiters". Das TEST ist für Langzeit-Transit-Durchmusterungen konzipiert. Mehrjährige photometrische Beobachtungen mit hoher Genauigkeit sollen zur Identifikation weiterer Transit-Planeten genutzt werden. Zusätzlich wurden mit dem TEST zur Unterstützung der CoRoT-Mission photometrische Nachfolgebeobachtungen durchgeführt.

In dieser Arbeit wird das TEST und seine erfolgreiche Inbetriebnahme an der TLS beschrieben. Die Auswertung der ersten zwei Jahre an Beobachtungsdaten werden vorgestellt. Insgesamt war es möglich mit dem TEST in den Jahren 2008 und 2009 in über 200 Nächten Beobachtungen aus knapp 1000 Stunden zu sammeln. Bei der Suche nach Transit-Planeten in drei ausgewählten Feldern, wurden erste Kandidaten für planetare Transits identifiziert. Die Kandidaten wurden teilweise mit dem 2-m Teleskop der TLS nachbeobachtet.

Entscheidend für die Suche nach extrasolaren Transitereignissen sind neben guten Beobachtungen auch die verwendeten Detektions-Algorithmen. Im Zuge dieser Arbeit wurde hierfür ein neuer Algorithmus entwickelt. Dieser Algorithmus geht von einem Kastenförmigen Transitsignal aus und berechnet die Signifikanz des Signals basierend auf dem statistischen F-Tests. Für einen Vergleich mit existierenden Algorithmen wurden mit dem TEST aufgenommene Lichtkurven mit simulierten Transitereignissen überlagert und anschließend analysiert. Es konnte gezeigt werden, dass die zusätzliche Anwendung dieses Transit-Detektions-Algorithmus die Entdeckungswahrscheinlichkeit von Transitsignalen in den Lichtkurven des TEST erheblich verbessert. Dieser Algorithmus ist sehr schnell und robust. Er erlaubt die Detektion von Transitereignissen auch ohne genaue Kenntnisse des zu erwartenden Signals.

In den drei Feldern, die über die zwei Jahre beobachtet wurden, konnten sechs Kandidaten für planetare Transits identifiziert werden. Einer dieser Kandidaten wurde mit Hilfe von Nachfolgebeobachtungen als

ein roter Zwergstern im Orbit um einen Unterriesen identifiziert. Während mittlerweile über hundert Transitplaneten bekannt sind, wurden bisher nur wenige solche M-Zwerg in Bedeckungsveränderlichen Doppelsternsystemen identifiziert. Dies ist umso erstaunlicher, als solche Zwergsterne  $\sim 70\%$  aller Sterne ausmachen. Die Beobachtung von Zwergsternen in Bedeckungssystemen erlaubt die genaue Bestimmung fundamentaler physikalischer Parameter dieser Sterne. Die stellaren Evolutionsmodelle können so überprüft und gegebenenfalls angepasst werden.

M-Zwerg spielen auch für die Planetensuche eine immer größere Rolle. Die habitable Zone um Zwergsterne ist wesentlich dichter am Stern, so dass Transitplaneten mit höherer Wahrscheinlichkeit in der habitablen Zone beobachtet werden können. Für Himmelsdurchmusterungen, die sich speziell der Suche nach Planeten in Orbits um solche Zwergsterne verschrieben haben, ist ein genaues Verständnis der stellaren Physik dieser Zwergsterne unabdingbar, um die Beobachtungen richtig zu interpretieren.

Zur Zeit sind nur vierzehn M-Zwerg in Bedeckungsveränderlichen Doppelsternsystemen mit einer Masse unter  $0.4$  Sonnenmassen veröffentlicht. Acht davon in vier Doppelsternsystemen im Orbit um einen anderen M-Zwerg, die restlichen im Orbit um F-Hauptreihensterne. Der in dieser Arbeit untersuchte Zwergstern ist der erste M-Zwerg, welcher einen Unterriesen bedeckt. Bestimmungen der Masse und des Radius des Zwergsterns zeigen leichte Abweichungen von der erwarteten Dichte. Dies unterstreicht die Besonderheit dieses Doppelsternsystems.

Neben den Transit-Durchmusterungen wurden in den vergangenen Jahren photometrische Nachfolgebeobachtungen für die CoRoT Satellitenmission unternommen. Ziel der CoRoT-Mission ist auch die Suche nach Transitplaneten. Die absichtlich defokussierte Optik des Satelliten verursacht allerdings eine hohe Rate an Kandidaten die durch Bedeckungsveränderliche Sterne, welche auch in der photometrischen Maske liegen, verursacht werden. Um diese zu identifizieren sind photometrische Nachbeobachtungen mit einer höheren räumlichen Auflösung notwendig. Mit dem TEST wurden seit 2008 in über 50 Nächten solche Nachbeobachtungen durchgeführt. In sechs Fällen konnte das Transit-Signal dem zentralen Objekt zugeordnet werden. Bei einem der Kandidaten wurde durch weitere Nachfolgebeobachtungen der planetare Charakter des Begleiters bestätigt. Das TEST Teleskop konnte so bei der Entdeckung des Planeten CoRoT-11b mithelfen. CoRoT-11b ist ein "hot Jupiter" Planet, welcher einen schnell rotierenden F-Stern umkreist. CoRoT-11b ist einer von nur vier bekannten Planeten, die um einen schnell rotierenden Stern kreisen. Mit einer Masse von  $M_p = 2.33 \pm 0.34 M_{Jup}$  handelt es sich um einen aussergewöhnlich schweren Planeten. Aus dem beobachteten Radius von  $R_p = 1.43 \pm 0.03 R_{Jup}$  berechnet sich eine Dichte von  $\rho_p = 0.99 \pm 0.15 \text{ g/cm}^3$ . Damit lässt sich schließen, dass es sich um einen aufgeblähten Wasserstoff-Gasriesen handelt.

Die Daten, welche für die Transitsuche aufgenommen wurden, wurden auch nach variablen Sternen durchsucht. Mehrere hundert periodische variable Sterne konnten so identifiziert und teilweise genauer klassifiziert werden.

Im Zuge dieser Arbeit wurde für das TEST ein robotischer Beobachtungsbetrieb entwickelt, der dauerhafte Beobachtung bei geringem personellen Aufwand erlaubt. Die gewonnenen Daten werden direkt in eine Datenbank eingepflegt, um einen selektiven Zugriff einfach zu ermöglichen. Das für das TEST entwickelte photometrische Auswertungsprogramm ist direkt an diese Datenbank angebunden. Auch für die Analyse der Lichtkurven wurde ein Programmpaket speziell für das TEST entwickelt.



## Abstract

Since the first exoplanet was discovered in 1990, the number of known planets outside of our solar system has grown to over 500. Most of the discovered planets are on close-in orbits with periods shorter than 10 days. These short orbital periods and the associated high probability of an occultation of the central star allows to search for such planets with the photometric transit method. In 1999 the first transiting planet was found. Follow-up examinations allowed for a much more detailed understanding of the planet compared to previously discovered exoplanets. As a result, several groups started surveys with small telescopes in search for such transiting planets. For this purpose two satellite missions have been launched in the last years. One is CoRoT, under the leadership of CNES, and the other is Kepler, financed by NASA.

The Thüringer Landessternwarte (TLS) has been involved in the planet search for a long time. The 2-m telescope is used for radial velocity surveys on bright stars. In addition, in support of the CoRoT mission, photometric follow-up observations are conducted using the Schmidt camera. In course of this thesis the Tautenburg Exoplanet Search Telescope (TEST) was set up 2007 at the TLS for automatic operation, to contribute to this scientific field. The TEST is designed for long-term transit surveys. Several years of photometric observations with high accuracy can be used to find new transiting planets. Additionally, in support of the CoRoT mission, photometric follow-up observations have been carried out.

In this thesis the TEST and its successful operation at the TLS are described. The evaluation of the first two years of observational data is presented. The TEST observed in over 200 nights during the years 2008 and 2009 for almost 1,000 hours. The transit survey was conducted on three selected fields, hereby first candidates for planetary transits were identified. Some of the candidates have been followed-up using the 2-m telescope of the TLS.

In the search for extrasolar transit events, next to good observations, the detection algorithms are very crucial. In the course of this work, a new algorithm was developed. This algorithm assumes a box-shaped transit signal and calculates the significance of the signal based on the statistical F-test. For a comparison with existing algorithms original light curves, observed with the TEST, were superimposed with an artificial transit signal and then analysed. The newly developed algorithm improved the probability to discover Transit signals significantly. This algorithm is very fast and robust. It allows the detection of transit events, even without precise knowledge of the expected signal.

In the three fields that have been observed over the two years, six candidates for planetary transits were identified. For one of these candidates radial velocity follow-up measurements were taken with the TLS 2-m Coude. The observed object was found to be a M-dwarf in orbit around a A<sub>0</sub>-subgiant. While over a hundred transiting planets are known, only a few M-dwarfs in eclipsing binaries have been published. This is surprising, as ~70% of all stars are dwarfs. The observation of dwarf stars in eclipsing systems enables the precise determination of fundamental physical parameters for these stars. This is needed to test the stellar evolution models.

M-dwarfs play also an increasingly important role in the search for habitable planets. The habitable zone around dwarf stars is significantly closer to the star, thus transiting planets can be observed with an higher probability in the habitable zone. For sky surveys that search for planets in orbits around dwarf stars, accurate stellar models are essential to correctly interpret these observations.

Currently only fourteen M-dwarfs with a mass below 0.4 solar masses are known to be in eclipsing binary systems. Eight of them are in four binary systems orbiting around another M-dwarf. The remaining six known transiting M-dwarfs are in orbits around F-main-sequence-stars. The M-dwarf investigated in this study is the first transiting M-dwarf, which is known to orbit a subgiant. The estimated mass and radius of the dwarf star shows slight deviations from the expected density.

In addition to the transit surveys, photometric follow-up observations for the CoRoT satellite mission were conducted with the TEST. The aim of the CoRoT mission is the search for transiting planets. The deliberately defocused optical system of the satellite causes an high rate of false positives. Some of them are caused by eclipsing binaries which are inside the photometric aperture of the CoRoT mask and contaminate the signal. In order to identify these false positives, photometric follow-up observations with a higher spatial resolution are necessary. In over 50 nights such follow-up observations were carried out with the TEST. For six candidates the signal was clearly identified to be caused by the object of interest. For one of the candidates further follow-up observations showed the planetary nature of the companion. Thus the TEST telescope was able to help to discover the planet CoRoT-11b. CoRoT-11b is a "hot Jupiter" planet, which orbits a rapidly rotating F-star. CoRoT-11b is one of only four known planets orbiting a rapidly rotating star. With a mass of  $M_p = 2.33 \text{ } pm0 : 34M_{Jup}$  it is an unusual heavy planet. The observed radius of  $R_p = 1.43 \text{ } pm0 : 03R_{Jup}$  gives for CoRoT-11b a density of  $\rho_p = 0.99 \text{ } pm0.15g/cm^3$ . Thus it was concluded to be an hydrogen gas giant.

The data, which were taken for the transit search, were also analysed for variable stars. Several hundred periodic variable stars could be identified and classified.

In the course of this work the TEST was enabled for a robotic observation mode. This allows continuous observation with a minimum of staffing requirements. The data obtained are directly entered into a database, in order to allow for easy access. The design for the TEST photometric analysis program is directly linked to that database. For the light curve analysis a program package was developed specifically for the TEST. This light curve analysis program is also linked to the TEST database.

# Contents

<b>I</b>	<b>Introduction</b>	<b>1</b>
<b>1</b>	<b>Extrasolar Planets</b>	<b>5</b>
1.1	Detection Methods . . . . .	7
<b>2</b>	<b>Variable Stars</b>	<b>11</b>
2.1	Intrinsic Variable Stars . . . . .	11
2.2	Extrinsic Variable Stars . . . . .	12
<b>3</b>	<b>Instruments for the Search for Transiting Exoplanets</b>	<b>15</b>
3.1	Small Aperture Telescopes . . . . .	15
3.2	Optical Lens Systems . . . . .	16
3.3	Space Missions . . . . .	17
3.4	General discussion . . . . .	18
<b>II</b>	<b>Method</b>	<b>19</b>
<b>4</b>	<b>The Tautenburg Exoplanet Search Telescope (TEST)</b>	<b>23</b>
4.1	The TEST System . . . . .	23
4.2	Automatic Operation of the TEST . . . . .	25
4.3	Data Management of the TEST . . . . .	27
4.4	Performance of the TEST . . . . .	29
<b>5</b>	<b>Data Reduction and Photometry</b>	<b>33</b>
5.1	Standard Reduction . . . . .	33
5.2	Photometry . . . . .	34
<b>6</b>	<b>Lightcurve Analysis</b>	<b>39</b>
6.1	Noise Reduction . . . . .	39
6.2	Variable Star Identification . . . . .	41
6.3	Detection of Sinusoidal Signals . . . . .	42
6.4	Transit Signal Search . . . . .	43
6.5	Automated Binary Components Identification . . . . .	48
<b>7</b>	<b>Classification of Host and Candidate</b>	<b>49</b>
7.1	Spectral Classification of the Host . . . . .	49
7.2	Radial Velocity . . . . .	50

7.3	Estimating the Mass and Density of the Candidate . . . . .	50
<b>8</b>	<b>CoRoT Satellite Mission</b>	<b>51</b>
<b>III</b>	<b>Results</b>	<b>53</b>
<b>9</b>	<b>Follow Up of CoRoT Candidates</b>	<b>55</b>
9.1	LRc01_E1_0499 . . . . .	57
9.2	LRc02_E1_0202 = CoRoT 11b . . . . .	57
9.3	SRc02_E2_1160 . . . . .	59
9.4	Conclusion . . . . .	59
<b>10</b>	<b>TEST Candidates</b>	<b>61</b>
10.1	Candidates Field F2 . . . . .	62
10.2	Candidates Field F15 . . . . .	70
10.3	Candidates Field P1 . . . . .	74
10.4	Conclusion . . . . .	77
<b>11</b>	<b>Variable Stars identified with he TEST</b>	<b>79</b>
<b>12</b>	<b>Conclusions</b>	<b>85</b>
	<b>Bibliography</b>	<b>89</b>
	<b>Appendices</b>	<b>97</b>
<b>A</b>	<b>Types of periodic Variable Stars</b>	<b>99</b>
<b>B</b>	<b>Periodic Variable Stars - Field F2</b>	<b>101</b>
<b>C</b>	<b>Periodic Variable Stars - Field F15</b>	<b>111</b>
<b>D</b>	<b>Periodic Variable Stars - Field P1</b>	<b>117</b>

# List of Tables

6.1	Transit Detection Algorithms . . . . .	47
9.1	Observed CoRoT fields . . . . .	56
10.1	Observed fields for the transit survey . . . . .	61
10.2	Candidate F2_7259 . . . . .	64
10.3	Candidate F2_7259 . . . . .	68
10.4	Candidate F2_35765 . . . . .	69
10.5	Candidate F15_33633 . . . . .	72
10.6	Candidate F15_63381 . . . . .	73
10.7	Candidate F15_7387 . . . . .	74
10.8	Candidate P1_10221 . . . . .	75
10.9	Candidate P1_40834 . . . . .	77
11.1	Found Periodic Variables . . . . .	81
11.2	Classified Binaries . . . . .	83
B.1	Periodic Variables in the F2 field . . . . .	101
C.1	Periodic Variables in the F15 field . . . . .	111
D.1	Periodic Variables in the P1 field . . . . .	117

# List of Figures

0.1	Ancient observatory in Goseck . . . . .	3
0.2	The TEST . . . . .	4
1.1	Detected exoplanets, by detection method . . . . .	5
1.2	Planets Mass-Orbit distribution . . . . .	6
1.3	Exoplanets Detection Methods . . . . .	8
1.4	Radial Velocity . . . . .	8
1.5	Observing Probability as function of Duty Cycle . . . . .	9
1.6	Light curve of a planetary transit. . . . .	10
2.1	Light curve of a Pulsating Star . . . . .	12
2.2	Eclipsing Binary . . . . .	13
3.1	SuperWASP-South Cameras . . . . .	16
4.1	The TEST System. The CAD diagram on the left shows the inner layout of the telescope.	23
4.2	Optical design of the Flatfield Camera by Lichtenknecker. A correction plate in the optical path allows a large field of view without distortion. . . . .	24
4.3	Schematic View of the TEST control . . . . .	26
4.4	Schematic View of a typical TEST observing night . . . . .	28
4.5	Observations taken with the TEST . . . . .	28
4.6	GUI for Image Database Administration . . . . .	30
4.7	Spatial resolution of the TEST . . . . .	31
4.8	Precision reached in two different nights . . . . .	32
4.9	Observations, colour coded by their quality . . . . .	32
5.1	TEST Photometry Software . . . . .	35
5.2	Example of the ISIS image subtraction . . . . .	36
5.3	Image subtraction vs. aperture photometry . . . . .	37
6.1	Design TEST Light curve Database . . . . .	40
6.2	Comparison of three different noise reduction techniques . . . . .	42
6.3	The variability based on the standard deviation . . . . .	42
6.4	Combined Variability index . . . . .	43
6.5	Test of the detection algorithms . . . . .	47
9.1	LRc01_E1_0499 - TEST observations and finding chart . . . . .	56
9.2	LRc02_E1_0202 - TEST observations and finding chart . . . . .	57

---

9.3	Low resolution Spectrum of CoRot-11 and RV measurements of CoRoT-11b . . . . .	58
9.4	SRco2_E2_1160 - TEST observations and finding chart . . . . .	59
10.1	Transit Survey - Field F2 . . . . .	62
10.2	Field F2 - Standard deviation in selected nights . . . . .	63
10.3	Field F2 - Night Selection and Orbital Coverage . . . . .	64
10.4	Candidate F2_7259 . . . . .	65
10.5	Candidate F2_7259 - Transit Events . . . . .	66
10.6	Candidate F2_7259 - Spectral fit (1) . . . . .	66
10.7	Candidate F2_7259 - Spectral fit (2) . . . . .	67
10.8	Candidate F2_7259 - Radial velocity measurements . . . . .	67
10.9	Candidate F2_7259 - Mass-Radius diagram . . . . .	68
10.10	Candidate F2_35765 . . . . .	69
10.11	Candidate F2_35765 . . . . .	69
10.12	Field F15 . . . . .	70
10.13	Field F15 - Observations and Orbital Coverage . . . . .	71
10.14	Candidate F15_33633 . . . . .	72
10.15	Candidate F15_33633 - Stellar Classification . . . . .	72
10.16	Candidate F15_63381 . . . . .	73
10.17	Candidate F15_63381 - Stellar Model Fit . . . . .	74
10.18	Candidate F15_7387 . . . . .	75
10.19	Candidate F15_7387 - model fit to object 1 . . . . .	75
10.20	Candidate F15_7387 - stellar model fit to object 2 . . . . .	76
10.21	Field P1 . . . . .	76
10.22	Candidate P1_10221 . . . . .	77
10.23	Candidate P1_40834 . . . . .	78
11.1	General Variability . . . . .	80
11.2	Periodic Variables - BEST vs. TEST . . . . .	81
11.3	Types of Periodic Variable Stars . . . . .	82





**Part I.**

**Introduction**



In the year 2010 the UNESCO World Heritage Committee endorsed a study on the heritage sites of Astronomy and Archaeoastronomy. Astronomy has always been an important science in human history. Already in prehistory, people were not only fascinated by the heavenly bodies, but also tried to understand the rules behind their movements and constellations. Some of the most imposing buildings of ancient time were influenced by the astronomical knowledge or like Stonehenge or the Goseck circle (Figure 0.1) (Ridderstad (2009)) were build for astronomical purposes. Next to the immediate gain, like calenders, the interest in astronomy was always driven by the attempt to understand our genesis through the search for extraterrestrial life and other Earth-like planets in the Universe. Today the quest to understand more of the universe and ourselves continues as satellites are send to space, and extremely large telescopes are built on top of mountains.



**Figure 0.1.:** *The reconstructed palisade of the Goseck circle. It is a Neolithic structure, considered to be the oldest known Solar observatory. It is located in the Burgenlandkreis district, in Saxony-Anhalt, Germany.*

In the year 1992 the first extrasolar planet detection was confirmed by Wolszczan & Frail (1992). This planetary system has nothing in common with the Solar System, as the host star is a pulsar, a rotating neutron star. Three years later, Mayor & Queloz (1995) announced the first planet orbiting a main sequence star. Until then all theories about planets, their formation and evolution were only based on observations of the Solar system. Until now 466 planets in 398 systems have been discovered<sup>1</sup>, 101 of them transiting their host star. In 2005 a small aperture telescope system called “Tautenburg Exoplanet Search Telescope” (TEST) (Eislöffel et al. (2007)), was set up at the Thüringer Landessternwarte Tautenburg. Its purpose is to contribute to the transit search of hot Jupiters<sup>2</sup> and support the CoRoT space mission. This small aperture telescope is the main instrument used for this dissertation.

In the course of this thesis starting in 2007, I configured the TEST system, adjusted it, and enabled it for robotic observations. In addition to the automation of the observations, I programmed an automated data management, reduction and analysis software to handle the expected amount of more than 500 hours of observations per year.

The TEST is now a semi-automatic<sup>3</sup> telescope with a special designed data-management system including data reduction, photometry, and basic light-curve analysis tools to find periodic variables and transit-like events. In this thesis, I will outline the search for exoplanets and variable stars conducted with the TEST, as well as the supporting observations for the CoRoT satellite mission in its search for exoplanets.

<sup>1</sup>State of July 2010, for up to date information check the interactive catalogue at <http://exoplanets.eu>

<sup>2</sup>hot Jupiters are Jupiter-sized planets in very close-in orbits (cf. Chapter 1).

<sup>3</sup>The TEST has no independent weather control system. Therefore human interaction is still necessary to start the observation depending on the changing weather conditions. Otherwise the TEST works automatically. As a night assistant is always present at the TLS, this semi-automatic operation proved to be an optimal solution.

The first part of this thesis will concern the scientific background. Here I will give an overview of the current knowledge about planets, their formation and evolution. I will present the most successful methods used to detect extrasolar planets and highlight their advantages and disadvantages. A focus will be on the radial velocity measurements and the transit method, as most known planets were found by either of these methods. During the search for transiting exoplanets, variable stars were identified and classified, therefore an introduction to variable stars will be given. In order to classify the TEST project I will end the introduction with an overview of similar projects.

In the second part of this thesis, I will start with a summary of the “Tautenburg Exoplanet Search Telescope”. A description of the telescope hardware, the automated observation mode and the data management of the observed images will follow. A short analysis of the performance will conclude this technical overview.

In Chapter 5 I will go on to explain the pipeline for data reduction and photometry, which I implemented to ease usability in downstream processes. In Chapter 6 I will address the light curve analysis. Key aspects in this section will be the noise reduction and identification of periodic signals including transit-like events, which have been used to determine candidates for transiting exoplanets. Radial velocity measurements have been performed with the Alfred-Jensch-Telescope in Tautenburg equipped with a high resolution Échelle-Spectrograph to verify the candidates. I will describe the data analysis of these radial velocity measurements in Chapter 7 as well as the spectral classification of the star.

Next to the search for variable stars and transiting exoplanets, the TEST was used to support the CoRoT satellite mission with photometric follow-up observations. In Chapter 8 the satellite, its mission, and the concept of photometric follow-up studies will be described.

The results of the CoRoT follow-up observations with a main focus on CoRoT-11b, an extrasolar planet, which was confirmed by the TEST, will be discussed in Chapter 9. In Chapter 10 the transit survey and the identified candidates for transiting exoplanets will be described in detail. Although none of the candidates proved to be an exoplanet, the obtained results demonstrate the capabilities and limits of small aperture telescopes like the TEST. The variable stars that have been identified in the observed fields will be presented in Chapter 11. A comparison to the “Berlin Exoplanet Search Telescope” (BEST), which previously observed two of the fields the TEST is observing, will be drawn. Finally a conclusion will complete this thesis.



**Figure 0.2.:** *The Tautenburg Exoplanet Search Telescope (TEST). A 30 cm aperture telescope with a square field of view with 2.2 degrees on each side.*

# 1. Extrasolar Planets

Nearly 500 extrasolar planets were discovered in the last twenty years, more than half of them in the last three years. Most of the known planets have been detected by radial velocity measurements, but the number of planets detected with the transit method has increased strongly during the last years (Figure 1.1).

The understanding of formation of planetary systems and their evolution has changed in this last 20 years. Planets have been found in so close orbits around their host star no one would have expected. Other planets display very high eccentricity in their orbits. All this combines to a much more differentiated view on planetary systems. Still, the 500 known planets are a very small sample compared to the variety of parameters found for these planets in order to get good statistical conclusions, especially when examining subsamples.

Planets can be classified by different parameters, such as mass, density, chemical composition, atmosphere, and temperature. A general classification taking all of these into account resulting in a complete classification system as it is known for stellar classification is not yet in place. At the moment the classification is generally done by size and orbital period. In reference to the Solar System the planets are referred to as Jupiters, Neptuns, Saturns, Super-Earth, and Earth-sized planets depending on their

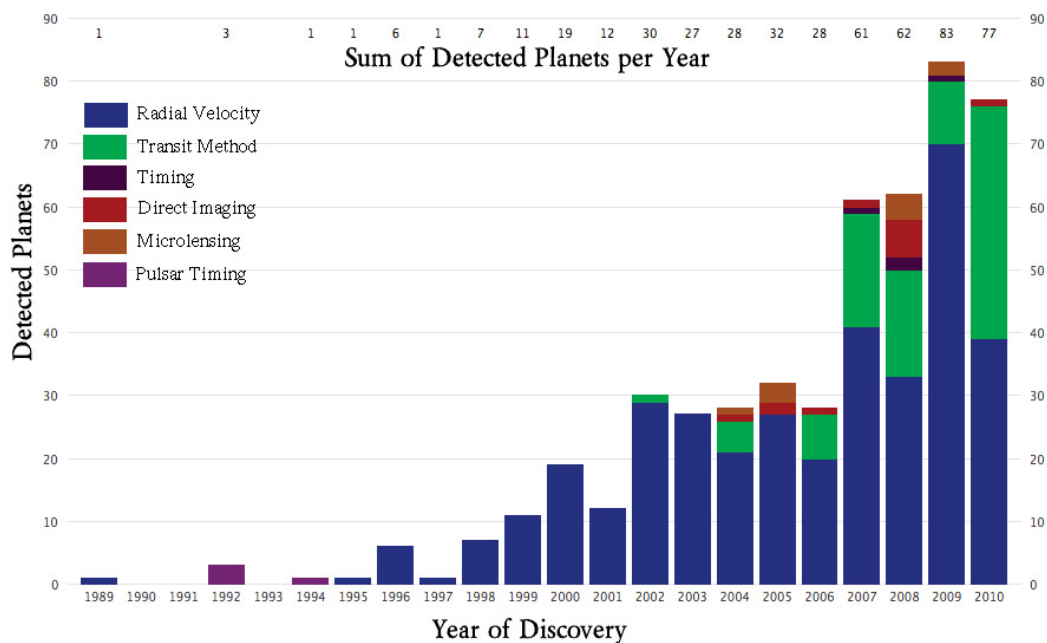
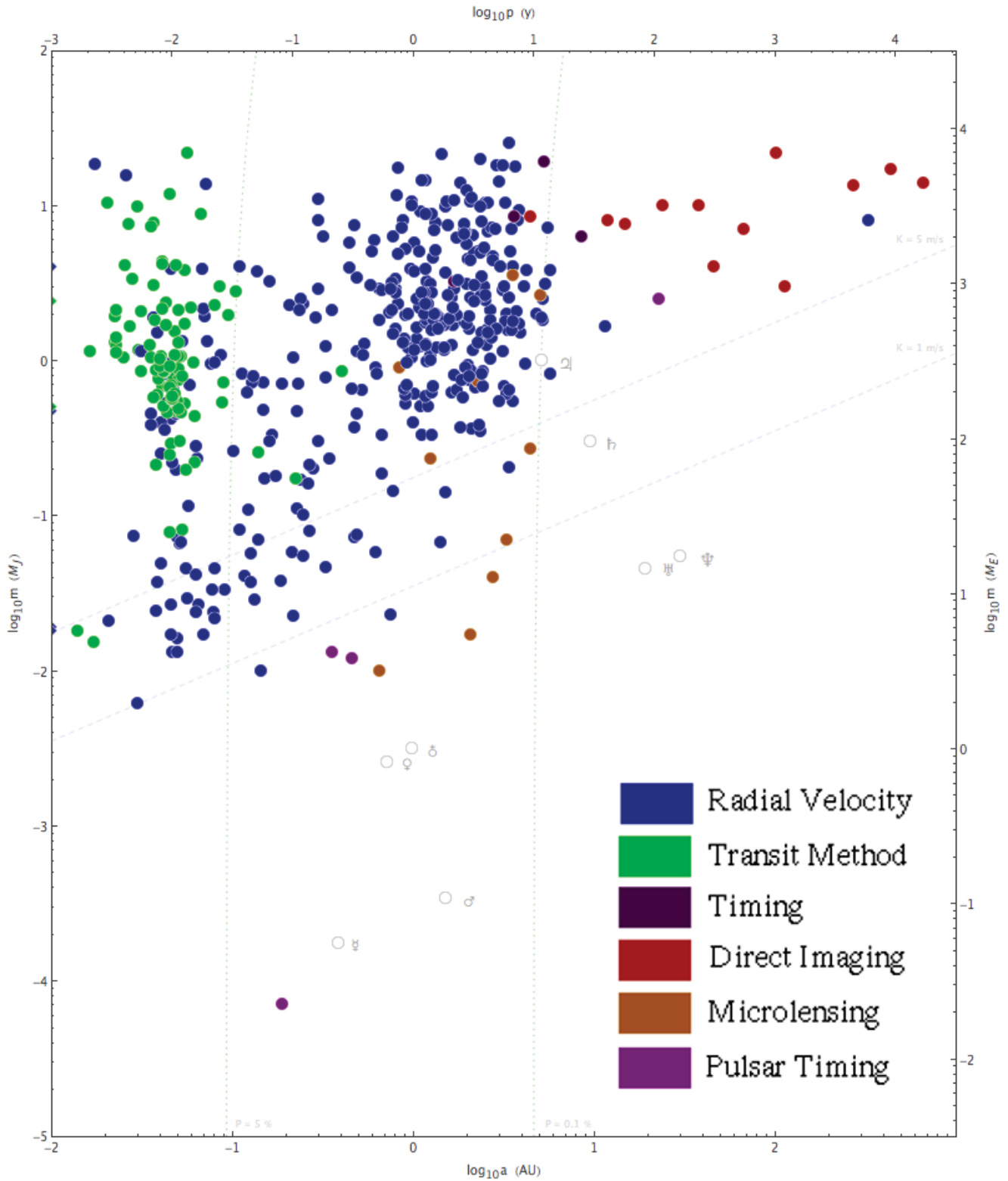


Figure 1.1.: Number of planets detected per year (status of 28th of August 2010), see Wikipedia (2010b). Each colour represents one detection method.



**Figure 1.2.:** Mass distribution of the detected planets plotted over the orbit (see Wikipedia (2010a)). Different colours are used for the different detection methods.

radius. Hereby the term Super-Earth refers to planets with a few Earth radii. The orbital period is characterised by the terms “hot” and “cold”. A “hot” planet is a planet with a very close-in orbit with a period of up to ten days. A “hot Jupiter” therefore is a Jupiter-sized planet on a close-in orbit (Figure 1.2).

Unfortunately the planets found so far are, due to the constraints of the methods and instruments applied, not representative for planets in general, but show a clear bias towards higher mass and to small orbits (Benz et al. (2006)).

Next to enlarge our observational base for theoretical models, a main goal of the ongoing planet hunt is the search for an Earth-like planet. Therefore it is obvious that the next step in planet detection will be to increase the sensitivity to find Earth-like rocky planets in a habitable zone to get first estimates on how common water planets like our own might be.

## 1.1. Detection Methods

To discover new planets a variety of methods are used, primarily based on dynamic effects, photometry, and micro lensing (Figure 1.3). In this thesis the focus is set to the transit method and the radial velocity measurements.

### Radial Velocity / Doppler Spectroscopy

As a planet revolves around its host star, not only the planet is moving, but the whole system is orbiting the common centre of gravity (Figure 1.4). The resulting movement of the star, projected parallel to the observers line-of-sight, can be measured by the spectral shift it causes (Doppler effect). The stellar mass can be derived through stellar models, allowing to calculate the  $M \sin(i)$  of the companion, where  $M$  is the actual mass of the companion and  $i$  the inclination of the orbital plane to the line-of-sight. As the inclination is often unknown, only a minimum mass can be determined. In combination with “Transit Method” (see below) it is however possible to determine the actual mass.

A main disadvantage of the radial velocity method is the amount of observing time needed on telescopes with a collecting area larger than two meters. This results in a pre selection of target stars, which are likely to host a planet, inflicting a selection bias on the results. Nevertheless the achievable accuracy allows to detect even Earth-sized planets.

### Transit Method

Planetary systems with an orbital inclination near  $90^\circ$  are characterised by high radial velocities compared to lower inclinations. In addition, it is possible to observe the planet eclipsing its host star. Figure 1.6) The combination of photometric observations of such a transit and radial velocity measurements of the host star allow for the determination of the planet mass and radius relative to the stellar mass and radius. Based on stellar models, the exact planet mass, density, as well as the eccentricity of the orbit can be determined. Unfortunately, such transit events are unlikely, especially for larger orbits Borucki & Summers (1984).

For an orbital radius of 0.1 AU, this gives a probability of  $\sim 3\%$ . For an orbit with a radius of 1 AU as the Earth orbit, the probability decreases to  $\sim 0.3\%$ . The probability to actually observe a transit is not only

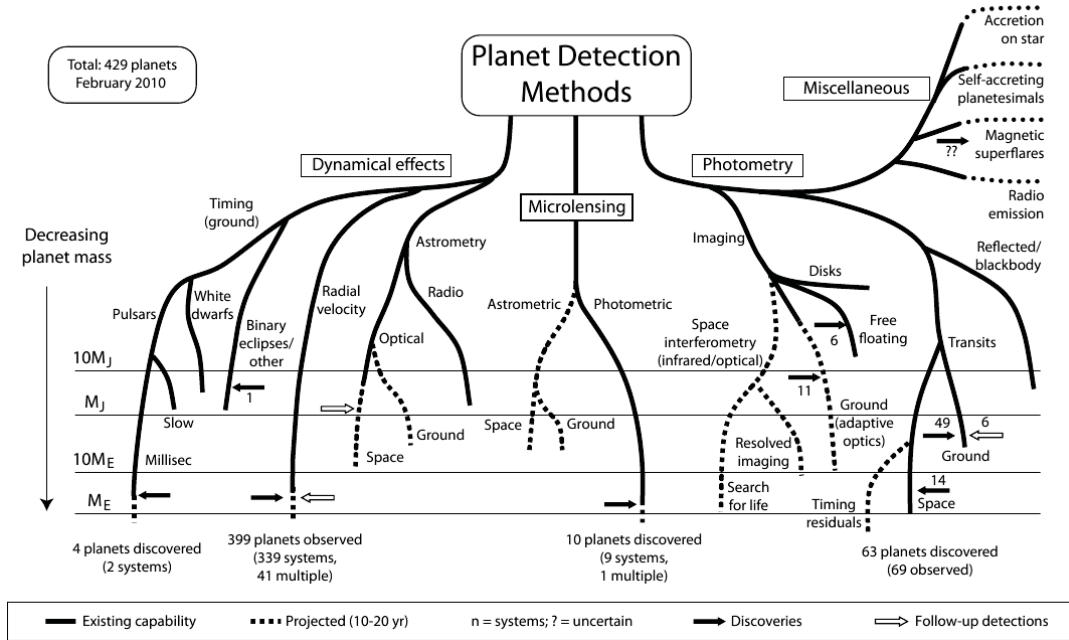


Figure 1.3.: Schematic overview of the different detection methods for extrasolar planets, created by Perryman (2000)

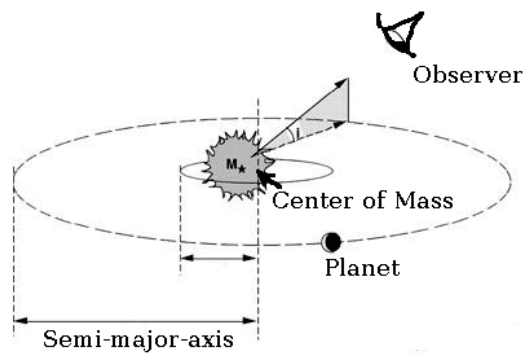
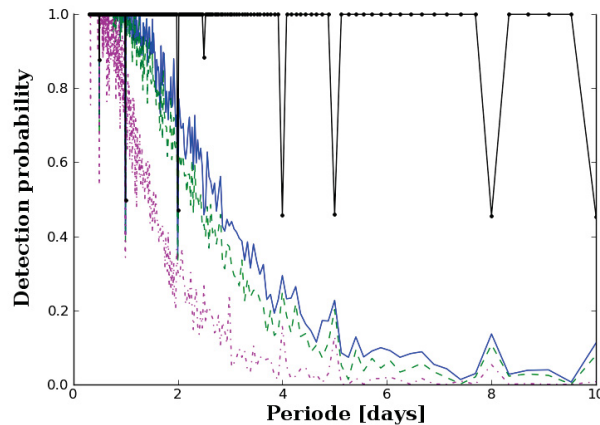


Figure 1.4.: Schematic view of a star and planet moving around the common centre of gravity.





**Figure 1.5.:** Probability to observe at least one complete transit event. Using the TEST data for the field F2, four different scenarios are displayed: black) the theoretical optimal possible, if all possible nights observations could have been conducted in the years 2008 and 2009, neglecting all bad weather conditions. blue) probability to observe at least one transit using all observations. green) probability to observe at least one transit, dismissing all really bad observations. magenta) using only data of highest photometric quality.

influenced by the chance of a star hosting a planet, and the planet transiting this star, but also depends on the number of observed stars and the duty cycle of the observing telescopes.

Depending on the ratio of the radius of the host star to the radius of the planet, the strength of the transit signal can vary from a few percent down to a few parts per million. The photometric precision of Earth-bound telescopes is mainly limited by the Earth atmosphere. Therefore, even small telescopes can observe the transits of Jupiter-sized planets around main sequence stars. For smaller planets, like an Earth, space missions are needed.

Another advantage of space missions is the possibility to continuously observe one field. In Figure 1.5 it is shown how important the duty cycle is in order to find a transiting planet. As can be seen, the probability of observing one complete transit of exoplanets with different orbital periods highly depends on the duty cycle. For two years of observation with the duty cycle of the TEST, the probability to observe one transit of an exoplanet with an orbital period of over ten days is negligible. Continuous observations instead would allow to detect such a transit with certainty. The CoRoT satellite mission gave a first estimate of how many hot Jupiters should be expected to be observed with a duty cycle of around 95 %, disregarding the differences in stellar populations. The CoRoT mission found that  $\sim 0.02\%$  of its observed stars host a hot Jupiter which is transiting its star. Therefore a large field of view, resulting in many observed stars ( $> 10,000$ ), and a high duty cycle are needed to stand a plausible chance of finding a planet.

If a transit is found, a photometric light curve with a high photometric accuracy (errors lower than one millimagnitude) provides additional information about the star. The transit depth is not constant over the time of transit, which is caused on the one hand by the limb darkening effect, depending on the stars atmosphere, on the other hand by star spots which are occulted during the transit (Figure 1.6).

For the search of Jupiter-sized planets such high accuracy is not needed. Small telescopes, that is telescopes with apertures below 1 m, are the ideal instrument for this cause. The needed accuracy can be

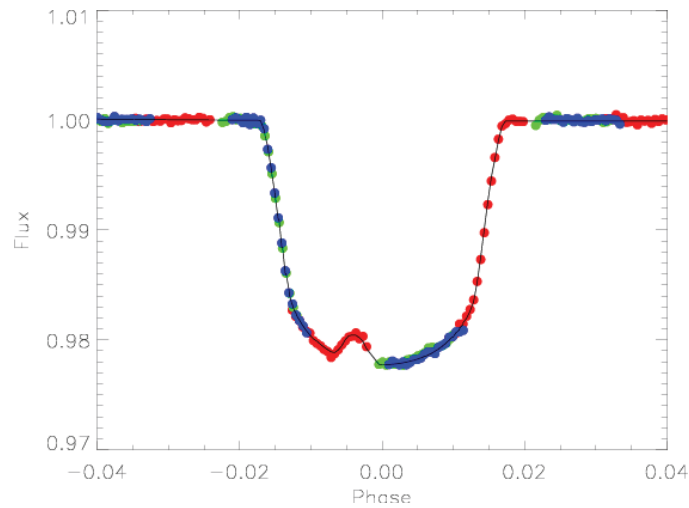


**Figure 1.6.:** *Light curve of a planetary transit of TrES-1 observed with the Hubble space telescope (Rabus et al. (2009)). The brightness of the star is reduced as the planet transits the star and darkens the disc of the star. The bump is caused by the planet transiting a star-spot.*

achieved, and large fields of view allow the observation of many thousands of bright stars at the same time. Additionally such small telescopes are not as expensive, this allows to dedicate the whole observation time to only one scientific goal. This is vitally important as long term observations with as good as possible time coverage are needed when searching for transit events.

As changes in the star brightness as seen in transits can also be caused by other physical processes, like grazing binaries, background binaries etcetera (cf. Almenara et al. (2009)) , follow-up radial velocity measurements are necessary to confirm a planet. In combination the transit method and the radial velocity method allow us to determine the exact mass and density of the planet. It is also possible to compute an exact orbital solution of the system.

For future prospects already detected transiting planets allow an even more promising aspect: as during transit parts of the starlight penetrates the planetary atmosphere, it will be possible for these planets to analyse their atmospheric compounds by analysing the transmission spectra taken during transit (e.g. Bean et al. (2010), Pont et al. (2008)).

## 2. Variable Stars

The photometric observations of stars in the search for transiting exoplanets allow also the detection and classification of variable stars. In this chapter I will shortly present the different types of variable stars and the cause of their variability.

Cuno Hoffmeister, a well known German astronomer, defined variable stars as stars whose optical brightness changes within a specified time significantly in the optical spectral range (Hoffmeister et al. (1984)). Although today the restriction to the optical spectral range would expectably lead to controversial discussions, as stars could also show variability in other spectral ranges, for this work it is sufficient as only observations in the optical spectral range are used.

Hence in the following, different classes of variable stars, and their physical causes of variability are discussed. A more detailed list of known variable stars with all the different types of groups is given by Kholopov et al. (1998).

### 2.1. Intrinsic Variable Stars

For intrinsically variable stars the change in brightness is caused by processes irrespective to the position of the observer. Pulsating variables, eruptive variables and cataclysmic variables are subsumed under intrinsically variable stars.

#### *Pulsating Variables*

In the interior of a star two forces directed against each other are present. First, the gravitational force that tends to contract the star, or in extreme cases leads to the collapse, and second, the radiation pressure acting towards it. When these two forces are not balanced, the result is a dynamic instability that leads to contraction or expansion of the star.

If the instability of the star is not too strong, an oscillation around the equilibrium occurs. Due to these periodic expansions and contractions a periodic change of the stellar radius resulting in pulsations in the intensity of the stellar brightness can be observed (Figure 2.1). Clearly visible is the sawtooth shape of the light curve. For some representatives of the pulsating stars, such as Delta Scuti stars, the light curve can also be sinusoidal.

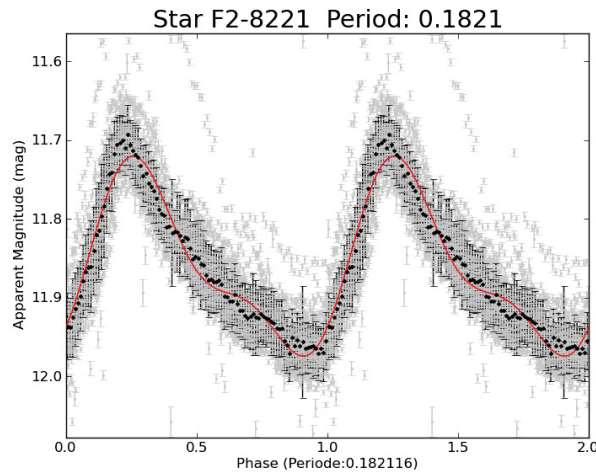


**Figure 2.1.:** This Figure shows a phase-folded and binned light curve of a pulsating star observed with the TEST. The sawtooth shape of the light curve is typical for pulsating stars.

### *Eruptive Variables*

The brightness variations in eruptive variables are caused by strong eruptions, such as flares. These eruptions are happening in the outer regions, in the chromosphere and the corona of the star. The consequence of these eruptions are mostly irregular light curves. Classifications are made based on the strength of the fluctuation as well as the shape of the light curve. The spectral type of the stars and the influence of surrounding matter clouds are also considered. Most of the eruptive variables do not show periodic variability.

### *Cataclysmic Variables*

Cataclysmic variables are often treated together with the eruptive variables. Strong bursts also lead to irregular light curves. In cataclysmic variables however, these bursts are based on a different physical process. Cataclysmic variables consist of two components: a white dwarf primary, and a mass transferring secondary. The stars are so close to each other that the gravity of the white dwarf leads to matter transfer from the companion. Instabilities in the accretion disc or the fusion of the accreted hydrogen lead to outbursts. Depending on which process is responsible for the explosions, these outbreaks occur periodically.

## 2.2. Extrinsic Variable Stars

Extrinsic variables only appear to change their brightness. There are two possible reasons: First, occultation and secondly rotation.

### *Occulting Variables*

As the most common multiple systems are binaries, here only these are presented. Eclipsing binaries have different amplitudes and period lengths in the variation of their light intensity, which depend on

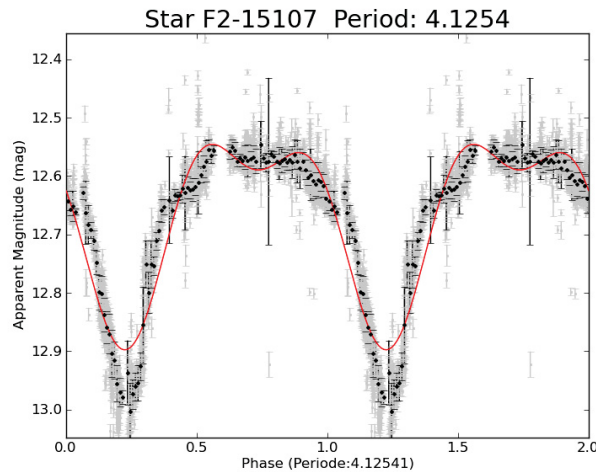


**Figure 2.2.:** Light curve of a typical eclipsing binary observed with the TEST. The two different minima can be seen. The Main minimum is caused by the fainter star eclipsing the brighter star.

various factors. The position of the observer in relation to the orbital plane of rotation of the binary system decides how much the components occult each other. The properties of the individual components such as luminosity, radius, mass, and at last the distance of the individual components to each other affects both, the coverage area and the period duration.

In general a multiple star system is formed of stars with different characteristics such as size and brightness. Therefore, in the periodic changes, main and secondary minima can be seen. The difference in strength of the minima is caused by varying coverage of the components and their differences for example in their brightness (Figure 2.2).

Of course brightness variations can also be caused by occultations of planets or proto-planetary disks. The variability caused by a proto-planetary disk depends on its inhomogeneity and composition. In contrast to planetary transits where a change in colour is not expected, proto-planetary disks can influence the spectrum of their host star, as dust is present. In addition young stellar objects display intrinsic variabilities.

### *Rotating Variables*

Due to the rotation of the star and strong differences in brightness on its surface, it appears to the observer as if the star changes its brightness. The unevenness in the brightness distribution on the star can be caused by sunspots, thermal or chemical irregularities, as well as by strong magnetic fields. In this group the distinction between variable stars and non variable stars is unclear. There is no star with a perfectly homogeneous surface, so that for all stars rotational variabilities can be detected at sufficiently high resolution observations.

Since the inhomogeneities on the stellar surface are also subject to change, fast rotation of the star is required for assignment to the class of the rotation variables. The rotation period must be short in relation to the change of surface inhomogeneity.



## 3. Instruments for the Search for Transiting Exoplanets

Even with small telescopes transiting exoplanets can be detected. Therefore many systems have been erected in the last years dedicated purely to the exoplanet hunt. In this section I will present some of the major projects. This will be covered in three groups: small aperture telescopes, optical lens systems, and spacecraft telescopes.

### 3.1. Small Aperture Telescopes

The photometric accuracy needed to detect transits of Jupiter-sized planets around Sun-like stars can be achieved with very small telescopes (main mirror  $\geq 10$  cm) combined with a CCD camera of high quality. The expected transit depth would be  $\sim 1\%$ . The main problem for Earth-bound telescopes is the duty cycle and the atmospheric distortion. During daytime and twilight observations are not possible on Earth. Furthermore, most of the small telescopes are not positioned at the best observing sites, resulting in many cloudy nights, or nights of high humidity, where observations are not possible. This decreases the chance to find exoplanets. To find planets with periods longer than ten days, the observations of a few years need to be used together, where in space 30 days would be sufficient.

Although the chances to find exoplanets are smaller than in space, long-term observations of a huge amount of stars will result in reasonable probabilities to find exoplanets. Small telescopes, with large fields of view promise ten thousands of stars to be observed simultaneously. This way short period Jupiter-like planets around bright stars ( $< 15$ th magnitude) can be found at reasonable costs. The Tautenburg Exoplanet Search Telescope (TEST), used for this thesis belongs to this group. A description of the TEST is given in Chapter 4.1. Other projects using mirror telescopes with small apertures are the following:

- The **Berlin Exoplanet Search Telescopes** (BEST and BEST II) are two small-aperture telescope systems (Rauer et al. (2004), Kabath et al. (2009b)). The first, BEST, a Lichtenknecker Flatfield camera with a main mirror of 20 cm, was tested at the Thüringer Landessternwarte from July 2001 to April 2003. It is now located at the Observatoire de Haute Provence, France, and operated remotely. The second telescope, BEST II, is a Baker-Ritchey-Chrétien telescope with an aperture of 25 cm. It has been operational at Observatorio Cerro Armazones, Chile, since April 2007. Both telescopes have been used to support the CoRoT space mission (Chapter 3.3). Transits of planets discovered by the CoRoT satellite have been identified in data observed ahead, as well as afterwards (Rauer et al. (2010)). Additionally variable stars in the observed fields of CoRoT were identified (e.g. Kabath et al. (2009a), Kabath et al. (2009c), Kabath et al. (2007)). The main advantage of the BEST II telescope is its observational site with about 73% photometric nights per year.





**Figure 3.1.:** *SuperWASP-South Cameras. Eight telephoto lenses mounted on a single mount. Photo by David Anderson*

- The **Trans-Atlantic Exoplanet Survey** (TrES) uses three telescopes with apertures of 10 cm each. The telescopes are located at Lowell Observatory, Palomar Observatory, and the Canary Islands. The different observational sites allow for a much better orbital coverage when combining the data (Alonso et al. (2007)). Four planets have been found<sup>1</sup>.
- A different approach to getting continued observations is pursued by the **Antartica Search for Transiting Extrasolar Planets** (ASTEP)(Crouzet et al. (2010)). The selection of Antarctica as observing site allows continuous observation for several months, avoiding the cycle of day and night.

### 3.2. Optical Lens Systems

Some projects do not use mirror telescopes, but photo lenses combined with astronomical CCDs. Such systems are used to look at even brighter stars, that is between 8th and 13th magnitude. The larger field of view compensates for the fact that there are fewer stars in this brightness regime. These projects use many such lenses to increase the chance of finding transiting planets.

- After the prototype of the Wide Angle Search for Planets (WASP) proved to have the necessary photometric accuracy **SuperWASP** was installed (Pollacco et al. (2006)). The WASP project consists of two telescope batteries. SuperWASP-North at Roque de los Muchachos Observatory on the

<sup>1</sup>cf. the exoplanet database (<http://www.exoplanet.eu>) for the updated number



Canary island of La Palma and SuperWASP-South at the South African Astronomical Observatory. Each observatory consists of an array of eight Canon 200 mm f1.8 lenses backed by Peltier-cooled CCD cameras (Figure 3.1). The field of view of each of these batteries is of about 500 square degrees. 64 planets WASP planets have been confirmed<sup>2</sup>.

- The **Hungarian Automated Telescope Network** (HATNet) project is a network of six small fully-automated photo-lens telescopes (Bakos et al. (2007)). In 2009 another six telescopes were erected for the HATNet-South. In difference to the SuperWASP project all the telescopes work independently. 30 planets have been detected<sup>3</sup>.
- The **XO Telescope** is a telescope located on Mount Haleakala on Maui, Hawaii (McCullough et al. (2005)). It is formed by a pair of 200 mm telephoto lenses. Five planets were found since 2006<sup>4</sup>.

### 3.3. Space Missions

One of the main problems for Earth-bound systems are the discontinuous observations. Transiting planets with longer periods are nearly impossible to being found. Not only is a transit with a wider planetary orbit much more unlikely to happen as mentioned before (Chapter 1.1), but also there are fewer chances to observe the transits. In addition Earth-bound observations with small telescopes are limited to Jupiter-sized planets due to atmospheric disturbances. For much smaller planets like Neptunes or even Earth-sized planets, the photometric accuracy is not sufficient if observing sun like stars<sup>5</sup>. With CoRoT and Kepler, two satellites are searching for transiting exoplanets at the moment.

- **CoRoT** (Convection Rotation and planetary Transits) is a space mission led by the French Space Agency (CNES). The two mission objectives are to search for extrasolar planets with orbital periods less than 50 days, and radii down to Super-Earth dimensions, and to perform asteroseismology by measuring oscillations in stars. The telescope has an aperture of 27 cm. To get also colour information, the defocused beam is directed through a prism, giving light curves in three different colours. To minimise the download data rate, the photometry is done on-board for 12000 pre-defined objects. As the spatial resolution of the instrument is rather poor, photometric follow-up as well as spectroscopic follow-up needs to be done to ensure the main target in the analysed aperture is causing the transit. In course of this thesis photometric follow-up observation for the CoRoT Mission have been made. In Chapter 8 this will be explained in more detail.
- The **Kepler** Mission is a NASA space observatory designed to discover Earth-like planets. Kepler will observe its fields for much longer duration and therefore hopes to find planets in Earth-like orbits.

---

<sup>2</sup>cf. the exoplanet database (<http://www.exoplanet.eu>) for the updated number

<sup>3</sup>cf. the exoplanet database (<http://www.exoplanet.eu>) for the updated number

<sup>4</sup>cf. the exoplanet database (<http://www.exoplanet.eu>) for the updated number

<sup>5</sup>Planets orbiting M-dwarfs give much higher signals and can therefore be detected much more easy. Here even Earth-sized planets can be detected by ground based telescopes.

### 3.4. General discussion

In the last decade many different approaches to detect transiting exoplanets have emerged. The most successful ground based projects have been proved to be systems of small lens systems. The large field of view allowed to observe large areas of the sky and to concentrate on bright stars. For planet candidates detected around host stars fainter than 15th magnitude the needed follow up is nearly impossible to realize. Future projects will thus go for even brighter stars than WASP and HAT already did.

The first two space missions dedicated to the transit search detected the first rocky planets. And Kepler with its observations of long duration allowed for the first time to detect transit timing variations in the orbital periods of the planets. Unfortunately as well CoRoT as Kepler will not detect Planets around very bright stars. This limits us in the ability to completely characterize the planets and their atmospheres in following ground based observations. A mission like the proposed PLATO satellite is still needed to detect earth like planets in the habitable zones around nearby stars.

**Part II.**

**Method**



The Tautenburg Exoplanet Search Telescope (TEST) is the main instrument used for the work presented in this thesis. The two key scientific objectives I pursued with the TEST are: a) long-term observations of selected star fields to search for unknown hot Jupiters and b) photometric follow-up observations in support of the CoRoT satellite mission.

In the years 2002 / 2003 the Berlin Exoplanet Search Telescope (BEST), operated by the *Institut für Planetenforschung*, of the *Deutsches Zentrum für Luft- und Raumfahrt (DLR)*, was located at the *Thüringer Landessternwarte (TLS)* Rauer et al. (2004). The good experiences made with the BEST led to the conclusion to permanently install a small aperture telescope at the TLS. This telescope, the TEST, had first light in October 2005.

In contrast to the BEST, which is operated remotely, for the TEST it was decided to completely automate the observations. Until recently such small telescopes were only used by amateur astronomers. Professional use was mostly not considered, as the main advantage of such small telescopes, their dedicated availability, also resulted in a high need of time and effort to be invested, in order to conduct long term observations. An automation of such telescopes therefore makes long term campaigns of this kind feasible for the first time.

As a main part of the work on this thesis, I automated the observing mode of the TEST. Thus, observations can now be taken at low effort, resulting in over 600 observing hours (not all of which were at photometric conditions) in the year 2009. To handle this amount of data, I designed a database for the TEST. This database is coupled to a photometric analysis pipeline, allowing an easier analysis of the selected fields.

In Chapter 4, I describe the TEST and its robotic observation mode, as well as the data handling. This is followed by a short overview of the reduction and photometry software I designed for the TEST (Chapter 5). In Chapter 6, I present the analysis of the light curves, including noise reduction, identification of variable stars, and the search for transit-like events as necessary part of the search for transiting exoplanets.

In order to verify the planetary character of candidates found with the TEST, I performed spectroscopic follow-up observations with the 2-m Coudé telescope of the TLS. In Section 7 the spectroscopic follow-up, as well as the procedure to determine physical parameters of the observed objects are specified.

Next to the search for transiting planets in selected fields the second main topic of this thesis are the photometric follow-up observations in support of the CoRoT mission. This mission and the motivation for the ground-based follow-up will be presented in Chapter 8.



## 4. The Tautenburg Exoplanet Search Telescope (TEST)

### 4.1. The TEST System

The TEST system consists several components, like the dome, the telescope, the CCD, the guiding system, etcetera . Additionally the TEST system includes an image database which is used to administer the observations done with the TEST. In this chapter the hardware components and their control software as well as the TEST database are presented.

#### The Telescope

The TEST is a Flatfield Camera (FFC) by Lichtenknecker with an effective aperture of 294 mm and 940 mm focal length. The focal ratio is  $1/3.2$ . The FFC is a folded Schmidt camera (Figure 4.2). The light passes the correction plate, which is an aspheric lens of 300 mm in diameter. Then the main mirror of

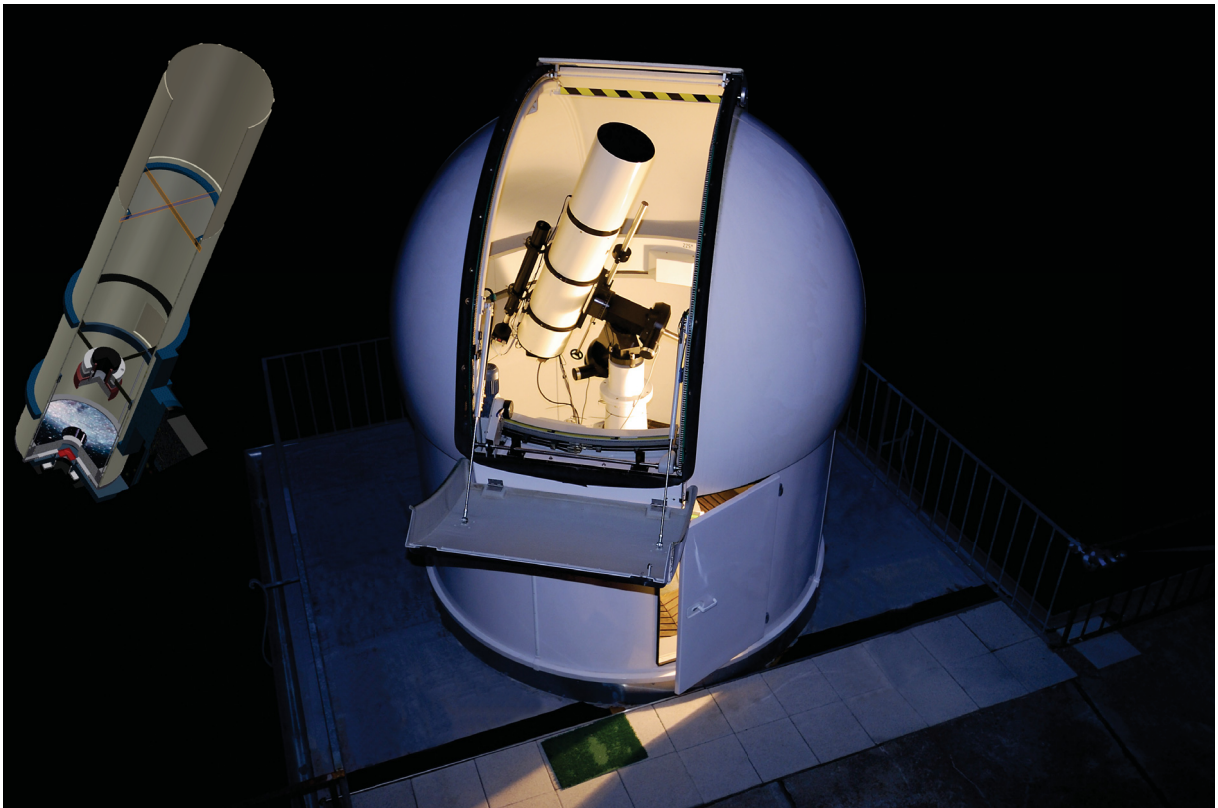
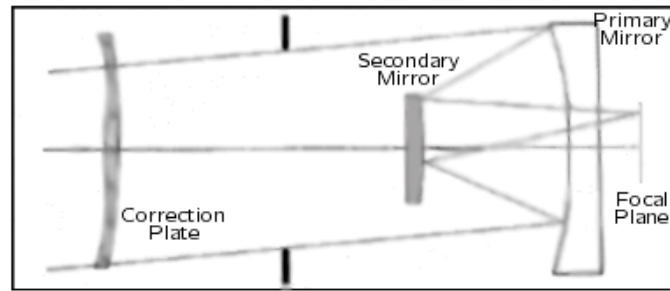


Figure 4.1.: The TEST System. The CAD diagram on the left shows the inner layout of the telescope.



**Figure 4.2.:** *Optical design of the Flatfield Camera by Lichtenknecker. A correction plate in the optical path allows a large field of view without distortion.*

300 mm in diameter reflects it to the secondary mirror (141.5 mm in diameter), which is mounted on the focusing unit. From there the light is reflected to the focal plane behind the main mirror.

The focus of the telescope is mainly stable and changes only slightly when large temperature shifts occur. The position of the primary and secondary mirror can be adjusted separately. The tube including the optical system has a weight of about 40 kg.

### The CCD

In the focal plane a CCD camera by Apogee (APOGEE AP16E) is placed. The camera has a Kodak KAF-16800 front-side illuminated chip. This chip has  $4096 \times 4096$  pixels with a size of  $9 \mu\text{m}$  per pixel, resulting in a  $36.8 \times 36.8$  mm detector area. In combination with the optical system a scale of about 2.0 arcsec/pixel is reached. In turn the field of view has  $2.2 \times 2.2$  square degrees. The digital resolution of the chip and readout electronics is 14 bits, with a saturation limit of 16384 ADU. A thermoelectric cooler with forced air allows the cooling of the CCD down to  $30^\circ \text{C}$  below ambient temperature. The readout noise is about  $15 e^-$ . A low dark current of  $0.2 e^-/\text{pixel}/\text{sec}$  is given for the cooled CCD. The readout time is  $\sim 30$  seconds. It can be reduced when reading out only sub-frames or using pixel binning to  $\sim 7$  seconds.

### The Mount

The TEST is mounted on a Lichtenknecker M145 German equatorial mount. Both axes are controlled by step motors. These step motors can be accessed by a hand paddle or via remote control. The mount control is realised by Quadrant Engineering, Inc., with the Coordinate III system. Coordinate jumps at noon and midnight inside this control system are one of the challenges of this mount. As step motors are sensitive to resonance, the fixation of the motors was changed in 2008 to a damped suspension in order to avoid unpredictable stops of the telescope which were observed in the first year of operation. With the awareness of the coordinate jumps and the improvement of the motor fixture, the mount can be used for automatic telescope control, although the pointing accuracy is not as good as some other mounts offer. As the mount is a German equatorial mount, a reversion of the telescope is needed when passing the meridian. When moving over the meridian while tracking, the mounts control system unfortunately fails to recognise that the reversion was not yet done. Therefore observations near to the meridian are not advisable. Instead it is necessary to actively slew to the other side of the meridian.



## Guiding system

The guiding optics is a refractor with an aperture of 80 mm. and a focal length of 900 mm. As guiding camera a SBIG ST2000XM camera is used. This camera consists of two separate CCD chips. The scientific chip has 1600 x 1200 pixel with a pixel size of  $7.4 \mu\text{m}$ . Next to this, a small guiding chip is installed, which is not used in the standard configuration of the TEST. Instead the Scientific Chip is used to select and follow a guiding star. The guiding is done automatically by the CCD control software CCD-Soft.

## Filter Wheel

In order to allow for multi-band observations, a filter wheel was added to the TEST system in January 2009. The IFW filter wheel by Optec, Inc. holds six square filters with a side length of 50 mm. In addition to the R-Johnson filter used for observations in 2008, observations with UBVRI-Kron filters are now possible. The filter wheel can be accessed remotely over a serial connection. The automatic observation mode of the TEST allows to observe a given field with alternating filters.

## The Dome

The TEST is placed in a 3-m dome by Baader Planetarium. As the dome is placed directly south to the dome of the 2-m Tautenburg telescope, observations directed to the north are only possible at altitudes higher than  $50^\circ$ . In all other directions observations down to  $20^\circ$  altitude can be achieved.

## The Weather Control

During the observation the weather conditions are monitored. Dew point and humidity sensors are installed at the TEST mount, tube, and dew cap. Furthermore, the data of the weather station of the Thüringer Landessternwarte gets evaluated during observations. In case of critical temperatures near the Schmidt plate, the dew cap can be heated during observations. In case the humidity gets to high inside the dome or at the weather station, the dome closes automatically and a dehumidifier will turn on. The dehumidifier is also used in the beginning of the observing run to ensure that no condensation builds up on the CCD.

Additionally, the immediate analysis of the guiding images during observations is used to identify incoming clouds. In case no guide star is found, the dome will also close and a warning message will be displayed in the control room.

## 4.2. Automatic Operation of the TEST

In cooperation with the technical staff of the Thüringer Landessternwarte I prepared the TEST for robotic observations in the year 2007. As at this time no automated control software for such a telescope system was available, a software bundle by Software Bisque, optimized for interactive observations was used as a starting point. This software bundle containing TheSky6, CCDSoft5, and AutomaDome was used to interface with most of the hardware components described above. AutomaDome gives a simple interface

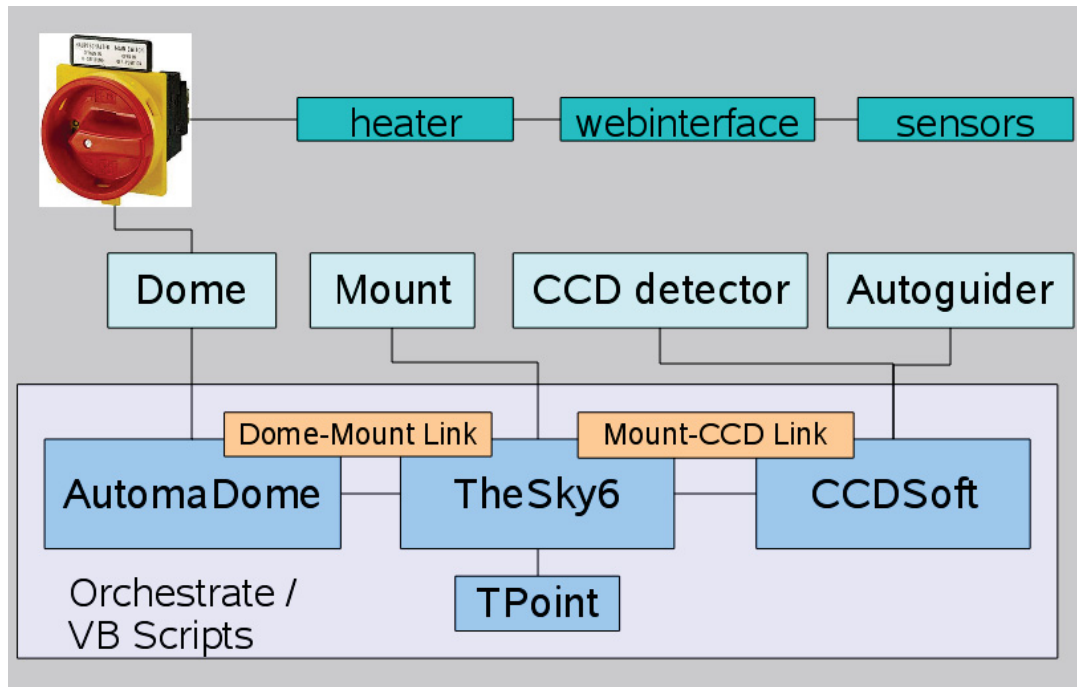


**Figure 4.3.:** Scheme of the automated software control of the TEST. The mount, dome, and CCD cameras are accessed using the software bundle by Software Bisque. For the automation and control of the additional hardware scripts were written embedding the commercial software in the robotic operation of the TEST.

to control the dome. TheSky6 allows to control the telescope. It is also connected with AutomaDome, ensuring that the slit of the dome and the telescope face the same direction. Star catalogues are included in TheSky6, allowing to calculate astrometric solutions in combination with the CCDSOFT5 program which is used to control the CCD and Guiding system. All these programs written mainly for amateur astronomers can be accessed via Visual Basic scripts. Scripts to simplify the interactive use of telescopes were already included. The programs of Software Bisque allow an easy access to the hardware and also provide useful tools like an automatic astrometric calculation, but they are optimised for interactive usage, not for a complete automation, which was needed. Therefore, I programmed an automated environment which is accessing the TEST hardware using the Software Bisque programs (Figure 4.3). The access to the mount, the dome, as well as the CCD cameras uses mainly the interfaces provided by the above mentioned commercial software. To allow for an as good as possible failsafe shutdown of the system, the mount is also accessed directly via the serial port when turning of the tracking of the telescope.

The CCDSOFT software allows to connect to a filter wheel as well, but unfortunately this interface is laid out for a four filter system only (luminance, red, green, blue). Therefore the TEST filter wheel is controlled directly through its serial port. The weather control system as well as the dehumidifier are also controlled separately.

The timeline of an observing night is laid out in Figure 4.4. I programmed the TEST to work completely robotic, starting with the cooling of the CCDs and ending in the next morning with their controlled warming. Such robotic observation modes are needed to allow for such longterm campaigns, which otherwise would not be possible in an efficient way.

When the TEST is started it first establishes the access to the hardware. When the connections are established and the scientific CCD camera is cooled down to  $\sim 25^\circ$  below ambient temperature, skyflat

images are taken during the dusk. These flatfields are taken in all filters. The exposure times are calculated using the equation presented by Tyson & Gal (1993). I limited the minimal exposure for skyflats to a few seconds. Thus the influence of the finite shutter speed is not influencing the flatfields significantly. Nevertheless, in the later presented reduction pipeline I allow to correct for the effects caused by the iris-shutter of the CCD camera. After skyflat images are taken, the TEST waits for the Sun to go below  $13^\circ$  under the horizon. Then the observation starts.

The fields to be observed are submitted to the TEST in an ASCII file. Name and coordinates of the object, as well as the exposure time and selected filter needs to be defined in this ASCII file. In addition, observation start and end time can be defined, as well as a combination of different filters to be used consecutively. When no starting observing time is given, the TEST will start with the first defined field in the ASCII file and check for its visibility. If the field is visible the telescope will slew to the position, otherwise the next defined field will be checked. As the slewing of the mount is not as precise, an automatic astrometry calibration is done. Using an image taken with the TEST an astrometric solution is calculated using TheSky6. After this the position of the mount is corrected accordingly.

If another field with higher priority gets visible, or the field observed at the moment disappears, the TEST will observe the next field.

All this time the guider is not only used to correct for tracking errors, but also to check the current weather conditions. When the guide star disappears, the guide camera is used to check for clouds, and if no stars are visible the closing of the dome is initiated.

During dawn, skyflat images again are taken. Afterwards the telescope is moved back to its parking position. At this point, before the camera is warmed up again, bias images as well as dark images, ten for each exposure time used during night, are taken. As a last step data gathered over night are copied to the TEST archive, and an e-mail including the observing log-file is sent to the observer.

### 4.3. Data Management of the TEST

During an average observation night, between 100 and 200 scientific images are taken, observing mostly not more than three different fields. These values depend of course of the length of the night, exposure time, and weather conditions. In Figure 4.5 the number of observed hours per night since 2008 are shown<sup>1</sup>. I took most of the observations of three defined fields in the search for transiting exoplanets. For the CoRoT follow-up observations I observed several different fields, but only at nights when transit-events observable with the TEST were expected. Besides the transit search and CoRoT follow-up, I looked at known variable stars in support of other projects. Partly these observations were taken in different filter bands and with different exposure times. All together, since January 2008 over 20,000 scientific images have been taken with the TEST. All these images need to be easily accessible for further data processing.

Hence I set up a user friendly, fast accessible, well structured data management system to access not only the scientific, but also the corresponding calibration images. The “TEST Data Management” system is

---

<sup>1</sup>In 2008 many gaps in the duty cycle are caused by malfunctions of the hardware. Especially the mount and the shutter of the Apogee CCD camera caused some trouble. Since 2009 the duty cycle is mainly shaped by night duration and weather conditions.

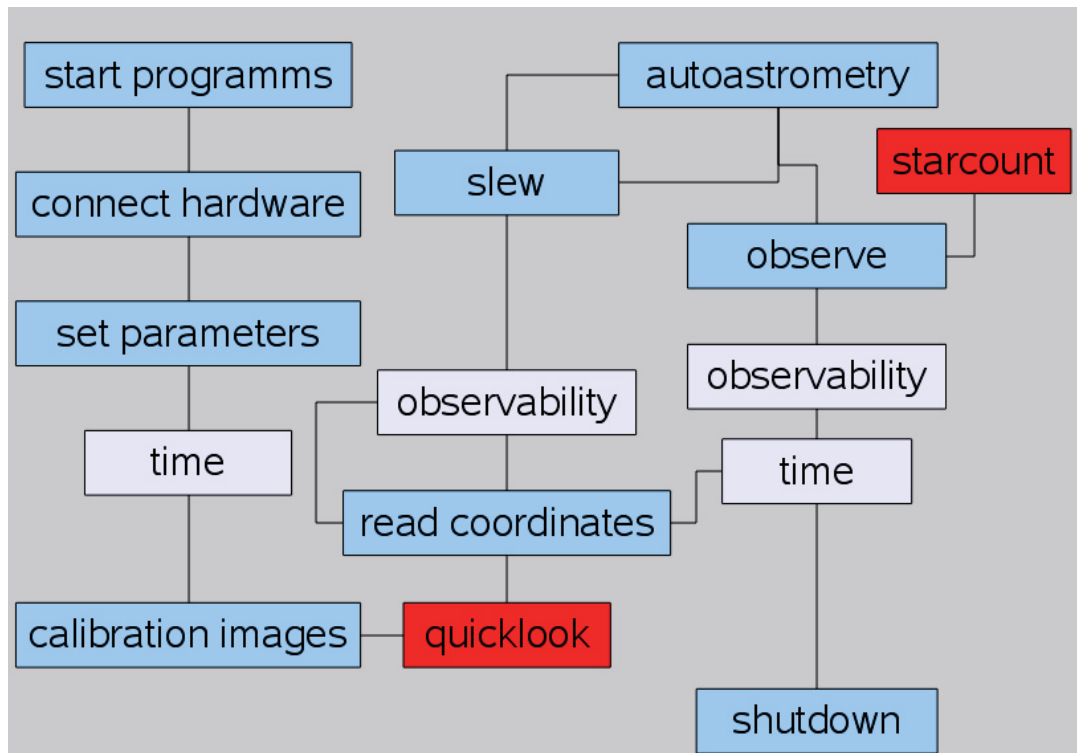


Figure 4.4.: Schematic View of a typical TEST observing night.

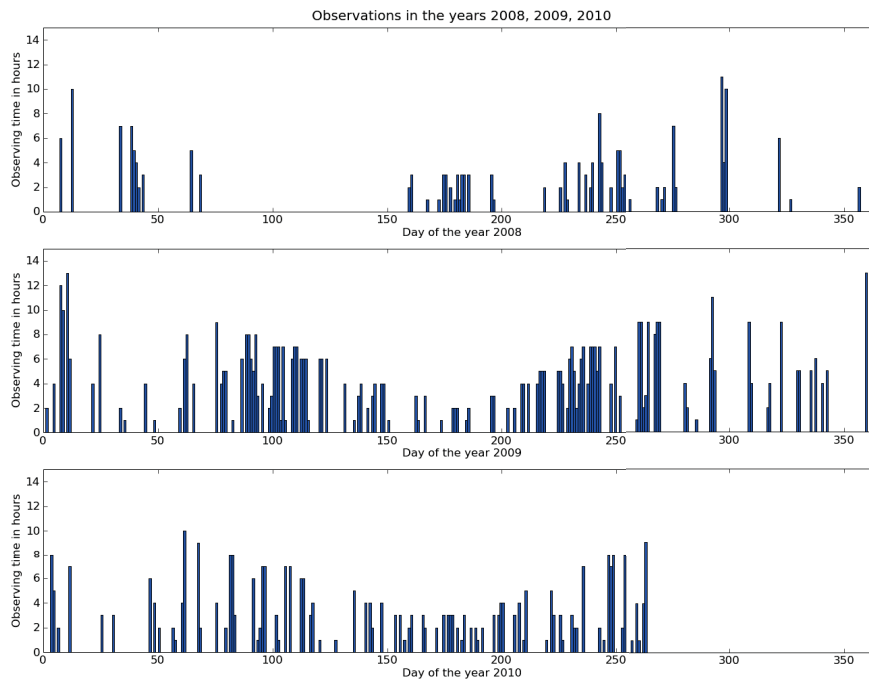


Figure 4.5.: Daily observing hours of the TEST for the years 2008, 2009 and 2010.

based on a PostgreSQL database, which allows a fast and easy selection of data by different parameters. The database is very simple structured and consists of three tables. Next to the original images, the master images created during the reduction (see Chapter 5.1) are listed, and finally the reduced scientific images are accessible via the third table. In the first mentioned table, next to the filename of the image file, all the image file header information is stored in separate columns, so that each column represents one header keyword. The filename is set to be a unique key, in order to avoid duplicated entries of files in the database. Some of the header keywords like *observing date*, *filter*, *exposure time*, *observed object* are indexed. This was done for keywords known to be used in the future to select a subsample of the images for further processing. Thus I ensure a fast access to the database. In the table administering the master images next to the filename of the created master file, the image type (master-bias, master-dark, or master-flat), the filter, exposure time, the used instrument and telescope, and the image size are stored. Next to this, references to the files used to create the master image are given, allowing to easily retrace its construction. In addition, statistical values like the mean value, as well as the standard deviation and an integer flag describing the quality of the image can be stored. The indices created for fast access to the master images are optimised for the TEST reduction routines. The information stored for the reduced images is basically the same as for the original ones. In addition, I store references to the original image which was reduced as well as to the master images used, in the database.

With such a database all the needed information for one image or a subsample of images can be accessed using the sql syntax by direct connection to the database. For the TEST, I created a graphical interface to this database using wxPython<sup>2</sup>. This user friendly interface allows fast and easy access to the TEST database, without the need to get familiar with the underlying database structures. This interface (Figure 4.6) allows one to select images, and to export their filenames, as well as additional information in an ASCII file. This feature was included to allow the use of routines, other than the ones I already included in the TEST photometry software. For the reduction and the photometry programs I used in this thesis, such an intermediate step is not needed as I included the database management directly into the graphical interface of the TEST reduction and photometry programs.

## 4.4. Performance of the TEST

The performance of the TEST is influenced by two major factors: a) the different hardware components, their individual quality and reliability and b) the observing site.

The TEST consists of many different hardware components, all of which went through some changes over the past years. Therefore also the performance changed over time. Especially in the years 2007 and 2008 many problems concerning the hardware were encountered. Repairs and modification of the system often improved the TEST. For example the installation of a dehumidifier increased the number of nights with good observations, as the fogging of the CCD when cooling down could be avoided.

Readout problems with the guide camera, as well as a malfunctioning shutter of the Apogee Camera were repaired. From time to time (approximately once a year) the correction plate in front of the telescope

---

<sup>2</sup>cf. <http://wxpython.org>

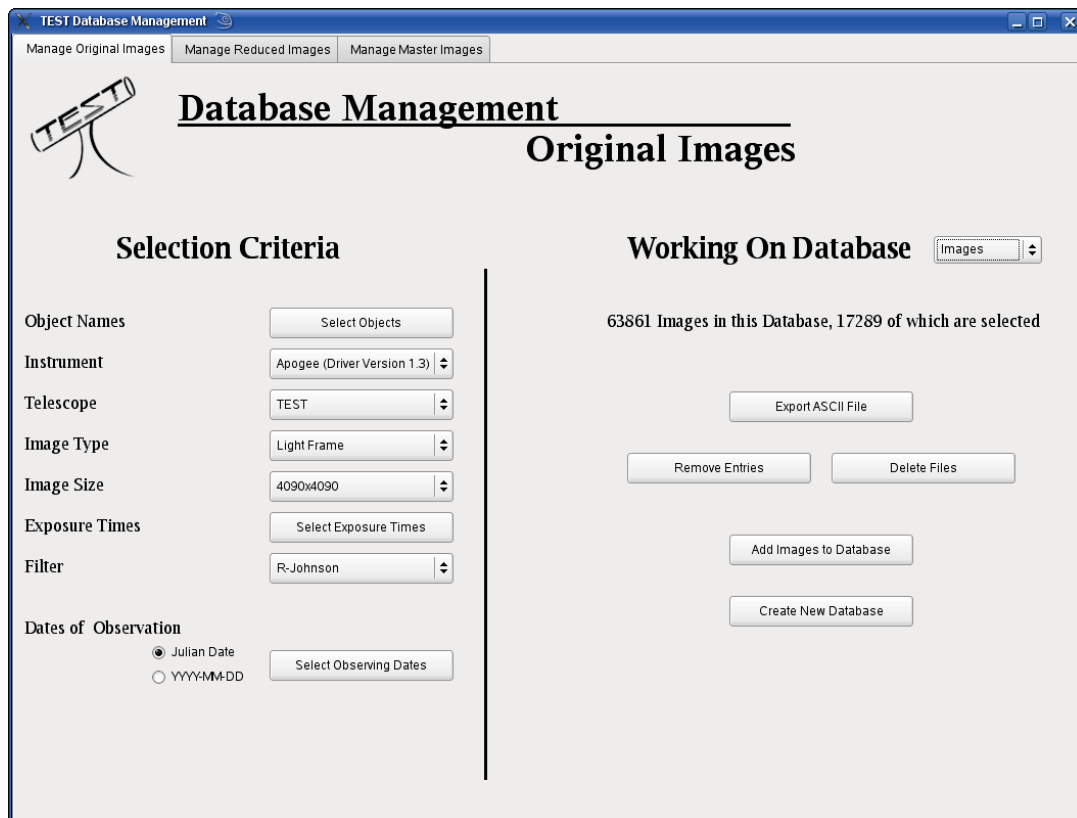


**Figure 4.6.:** A graphical interface to administer the original as well as reduced images. A connection to the TEST image database allows to select subsamples of the images stored in the database. An ASCII list of these subsamples can be exported for further use with other programs.



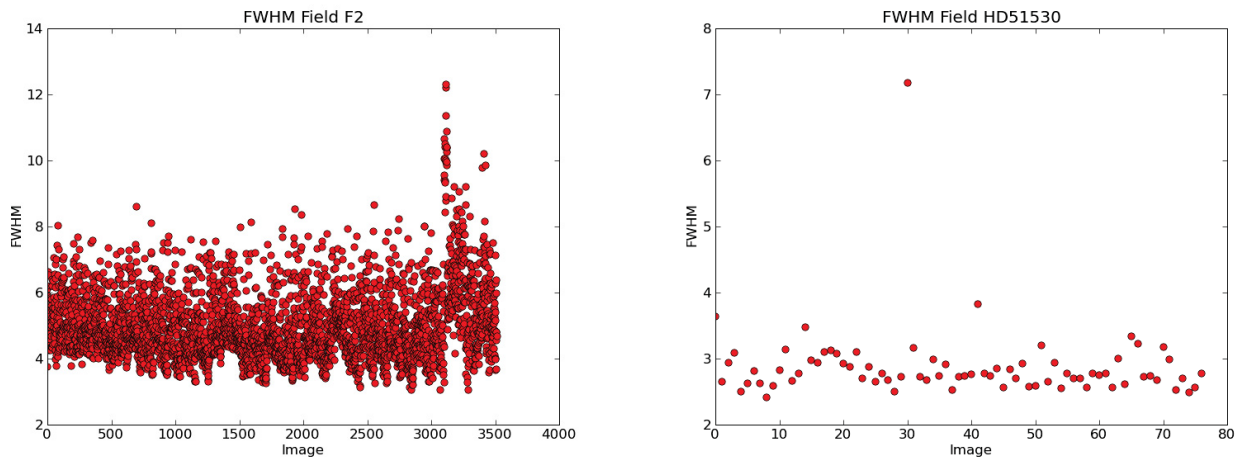


**Figure 4.7.:** *The FWHM in pixels for images of the F2 field taken in 2009 (R-Johnson, 120s exposure) on the left, and on a night with good seeing taken in the U-Kron band with 1 s exposure time*

needs to be cleaned as insects and pollen settle on it over time, even though a cover is protecting the telescope when not observing.

Lots of my attention was spend on the mount of the telescope. Malfunctions encountered when slewing the telescope to a new position were completely removed, jerky movements of the mount when tracking were reduced to an acceptable limit. Unfortunately the pointing of the mount is still not better than 20 arc-minutes. Therefore astrometric corrections need to be done when slewing to an object. Using this correction, a pointing accuracy of a few arcseconds can be reached by the loss of around one minute reaction time.

The resolution of the TEST as given by the CCD is two arcseconds per pixel. To ensure a good fit of the point spread function as well as to distinguish between cosmics and stars, the stars light should be spread over a few pixels, giving us a minimum value of four to six arcseconds full-width-half-maximum (fwhm) that would be possible to reach. In reality a fwhm less than five arcseconds has not been observed with the TEST, although with the 2-m telescope in Tautenburg a seeing of two arcseconds and better has been observed. This might be caused by air fluctuations inside the TEST dome or even moving layers of air inside the closed tube of the TEST. In Figure 4.7 the fwhm is shown for all observations of the F2 field in the year 2009 using the R-Johnson filter with an exposure time of 120 seconds. The best seeing would be at around three pixels, corresponding to six arcseconds, but the mean value would be between four and five pixels corresponding from eight to ten arcseconds. At the right side the observations of a very good night are shown using the U-Kron filter with an exposure time of 1 second.

The photometric precision that can be reached is mainly influenced by the observing site, and its weather conditions. In Figure 4.8 the theoretically expected and actually observed precision is shown for two different nights. As can be seen this can change quite significantly from night to night. A good estimate for the photometric goodness of a night is given by the number of stars in a given field that show a standard deviation below 1%. When looking at the two graphs in Figure 4.8 this is represented by the horizontal red line. In the left graph over 1000 stars are well below this line, whereas in the right graph no star at all can reach this precision.

When looking at all nights in the years 2008 and 2009, one finds that only 50% of the nights used for observations show conditions to reach the photometric precision needed to find transiting exoplanets.

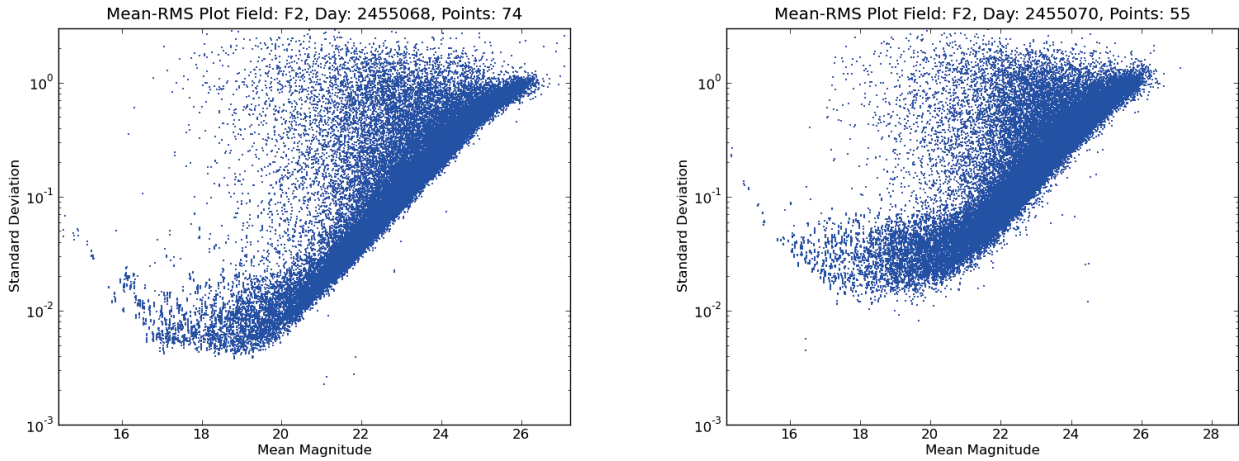


**Figure 4.8.:** The standard deviation of the light curves of observed stars plotted over their mean magnitude for two different nights, indicating the precision reached in each case. The precision can vary very strongly. Nights that show a certain amount of stars with a standard deviation below 0.01 magnitude are considered to be good. The number of stars depends on the field.

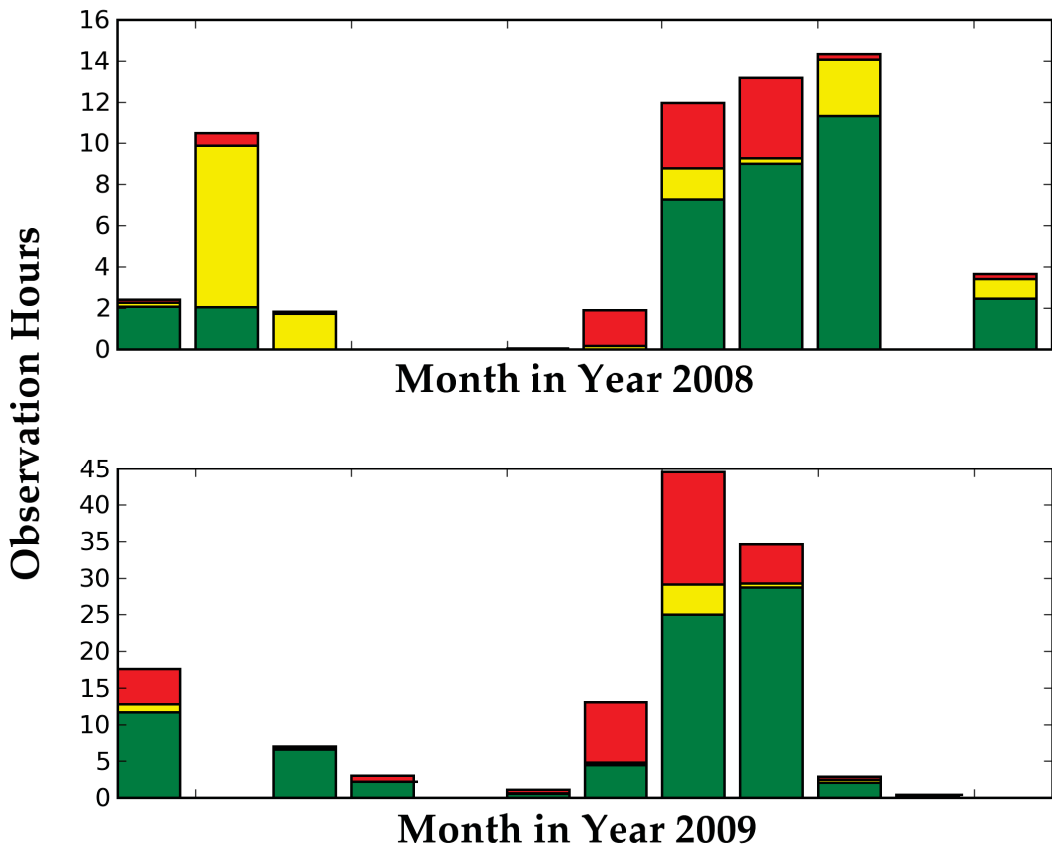


**Figure 4.9.:** Observations of the field F2, colour coded by their quality: red) observations not usable. yellow) bad photometric quality. green) observations used for transit search.

For the Field F2 this is shown in figure 4.9. In combination with the typical duty cycle of the TEST as shown in Figure 4.5 a yearly amount of around 500 hours of observation in “photometrically good” nights can be estimated for the TEST for future years.



## 5. Data Reduction and Photometry

### 5.1. Standard Reduction

Observed scientific images unfortunately are influenced by many sources of errors. The purpose of the image reduction is, to minimise the effects introduced to the observations by your instrument.

For the reduction of the scientific images I applied a standard reduction pipeline using IRAF (Tody (1986), Tody (1993)). This standard reduction includes bias and dark subtraction, as well as flatfield correction.

At the end of every observing night ten bias images are taken. Additionally, for each exposure time used during night, ten dark images are taken. Before creating masterbias and masterdark images, the quality of each image is controlled. For this the bias and dark images are arranged in blocks by observing nights and in case of the dark images also by exposure time. For each image the mean value, as well as the standard deviation is calculated. Images which deviate strongly from the other images are marked as bad and are not used to create the according master image.

The ranking of flatfields proves to be much more difficult. Flatfields are taken during the dusk and dawn twilight on the sky in all filters. The change of the exposure times between two exposures is calculated based on Tyson & Gal (1993). The minimum exposure time is set to be a few seconds, thus the shutter time of the iris will not influence the flatfields. Nevertheless, when creating a masterflat, it is possible to correct the flatfields for the effects caused by finite shutter speed as described in Surma (1993). For the automated determination of the quality of the flatfields, I developed a routine based on morphological image processing. The combination of the two fundamental morphological operations, erosion and dilation, to the opening operation, reduce the flatfields to their large structures. The kernel size used for the erosion and dilation needs to be large compared to expected changes between different flatfields (e.g. stars), but small compared to structures expected to be displayed on bad images (e.g. caused by filter displacement or dew on the CCD). For the TEST data the kernel is set to a circle with 50 pixels in diameter. Thus the flatfields can be compared to each other even if stars of the twilight sky may be present. Although these operations are not very common in astrophysics, they are widely used in image processing and serve as a basic tool of morphological noise removal. A more detailed description of these operations can be found in Serra (1983).

The created master images are rated in a similar fashion. For all masterbias and masterdark images mean value as well as the standard deviation is determined. Images that deviate a lot from the other master images are labelled to be of bad quality. The quality of masterflats is established by manual examination. A simple graphical interface plots all the masterflats and allows an easy manual selection

of masterflats of good quality. Information about the master images like their quality, the names of the combined images, and averaged observation date are stored in the TEST database.

For the reduction of the scientific images, the appropriate master images are selected by the filter (for flats), exposure time (darks), average observation date and their quality. The reduction of the scientific images, as well as the creation of the master images is done using the “TEST Data Reduction Program”. The graphical interface is programmed using wxPython, the same as the “TEST Data Management”. It is connected to the TEST database, and allows therefore an easy selection of the images that need to be reduced. The IRAF routines used for the data reduction are called using PyRAF<sup>1</sup>. The reduced images are implemented into the TEST database for further access.

## 5.2. Photometry

The TEST photometry package uses also a graphical interface similar to the one I designed for the data reduction. An image selection by field, exposure time, date of observation and several other parameters allows to do photometry for any subgroup of the TEST images (Figure 5.1). Images with different sets of parameters can also be selected simultaneously. In such case the images are sorted according to the observing parameter (observed field, exposure time, filter, etc.) and the following steps are executed for each set of images separately.

In a first step the quality of each image is determined. For this each image is compared to other images of the same parameter set (observed object, exposure time, filter). Using Source Extractor by Bertin & Arnouts (1996) the number of stars and the median full-width at half-maximum (fwhm) for all stars in the images are identified. Furthermore the actual position and rotation of the image in sky coordinates are determined using the astrometric calibration software by astrometry.net (Lang et al. (2010)). The astrometric solution as well as the number of identified stars and the apparent seeing conditions are then used to evaluate the quality of the image. Discrepancies in the number of stars may be caused by cloudy weather, or jerky movements of the mount during the exposure. Errors in position or rotation angle indicate slewing problems of the mount or errors in the astrometric calculation which also can be caused by in-moving clouds or other artefacts visible on the image.

The fwhm computed by the Source Extractor is then used to identify the images with the best seeing. These images, 50 at maximum, are combined to a reference frame. This again is done using IRAF routines. The reference frame, showing a high signal-to-noise ratio, is used to create a final catalogue of stars in the field-of-view using Source Extractor. In order to ensure the completeness of the catalogue, found stars are subtracted from the image by the IRAF daophot/substar routine. The subtracted image is re-analysed for stars previously not found. Using the astrometric solutions previously calculated with astrometry.net, all images are shifted to the coordinate system of the reference frame.

Finally the magnitude of each star is calculated. Two different routines are integrated in the TEST photometry program for this task. A simple and fast approach is the aperture photometry included in the

---

<sup>1</sup>PyRAF is a product of the Space Telescope Science Institute, which is operated by AURA for NASA. It is a command language for running IRAF tasks that is based on the Python scripting language. More information can be found at [http://www.stsci.edu/resources/software\\_hardware/pyraf](http://www.stsci.edu/resources/software_hardware/pyraf).

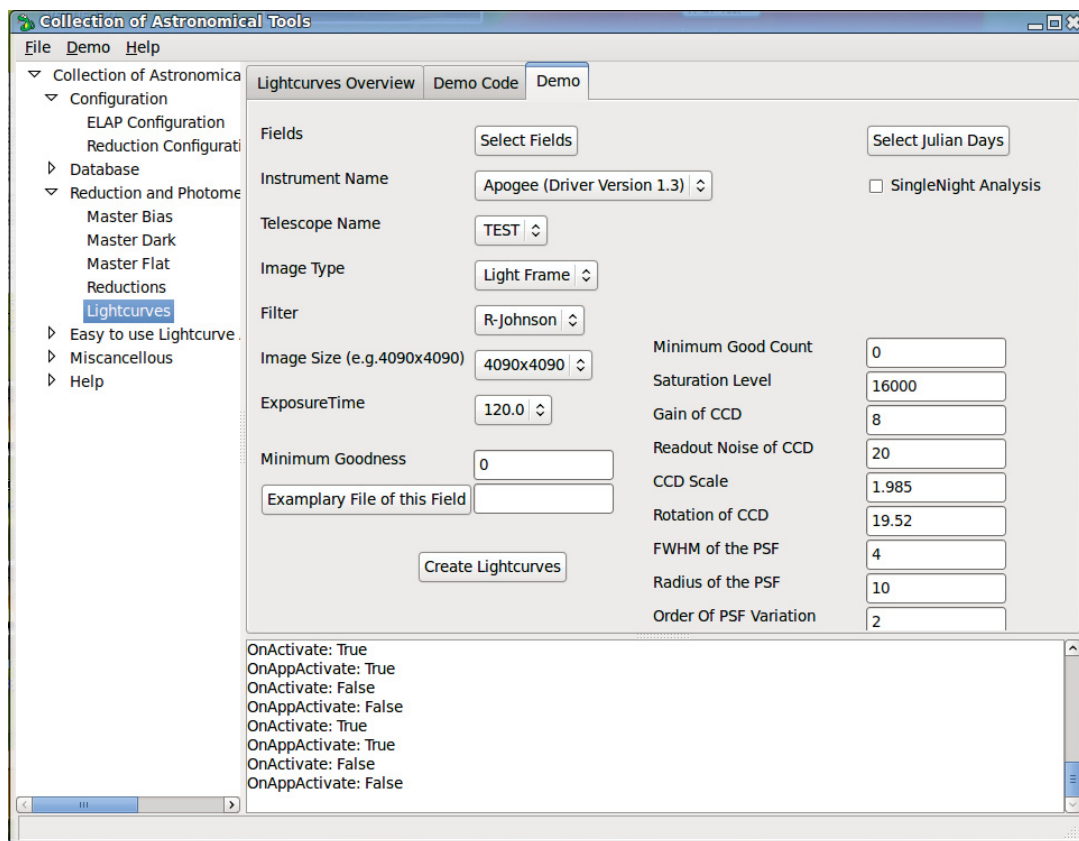


**Figure 5.1.:** The front end for the TEST photometry. Using the TEST database already reduced images can be selected by different criteria. The selected images will then be analysed. Some major parameters can be set manually in this program.

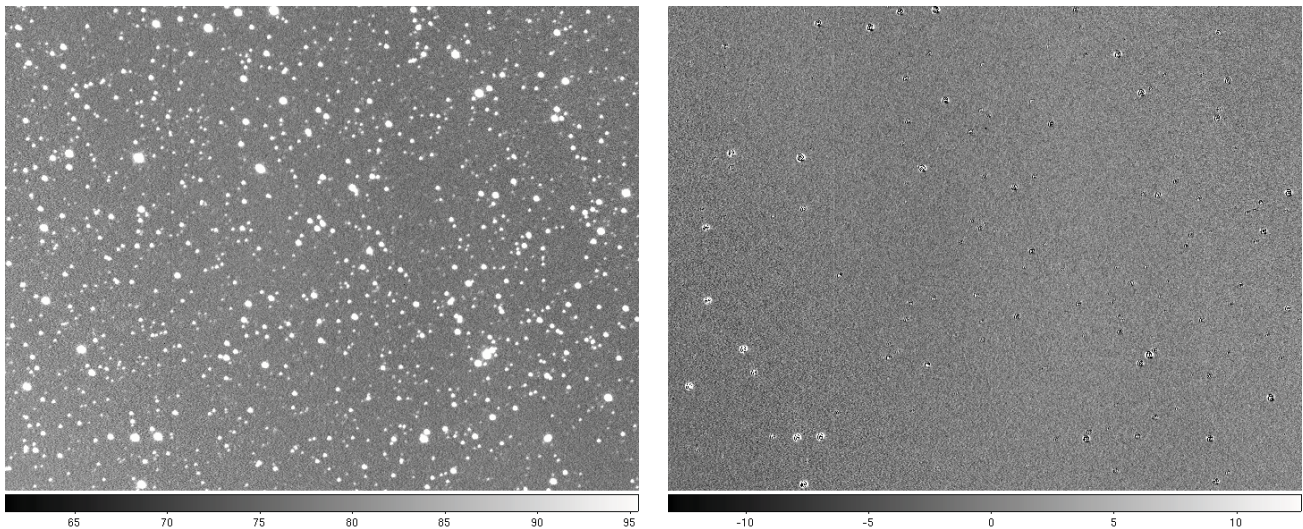


**Figure 5.2.:** *The differential image subtraction as seen above is conducted using the ISIS code by Alard (2000). As can be seen especially bright objects cause some trouble. But most stars can easily be subtracted and therefore allow a much higher accuracy when determining the variability of stars especially in crowded fields.*

IRAF daophot package. Computationally more intensive is the second approach, the image subtraction. In the following I will give a short description of these two methods and will compare the results and photometric precision reached with these two methods and discuss the pros and cons.

### Image Subtraction vs. Aperture Photometry

Aperture photometry is a very basic and well understood method to calculate the flux of a star. At this I measure the intensity of a circular region around the target star and subtract the estimated background contribution. The background is estimated by an annular region surrounding the star at a given distance. When using aperture photometry the resulting light curves are dominated by seeing effects and influences due to sky background and cirrus clouds. In order to compensate for the changing observing conditions I build a reference light curve out of the stars showing the least variability. I then use this reference light curve for calibration. This will be described in Chapter 6.1 in more detail.

In contrast to this, image subtraction is a method where a reference frame is subtracted from a number of frames using image convolution. The reference image, a selected image of high photometric quality, is convoluted with a kernel in order to match each image as close as possible by seeing and sky background. This convoluted image is then subtracted from the current image, producing a difference image. In the resulting difference image I measure the discrepancy between the reference image and the current image using aperture photometry, as above. In Figure 5.2 an example for the image subtraction is showed. As can be seen most of the stars are completely removed. At the position of some stars residuals, positive or negative can be detected, showing the change in brightness between the images. The convolution works also as a calibration of all images to the same photometric conditions. Therefore a calibration for atmospheric changes using a reference light curve is not necessary.

The “TEST Photometry” program uses the ISIS image subtraction program by Alard & Lupton (1998) with a spatially variable kernel as described in Alard (2000).



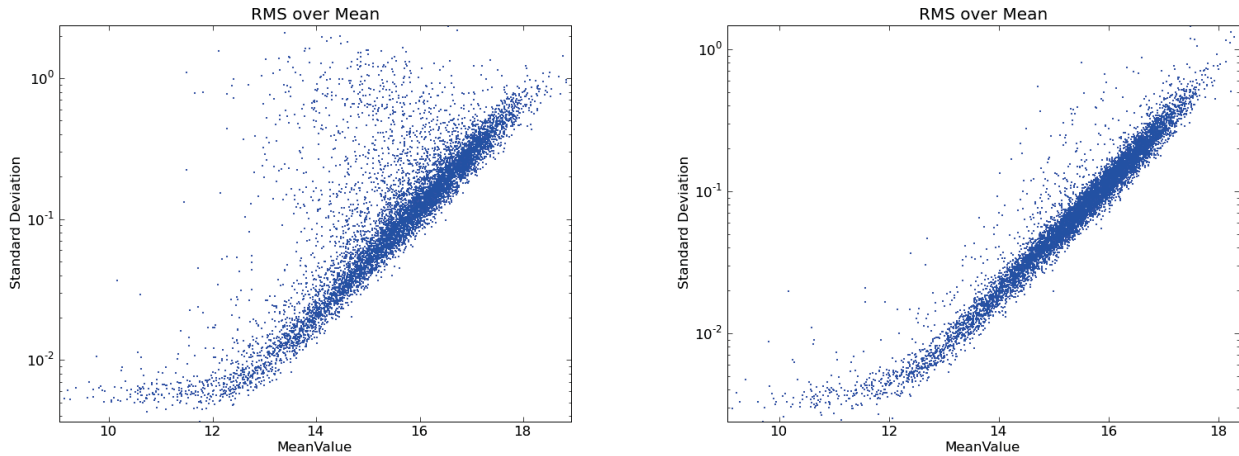


**Figure 5.3.:** *A single night observation at good weather conditions. The standard deviation over the mean apparent magnitude. Left the results for pure aperture photometry, whereas on the right side the photometry was done by image subtraction. For some of the not so bright stars real improvement can be seen, for brighter targets the difference is small.*

When comparing the results gained with these two methods, it is clear that in general the image subtraction gives much better results, even if the calibration is applied to the pure aperture photometry (Figure 5.3). But unfortunately for the brightest sources the image subtraction encounters sometimes problems. Additionally the results depend much by used parameters, such as the kernel size for the convolution. The pure aperture photometry allows a much more robust analysis without much need for optimization of the parameter set. This given the “TEST Photometry Program” allows to choose between these two methods. Aperture photometry also proves to be superior when images with very few stars are analysed. The image subtraction routine is not able to get a proper normalization of the images when only few stars are given and fails completely, whereas the aperture photometry is possible although the reference light curve build for calibration gives large errors in such a case.



## 6. Lightcurve Analysis

The light curve analysis consists of four main sections: noise reduction, identifying variable stars, finding sinusoidal signals, search for transit-like events. In addition, stars which were identified to be binary systems are further analysed with the DEBiL/MECI programs (Devor (2005), Devor & Charbonneau (2006)) in order to determine stellar types of the components of binary systems.

The light curve analysis is based on the analysis tools described in Eigmüller (2006). In order to improve the compatibility with the photometry, reduction and data management of the TEST, I rewrote the data analysis in Python, using major modules like SciPy and NumPy<sup>1</sup>. I transformed code that was available in Fortran and C to Python modules, thus allowing an integration into the TEST analysis pipeline. The frontend of the “TEST Light curve Analysis Program“ is programmed using wxPython, similar to the TEST-Data-Management and TEST-Photometry package.

The photometric light curves are managed in a PostgreSQL database (Figure 6.1). Next to the light curve identification number (ID), its filename, information gained by the light curve analysis as well as colour information obtained by cross referencing to the 2MASS catalogue is stored in this database. For a fast access to the light curves showing variability in general, or even periodic sinusoidal signals, views of these subgroups are created in the database<sup>2</sup>. The parameters found with the transit search algorithms (Chapter 6.4) or sinusoidal fit (Chapter 6.3) are stored in separate tables, using the light curve ID as reference to the main table.

### 6.1. Noise Reduction

Light curves are often dominated by noise. Sources of noise are for example atmospheric effects. In order to detect such small signals like transit events of planets, the noise needs to be minimised. For the noise reduction three different algorithms are implemented. They can be applied alone, as well as in combination. The first algorithm is based on the subtraction of an averaged light curve (further referred to as SAL algorithm) (Scholz & Eislöffel (2004)). Out of a sample of light curves the ones showing the least variability are selected. Their light curves are used to build a reference light curve showing a signal common to all stars in the field. This light curve then is subtracted from all light curves.

I modified this algorithm in order to use it with the TEST data. The quality of the result of this algorithm depends strongly on the amount of stars selected. Too many selected stars increase the noise, as faint stars with lower signal-to-noise ratio will dominate the reference light curve. If on the other hand, too

---

<sup>1</sup>cf. <http://www.scipy.org>

<sup>2</sup>In database theory, a view consists of a stored query accessible as a virtual table. This virtual table is composed of the result set of this query.

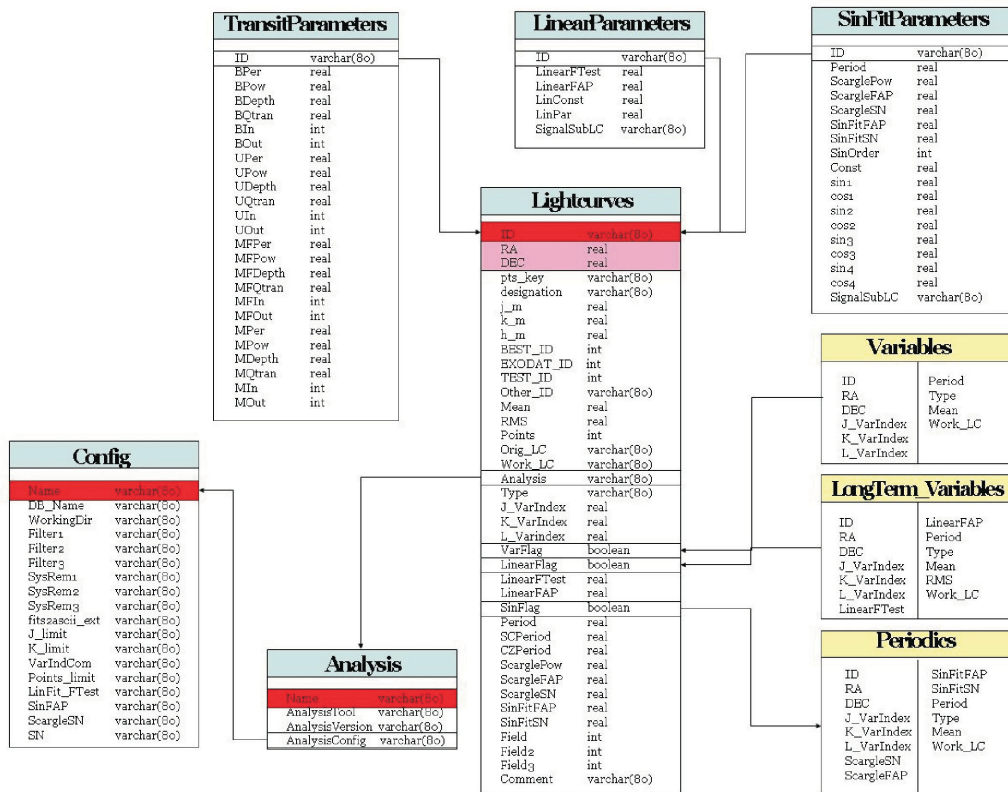


**Figure 6.1.:** The light curves are managed using a database with the above design. The main table contains all information about all light curves, different views show all the light curves identified to show variability, sinusoidal signals, or transit-like events.



few stars are selected, signals, present only in a single light curve, can influence the reference light curve strongly and create artificial signals.

In contrast to the original algorithm, which used only stars showing valid data points for the whole light curve, I allow the usage of stars if successful photometry could be achieved in at least 80% of the images. This modification was necessary for the TEST data, as many images of poor photometric quality are present. Without this modification, often the amount of light curves usable for building the reference light curve is too small to ensure the selection of a sufficient number of non-variable stars.

Furthermore two additions were included to the initial algorithm for the analysis of the crowded fields, observed with the TEST. The huge amount of stars allows not only to calculate one, but several reference light curves, using different stars. The different reference light curves can be calculated depending on the area on the CCD, colour information from the 2MASS catalogue or distributed randomly. For images of bad quality these different reference light curves sometimes differ quite a lot. In general, the images showing large differences in these different reference stars, are partly covered by clouds or show similar effects, and thus need to be deselected from further analysis to improve the overall light curve quality.

The calibration of the light curves with a constructed reference light curve is needed especially for the light curves calculated with aperture photometry. In these light curves often a change of brightness, common to all stars, can be observed. These changes are caused by variable weather conditions and the change of airmass due to the rising and setting of the field. These changes may rise up to a few tenths of a magnitude.

Light curves extracted from subtracted images using ISIS (see Section 5.2) show almost no such common variability. Here, such a normalisation is already done with the convolution of the images and therefore the SAL algorithm is not needed. Nevertheless, even for light curves obtained using image subtraction the error of the built reference light curve can be used to evaluate the quality of the images.

In addition, routines for noise reduction using the SysRem algorithm by Tamuz et al. (2005) and trend filtering algorithm (TFA) by Kovács et al. (2005) can be used. None of these both algorithms showed a clear advantage over another for the TEST data (Figure 6.2). A combination of the different algorithms is possible, and shows slight improvement. For all these algorithms different parameters can be set to optimise the results. The optimal parameters differ for each data set. In general the experience with the TEST data showed that the photometric quality of the resulting light curve is mainly influenced by careful selection of observations with high photometric quality, and much less by the different noise reduction algorithms.

## 6.2. Variable Star Identification

The identification of variable stars is based on two indices. Firstly the modified Stetson variability index is used (Welch & Stetson (1993), Stetson (1996)). This index is based on the assumption that variability which is caused by noise will show a completely random distribution. When normalising this light curve to a mean value of zero, the probability that two neighbouring data points have the same sign is  $\sim 50\%$ . But if the light curve is showing a signal, neighbouring data points would more likely show the same

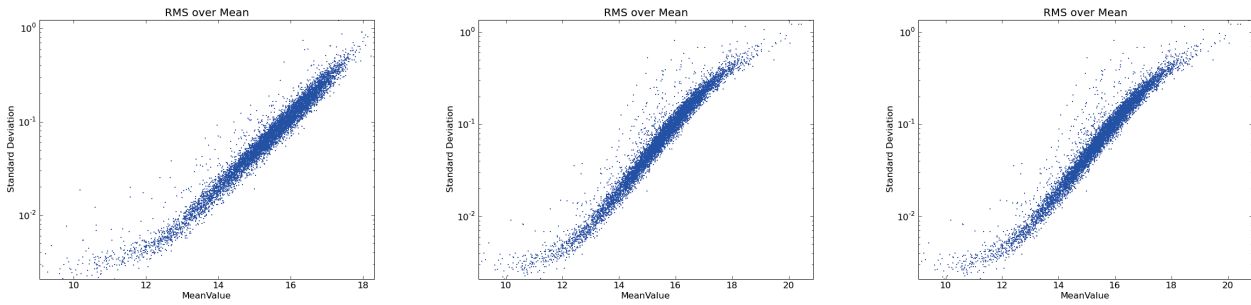


**Figure 6.2.:** The standard deviation plotted over the mean magnitude values after three different noise reduction techniques have been applied. Starting from the left: SAL, SysRem and the TFA algorithm.

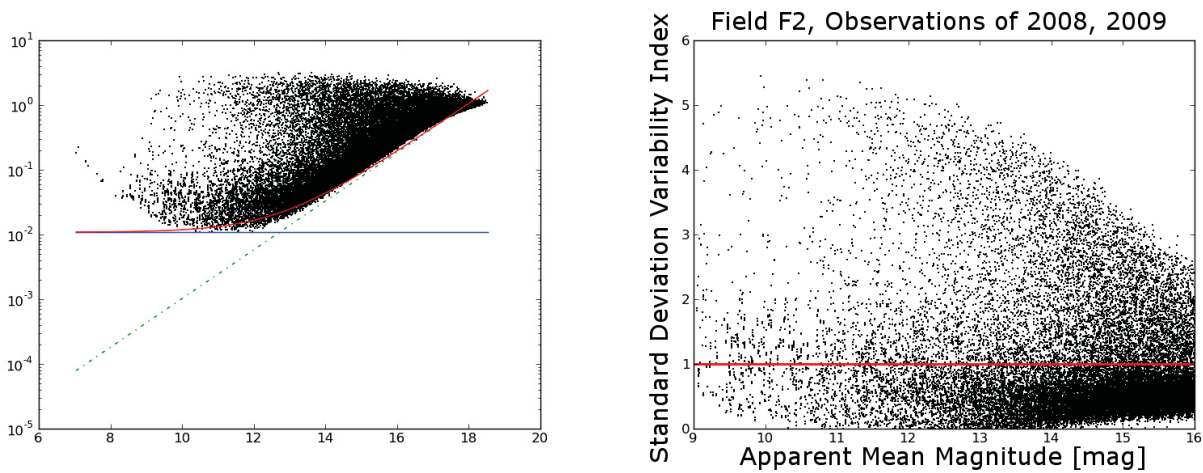


**Figure 6.3.:** The left image shows a typical distribution of standard deviation over mean magnitude of stars as observed with the TEST. An exponential function is fitted to the lower envelope of the distribution (red line) and used for a normalization. The right figure shows the resulting variability index.

sign.

In the modified version as introduced by Zhang et al. (2003) a weight which emphasises values which are separated by only a short amount of time is used. This allows to apply this index to light curves with non-evenly spaced values. This is needed as the time sampling of the TEST data is highly irregular. The other indicator for variability is given by the standard deviation of the light curve. The standard deviation is not only influenced by the variability of the star but also by the noise introduced by the observing site and instrument. This noise is correlated to the observed magnitude of the star. Therefore the standard deviation needs to be corrected by a magnitude dependent function before it can be used to estimate the variability of a star (Figure 6.3).

For further analysis stars can be selected as variables by either of the algorithms as well as their combination (Figure 6.4). As the combination of the algorithms shows a higher precision, it is the default selection method.

### 6.3. Detection of Sinusoidal Signals

As a next step, the search for sinusoidal signals is conducted for all stars found to show variability with the above mentioned method. For each of these light curves the Scargle-Lomb periodogram is calcu-

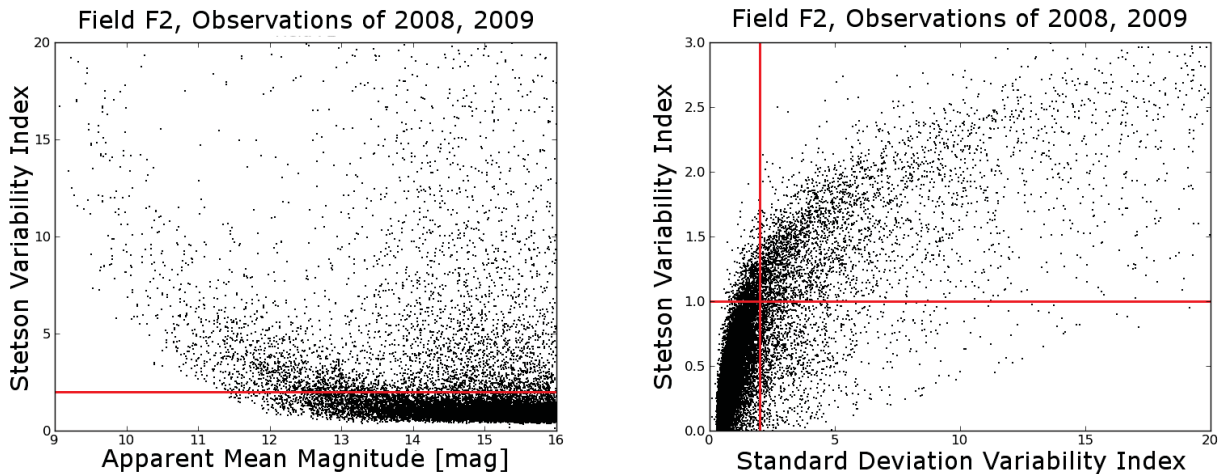


**Figure 6.4.:** *On the left the Stetson Variability Index is plotted for the same stars as seen in Figure 6.3. On the right side both variability indexes are plotted to each other. The red lines indicate the selection criteria. Stars can be select to be variable by either of the indices separately (right of the red line / above the red line), or in combination of both indices. The default selection criteria is that at least one index suggests the variability of the star (all stars, but lower left corner in the right graph).*

lated. For this task a program based on an algorithm presented in Press et al. (1992) was used in a slightly modified version<sup>3</sup>. As the following CLEAN deconvolution algorithm is computationally intensive, only light curves whose periodograms show a significant power are selected for further analysis.

The frequency spectra as calculated by the Scargle-Lomb algorithm are distorted by the limited frequency resolution and spurious responses. These are caused by the finite time span of the observations and the irregular time sampling. The latter can be handled by the CLEAN algorithm, which deconvolves the spectral window function from the discrete Fourier Transform (Roberts et al. (1987))<sup>4</sup>. Thus in the final periodogram only the real signal will show.

## 6.4. Transit Signal Search

As known from signal theory, simple algorithms are the most efficient algorithm when trying to detect a signal (Kay (1998)). Therefore the most common transit detection algorithms are based on a simple box fit. When fitting a box signal to a lightcurve four free parameters need to be determined: the period, the box width, the box depth and the midpoint of the box. A very fast routine to search for the most significant signal at all periods was published by Kovács et al. (2002). Using a minimization technique the depth as free parameter can be eliminated, thus limiting the free parameters to three.

This routine was improved to meet the concerns of the very noisy TEST data in the following way. The phase-folded light curve is binned. For each bin the weighted mean is calculated as well as the weighted

<sup>3</sup>the C-Program was written by George B. Moody. It is published under the General Public License. I modified it for the TEST analysis program so that formerly fixed parameters could be defined by the user. It was changed to a Python library.

<sup>4</sup>For the CLEAN process a Fortran program by Joseph Lehar was used. Modifications have been made, to allow the passing of parameters.

error. The usage of a weighted mean and weighted standard deviation in contrast to a normal mean and standard deviation is extremely important for data sets such as the light curves obtained by the TEST. With the changing photometric qualities in different nights, the errors of the observations can change in order of several magnitudes. A simple binning of the light curve would not account for these changes in the quality of the data. This would allow easily to hide transit signals obtained in nights of good photometric quality by observations of less quality when folding the light curves. Additionally false positives could dominate the detection algorithm.

### The Transit Detection Statistics

The main difference between the different box-fitting algorithms is not the fitted signal but the statistics to determine the significance of the detected signal. When searching for signals near the noise limit a good statistic is essential in order to avoid your signal to be overlaid by false positives. The most popular two box fitting statistics used at the moment are the ‘Box-fitting Least-Square’ (BLS) algorithm (Kovács et al. (2002)) and Matched Filter (MF) (Doyle et al. (2000)) algorithm. The performance of these two algorithms have been compared and slightly improved by Tingley (2003). One of the main results of this comparisons was that the minimization technique leads to a slight loss in detections. Otherwise none of the algorithms showed significant advantage over another.

Following these improvements, the modified Matched Filter (MF) and BLS algorithm (BLS) have been used in this work. The significance of a signal using the MF statistics is given by

$$T = d \left( \sum_{n=in} \frac{x_n}{\sigma_n^2} \right) - \frac{1}{2} d^2 \sum_{n=in} \frac{1}{\sigma_n^2} \quad (6.1)$$

where  $\sum_{n=in}$  is the sum over the in-transit binned points,  $x_n$  are the mean differential magnitudes in the according bin and  $\sigma_n$  the corresponding standard deviation.

For the BLS statistic the significance is given by

$$T = \frac{rd^2 - 2sd}{1 - r}, \quad (6.2)$$

with the following definitions:

$$r = \sum_{n=in} \sigma_n^{-2} \left[ \sum_{m=1}^N \sigma_m^{-2} \right]^{-1} \quad (6.3)$$

$$s = \sum_{n=in} \sigma_n^{-2} \left[ \sum_{m=1}^N \sigma_m^{-2} \right]^{-1} x_n \quad (6.4)$$

$$d = \sum_{n=in} \frac{x_n}{\sigma_n^2} \left( \sum_{n=in} \frac{1}{\sigma_n^2} \right)^{-1} \quad (6.5)$$

$\sigma$  defined as above and  $N$  giving the number of all data points (in and out of transit)<sup>5</sup>.

These both statistics show clear similarities, although the BLS acknowledges the point-to-point noise outside the transit whereas the MF only uses the data inside the transit to determine the signals significance. Surprisingly even as the BLS uses more information of the light curve to determine the significance, the MF algorithm performs slightly better in the previously mentioned test done by Tingley (2003).

In the noisy data collected with the TEST, both these algorithms show clear disadvantages. As told above the MF is not using the information of the whole light curve but only of the in-transit points, whereas even as the BLS uses some additional information it shows to be counterproductive with the TEST data.

The BLS normalizes the errors inside the transit with the sum of the errors of all bins. Thus It not only emphasizes on small errors inside the transit, but also on large binning errors outside the transit. This is not problematic with data of equally good quality, but for changing photometric quality this can lead to false positives which prevents from detecting real signals. The statistical F-test, comparing the variance of two different sets of data samples, was found to be a much more robust way to estimate the significance of a signal and was therefore implemented in the TEST transit search. I implemented the F-test in combination with the box fitting algorithm as "Box-fitting F-test algorithm" (BFT), in the following way.

The photometric light curve is phase-folded in the wanted frequencies and then binned. The size of the bins can be varied. The value for each bin is calculated using the weighted mean, considering the errors of each original data point. The value  $v_n$  of the  $n$ -th bin including  $k$  data points  $x_i$  with the error  $\sigma_i$  is defined as

$$v_n = \frac{\sum_{i=1}^k \frac{1}{\sigma_i^2} * x_i}{\sum_{i=1}^k \frac{1}{\sigma_i^2}}. \quad (6.6)$$

The error  $e_n$  is defined by the unbiased weighted standard deviation in each bin.

$$e_n = \frac{\sum_{i=1}^k \frac{1}{\sigma_i^2} (x_i - \bar{x})^2}{\sum_{i=1}^k \frac{1}{\sigma_i^2}} \quad (6.7)$$

The distributions of the errors of all the bins gives a first estimate whether a periodic signal is found at this frequency. If the size of a bin is sufficient small compared to to the signal period, the standard deviation inside each bin should be significantly smaller than the overall standard deviation of the light curve. This is due to the fact that in such a small bin of the phase-folded light curve, a signal with this period will not contribute to the standard deviation.

---

<sup>5</sup>For more details on the derivation of these equations see Tingley (2003).

Therefore the error of a bin  $e_n$  should be similar to the standard deviation of the original light curve in case no signal is seen, whereas it would decrease if a signal is present in the phase-folded light curve. The significance of a signal at this period, independent of the signals shape, can therefore be defined as ratio of the mean error of all bins and the standard deviation of the light curve:

$$P = \frac{\sum_{n=1}^l e_n / l}{\sum_{i=1}^m \frac{1}{\sigma_i^2} (x_i - \bar{x})^2 / \sum_{i=1}^m \frac{1}{\sigma_i^2}} \quad (6.8)$$

The number of bins is given by  $l$ , whereas  $m$  is the number of data points in the light curve. A high signal-to-noise ratio therefore results in a low value for  $P$ . This is limited to signals larger than the size of one bin and only possible when the points per bin allow for reliable statistics. Now that the significance of any periodic signal was determined, the focus will be shifted to the box-shape signal as such signals are expected by planetary transit.

In order to search specifically for transit-like signals a box fit is applied to the phase-folded light curve and subtracted from the light curve. The F-test is now defined as the ratio of the standard deviation of the original binned, phase-folded light curve  $\sigma_{Original}$ , and the standard deviation of the light curve after the signal is subtracted  $\sigma_{Subtracted}$ :

$$F = \frac{\sigma_{Original}^2}{\sigma_{Subtracted}^2} \quad (6.9)$$

As the F-test showed to favour stronger sinusoidal signals over low amplitude transit like signals, I modified the F-test to emphasize the box-like shape of a signal. For this the F-statistics is normalized by the previously calculated P-index which gives the significanz of any periodic signal, independent of its shape:

$$F_{final} = \frac{P + \sigma_{Original}^2}{P + \sigma_{Subtracted}^2} \quad (6.10)$$

### Performance of the Transit Detection

The BFT, BLS, and MF algorithms were tested using original TEST light curves superimposed with periodic transit signals (Table 6.1). All these algorithms can be used with a fixed or variable number of bins, in the later case the number of bins is decreased for smaller periods in order to speed up the calculation.

For the test of the algorithms 10,000 randomly selected light curves of the crowded field F2 were superimposed with transit events. The transit depth was randomly selected in a range between 1.0% and 10.0%, the orbital period between 0.8 days and 4 days, and the transit length ranging between half an



**Table 6.1.:** Performance of the Transit Detection Algorithms. TEST light curves have been superimposed with transit signals. In this table the ratio of transits detected by a defined algorithm to all detected transits is shown. Each of the three tested algorithms was used with a static number of bins and with the bin number changed, dependent on the frequency.

Algorithm	constant bin number	variable bin number
uBLS	55.0%	49.5%
mMF	53.5%	49.2%
BFT	58.7%	52.4%

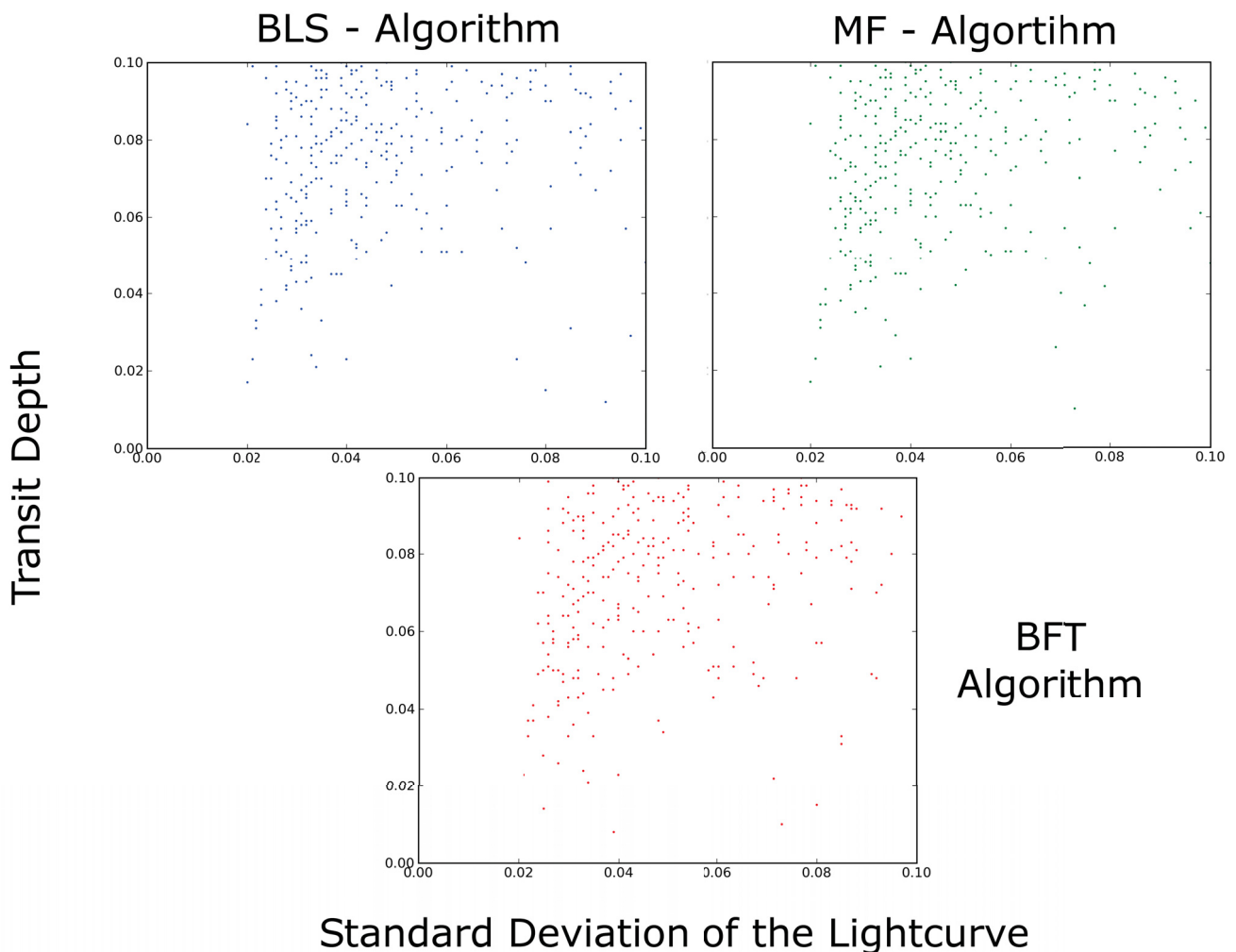


**Figure 6.5.:** Comparison of the detection algorithms. For each of the three detection algorithms the detected stars marked with the transit depth over the standard deviation of the light curve. As can be seen, many of the transits have only have been detected by one or two algorithms. A combination of the different algorithms therefore assures the best detection results.

hour and three hours. Around 11.8% of the created transits have been detected by at least one detection algorithm (Figure 6.5). This low detection rate is caused by the orbital coverage of the light curves, variability in the stellar light curves, and the low brightness of most stars which results in high noise compared to the transit signal. High noise is also introduced by non-optimal photometric conditions.

In comparison with the other algorithms the newly developed BFT algorithm shows slightly better results. But the most important result is that a significant improvement can be achieved, when combining different detection methods. When using only one detection algorithm the detection rate drops from nearly 12% down to ~6%. Combining the Box-Least-Square-fit algorithm and the matched filter algorithm, the detection rate of 8% is still well below the detection rate that can be achieved when including the newly developed BFT algorithm. The TEST data were therefore analysed with all three algorithms.

All the three algorithms (BFT, BLS, MF) used to calculate the significance of a box-like signal can of course be used not only on phase-folded light curves, but also on single night light curves. The single night detection has to be used very cautious, as several effects can mimic a planetary transit. Such false positives can be caused by the instrument (e.g. star wandering over bad pixels) as well as by the star itself (e. g. star spots). Nevertheless, in order to effectively use the few very good observing nights, the single night analysis was also conducted on these data. The many nights with mediocre photometric conditions otherwise prevent the detection of low amplitude signals, that might have been observed in a good night.

## 6.5. Automated Binary Components Identification

Binary stars detected either with the Scargle/CLEAN algorithm or when searching for transit-like events can be analysed further with the “Detached Eclipsing Binary Light curve fitter” (DEBiL) Devor (2005) and the “Method for Eclipsing Component Identification” (MECI) Devor & Charbonneau (2006). A part of the found binaries can thus be categorised in a much more detailed way. DEBiL models light curves of eclipsing binaries and tries to fit these models to the observed data. By iterating the parameters of the components a best fit will be produced. The results of this fit will be used by MECI. In combination with colour information, extracted from catalogues (2MASS) the likeliest set of parameters, like mass, radius, metallicity is determined for both components.



## 7. Classification of Host and Candidate

Observed transit-like events can be induced by different causes. Many of them can be excluded as soon as the signal is periodic, but some, like grazing binaries or background binaries, can only be excluded by measuring the radial velocity. Next to a clear determination whether the observed signal is caused by a planetary transit, radial velocity measurements allow to determine the actual mass of the companion in comparison to its host star. The spectra taken for radial velocity measurements can also be used for spectral classification of the star using stellar models. This allows to properly determine the system and verify the character of the companion. In order to reach the necessary precision to detect hot Jupiters around Sun-like stars, well calibrated spectra with a good signal to noise ratio are needed. Unfortunately, the targets observed with the TEST are too faint to do the follow-up observations with the Échelle spectrograph at the TLS using the Iodine cell (cf. Hatzes et al. (2003)). Therefore, the calibration of the spectra has to be done with spectra of the Thorium Argon lamp, which are to be taken right before and after the observations of the star. For a sufficient signal-to-noise ratio when observing a star fainter than 10th magnitude, an exposure time of one hour is needed. Such long exposure times result in a high contamination of the spectrum with cosmic rays. Therefore, the exposure is split into two exposures, each of 30 minutes. The data are reduced using standard calibration techniques. A bias image correction, as well as a flatfield correction is applied to all observed spectra. Using a spectrum of a bright target, the orders are identified and extracted. To correct the Échelle blaze function superimposing the spectrum, this is fitted in one dimension. Only for the very strong lines, where absorption lines might influence the fit, an interpolation using the neighbouring orders is used. The calibration of the spectral wavelength is done, as mentioned above, using spectra of the Thorium Argon lamp. These calibration spectra have been taken immediately before and after the observation of the target. For the calibration between these two spectra an interpolation is made. In a last step the spectra taken in different nights are corrected for different red shifts caused by the motion of the Solar system and the Earth movement.

### 7.1. Spectral Classification of the Host

For the spectral classification of the host star, a spectrum as good as possible is needed. Therefore all spectra taken of this star are combined. This also helps to get rid of cosmics that still are visible in the single spectrum.

In a next step, spectral lines which are obviously not caused by the star, but by light pollution of the nearby residential areas, have to be corrected. The spectral range of the Tautenburg Échelle spectrograph reaches from about  $4750\text{\AA}$  up to  $7000\text{\AA}$ . For the spectral classification the range including the  $H\alpha$ ,  $H\beta$ , and the metal lines in between, is used. The depth and form of these lines allow us to estimate the metallicity, temperature, and surface gravity of the star. This spectral classification was done by A. Tkachenko using models as described in Lehmann et al. (2010).

## 7.2. Radial Velocity

The radial velocity of the star<sup>1</sup>, needed to determine the cause of the observed transit event, is calculated using the cross-correlation technique. The different spectra are cross-correlated either with the best spectra taken, or with an artificial spectrum calculated when determining the spectral type of the star. The cross-correlation is done for several spectral ranges. The best lines to identify the radial velocity of the star are the metal lines. The centre position of the hydrogen lines can only be determined with large errors, as these two lines ( $H\alpha$ ,  $H\beta$ ) are very broad. Therefore small errors, that might be significant for radial velocity measurements, can easily be introduced when correcting for the Échelle blaze function.

## 7.3. Estimating the Mass and Density of the Candidate

At this point the host star is classified. Especially its radius and mass are known from the stellar models. For a first estimate of the companion parameters, the inclination of the system is assumed to be at  $90^\circ$ . This is a first good estimation as large discrepancies of this value would render the observation of a transit impossible. The photometrically observed transit can be used in a next step to calculate the radius of the companion. The depth of the transit is given by the relation of the radii of the host and its companion.

---

<sup>1</sup>for details on the radial velocity method see e.g. Hatzes (2002), Desort et al. (2007), Chelli (2000)

## 8. CoRoT Satellite Mission

Next to the transit survey, the TEST supported the CoRoT space mission by photometric follow-up observations. The CoRoT space telescope was launched in December 2006. This space mission is led by the French Space Agency (CNES) in cooperation with other national space agencies (like the Deutsches Zentrum für Luft- und Raumfahrt (DLR) in Germany) and the European Space Agency (ESA). The two objectives pursued are the search for transiting exoplanets (Barge et al. (2008)) and the astero-seismic analysis of bright stars (Baglin et al. (2006)). The photometric precision reached with the telescope allows to detect transiting planets down to the size of a super-Earth (cf. CoRoT-7b (Léger et al. (2009), Hatzes et al. (2011))). The CoRoT telescope observes perpendicular to its orbital plane, allowing up to 150 days of continuous observation. Periods found are therefore limited to below 100 days (cf. CoRoT-9b with a period of ~95d (Deeg et al. (2010))). In each field high precision photometry of 12 000 pre-defined stars is taken. To minimize the necessary amount of data to be sent to Earth, the photometry is done on board, and only light curves are transmitted to the ground.

Several effects can mimic a transit-like signal (i.e. background binaries, grazing binaries, etc. see Brown (2003)), therefore follow-up observations are an essential part of this mission. The observation of a single field leads typically to about 50 light curves showing transit-like events. Only a tenth of these candidates stand up to scrutiny. In order to confirm the planetary status of the candidates, three steps are conducted. First a detailed analysis of the light curve and the observed signal is done. Then photometric and spectroscopic follow-up observations will confirm the candidate. Here I will focus on photometric follow-up, as was done with the TEST telescope.

Obviously the photometric precision reached with Earth-bound instruments is much lower than with the CoRoT telescope itself. Nevertheless, photometric follow-up is needed due to the limited spatial resolution of the satellite. The typical Point-Spread-Function (PSF) of CoRoT has a size of  $35'' \times 23''$ . This is caused by a dispersion device included in CoRoT's light path, allowing to get multicolour photometry. On the one hand, this multicolour photometry allows us to get rid of some of the false positives, as a transit event is expected to show similar signals in all colours. On the other hand, the resulting poor spatial resolution brings the problem of additional false alarms due to background binaries, which contribute to the flux inside the PSF of the object of interest.

In order to minimize the telescope time used to verify a planet, such false positives are excluded using photometric follow-up observations. Even for transit events not deep enough to be detected directly by Earth-bound telescopes due to their limited photometric precision, a photometric follow-up allows us to confirm the signal by the observation of the neighbouring weaker stars, and to rule out their contribution to the signal (Deeg et al. (2009)).



**Part III.**

**Results**



## 9. Follow Up of CoRoT Candidates

Starting in 2008 the TEST conducted photometric follow-up observations for the CoRoT satellite mission. As described in Deeg et al. (2009) the common strategy for photometric follow-up, are “on / off observations”. Around ten observations are taken during the transit and before or after the transit occurred. This will not give a complete transit curve, but the observed different magnitude during the transit and outside of the transit will allow to verify on which star the transit event occurred. With telescopes in the one meter regime, such an approach is optimal, as it reduces the needed observing time.

As the targets of the CoRoT mission are quite faint, between 12<sup>th</sup> and 15<sup>th</sup> magnitude, exposure times of the TEST were set to 300 seconds. Taking additional 30 seconds readout time into account, one hour of observation is needed for ten images during transit, as well as one hour after the transit for the off observation. Additionally “off observations” are taken automatically when observing another CoRoT target in the same field.

As it turned out the targets, observable with the TEST, are limited to the bright target stars with strong transiting signals. Therefore only a few targets are in the observing queue of TEST, and due to observational breaks caused by bad weather, time spans of up to a few weeks between the observations during transit and off transit were common. For changes in brightness over such long time scales, it is quite difficult to distinguish between stellar variability and a dimming caused by a transit event. Therefore the strategy was changed in 2010. Now the TEST is trying to observe the whole transit event in one night, if possible. The observation of the target for the duration of the whole night additionally increases the sensitivity of the TEST as the data can be binned to reach a higher signal-to-noise ratio.

As described in Chapter 8, the photometric follow-up is necessary to compensate for the poor spatial resolution of the CoRoT satellite. The TEST spatial resolution is outlined in Chapter 4. Only for contamination sources separated by at least 8 arc seconds conclusions can be made.

In cause of this follow-up eleven different CoRoT fields have been observed (Table 9.1). For five CoRoT candidates the photometric follow-up with the TEST lead to a clear identification of the signal source. For the majority of the observed transit candidates no final conclusions could be drawn using the TEST observations. Nevertheless, one of the candidates for planetary transits observed with the TEST indeed proved to be a planet. CoRoT-11b, a hot-Jupiter in a prograde orbit around a F-type dwarf star is one of the most massive planets known so far. Here I present selected results of the TEST CoRoT follow-up.

**Table 9.1.:** Observations done with the TEST in course of the CoRoT photometric follow-up.

CoRoT Field	Observing Nights (All / Good)	hours of observation (All / Good)	conclusive results
IRo1	2 / 1	3.8 / 2.4	0
LRa01	5 / 3	8.3 / 5.2	0
LRa03	1 / 1	0.9 / 0.8	0
LRc01	8 / 5	15.1 / 10.5	2
LRc02	9 / 6	15.5 / 8.2	2
LRc03	15 / 12	17.4 / 11.9	0
LRc04	1 / 1	1.7 / 1.6	0
SRA01	2 / 1	1.6 / 0.3	0
SRA02	1 / 1	2.4 / 2.1	0
SRc01	10 / 2	14.7 / 3.7	0
SRc02	20 / 9	29.5 / 12.8	1
+			

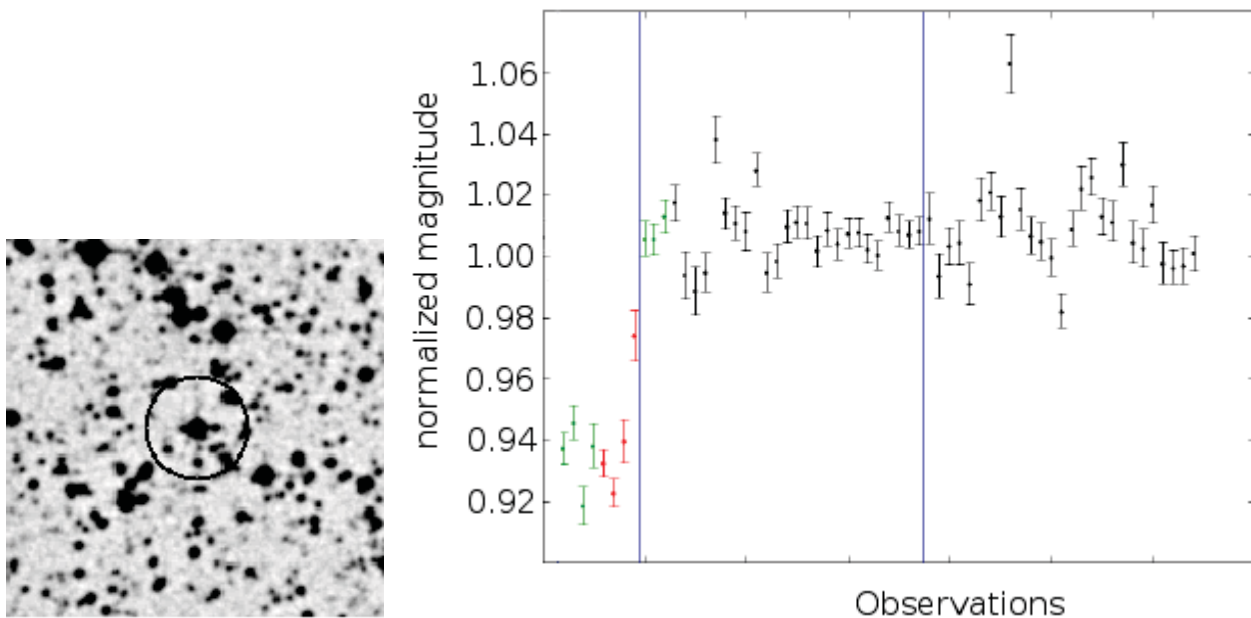


**Figure 9.1.:** CoRoT - Object LRc01\_E1\_0499. On the left the finding chart is plotted. Several nearby sources can be seen. The right graph shows the light curve as taken with the TEST. All observations plotted directly next to each other ordered by the observing date, the vertical blue lines mark the separation between different observing nights. The red dots show the values calculated to be in transit (“on”) whereas the green dots show the expected ingress or egress. The black dots show the comparison data when no transit is happening (“off”).



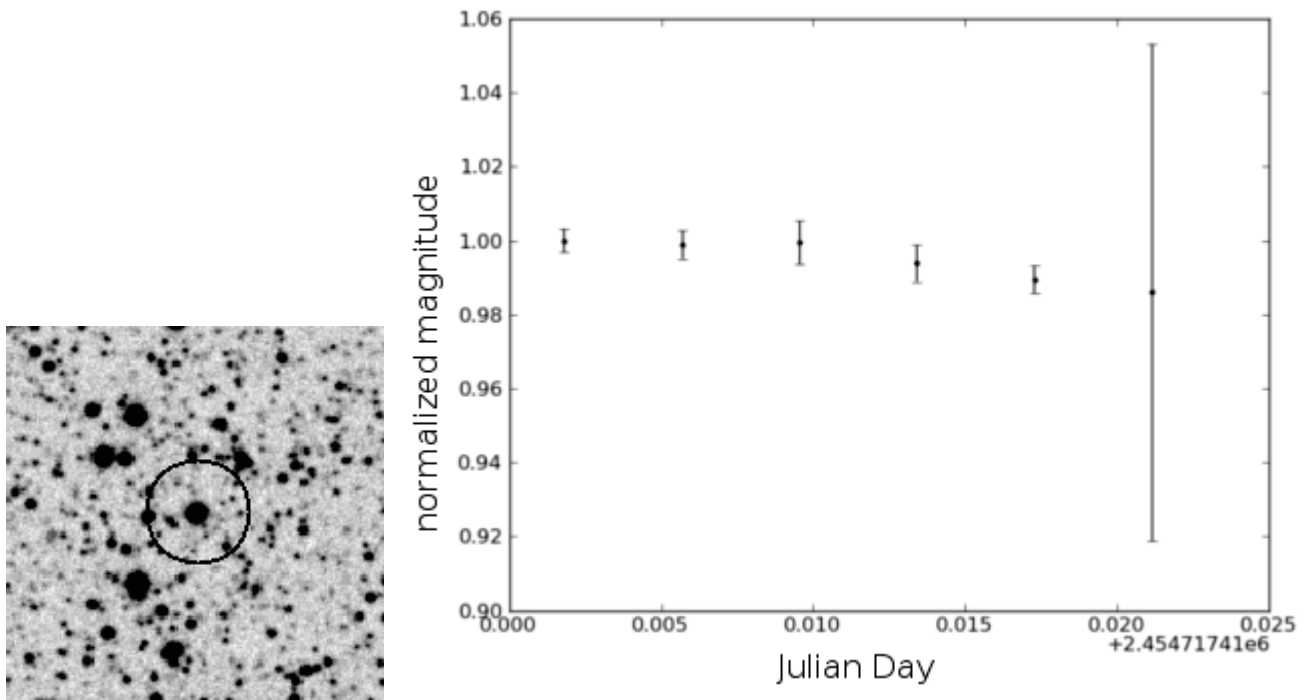


**Figure 9.2.:** CoRoT - Object LRc02\_E1\_0202. On the left the finding chart is plotted. The right graph shows the light curve as taken with the TEST. A slight decrease in brightness can be seen in the light curve, which was not observed in any neighbouring star.

### 9.1. LRc01\_E1\_0499

The period observed for the CoRoT candidate LRc01\_E1\_0499 is 4.86 days, the transit depth is given with 5.5%, the transit duration including ingress and egress takes 4.8 hours. The target has a brightness of 13.3 magnitudes. In a radius of 23 arc seconds around the target nine stars are listed in the 2MASS catalogue. The eight possible contamination sources are between two and four magnitudes fainter than the target star.

I observed the candidate LRc01\_E1\_0499 on three different nights. The transit event was observed in the night of the 14<sup>th</sup> of August 2010. The following observing nights were five and ten days later. The transit event is clearly visible on the target object, although a slight shift in the transit time seems to be apparent. One of the neighbouring objects is only separated by seven arc seconds from the target star. This object could not be excluded from contributing to the transit signal by TEST observations.

These results were confirmed by independent observations at the the Instituto de Astrofísica de Canarias (IAC). For final results of the state of the candidate further radial velocity follow-up needs to be conducted.

### 9.2. LRc02\_E1\_0202 = CoRoT 11b

CoRoT-11b is a "hot Jupiter" planet detected with the CoRoT satellite (Gandolfi et al. (2010)). The period of the transit signal, found in the photometric data is  $2.994329 \pm 0.000011$  days. The transit depth is

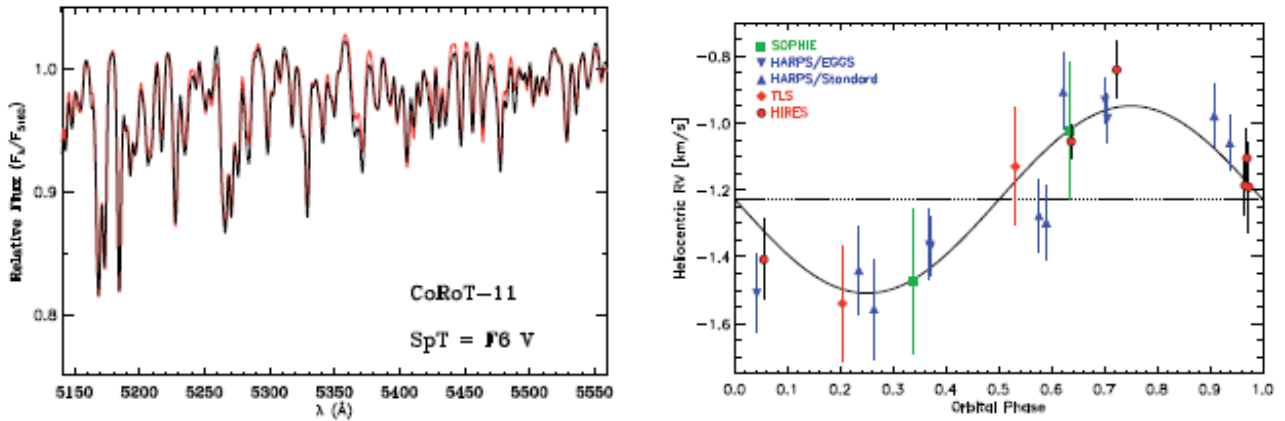


**Figure 9.3.:** Left: Part of the low resolution spectrum of CoRoT-11 taken at the TLS (black). The red line is the best fitting F6 V template. Right: Phase-folded radial velocity measurements of CoRoT-11b, and the best fit to the data.

given with 0.92%, the transit length is about 2.4 hours. The target has a brightness of 12.9 magnitudes. I observed the object with the TEST on several nights. All but one night were observed off transit. During one night the ingress of the object was observed with the TEST (Figure 9.2, right). The ingress is clearly visible in the TEST data. With these data, the possible sources of the transit were limited to two possible sources. All other contaminations inside the CoRoT photometric aperture were excluded. The 2MASS catalogue list three neighbouring stars with a distance less than 23 arc seconds to the target object (Figure 9.2, left), all of which could have caused the observed signal. In addition one neighbouring object separated by only 2 arc seconds is listed in the CoRoT Exodat database, this object could not be excluded with the TEST as the spatial resolution is not sufficient. This nearby object was excluded with measurements at the IAC, done by collaborators.

By analysing the spectra, the host star was confirmed to be a fast rotating F6-dwarf (Figure 9.3 (left); see Gandolfi et al. (2010)). Radial velocity measurements by the CoRoT team lead to the conclusion that this candidate indeed is a hot-Jupiter orbiting its star. The planet is one of the most massive exoplanets detected so far ( $M_p = 2.33 \pm 0.34$ ). The large error in the mass determination is caused by the fast rotation of the host star ( $v \sin i = 40 \pm 5 \text{ km/s}$ ). The rotation of the host star causes a broadening of the spectral lines, which decreases the accuracy in the determination of line position and therefore results in large errors when measuring the radial velocity. For this planet, 20 radial velocity measurements were needed to determine the mass with an error of 15% (Figure 9.3 (right)). CoRoT-11b is one of four planets known so far orbiting a rapidly rotating star. This small number is caused by the observational bias introduced with the radial velocity measurements. As this bias limits our detection abilities to late type solar like stars, our understanding of planetary evolution around more active and fast rotating stars is very limited. The detection of such planets around fast rotating stars ( $v \sin i > 10 \text{ km/s}^{-1}$ ) will broaden our parameter space in testing planet evolution models.

CoRoT-11b is one of the quite few very massive "hot Jupiters". Most of the "hot Jupiters" observed so far show masses well below two Jupiter masses. This cannot be explained with an observational bias, as the transit and the radial velocity method both would favour large high mass planets on close-in orbits. The quite low density of CoRoT-11b can be explained with a planetary model for an inflated hydrogen-gas-planet. This assumption was used to model the age of the planetary system. The most probable age is  $2.0 \pm 1.0 \text{ Gyr}$ .

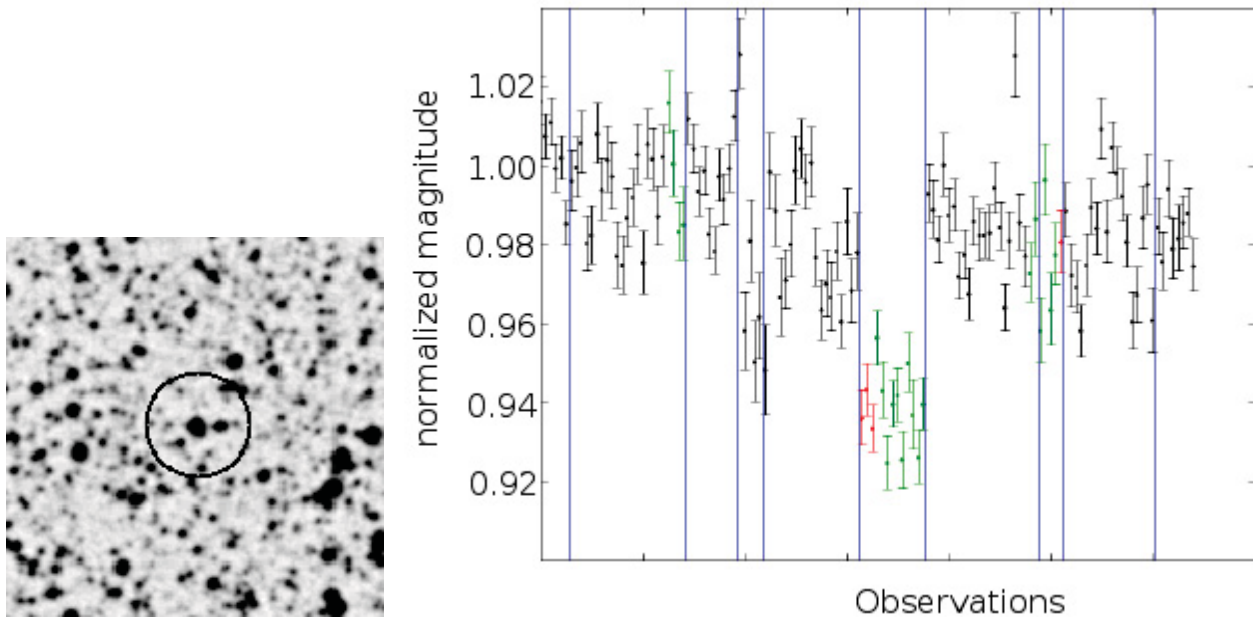


**Figure 9.4.:** CoRoT - Object SRc02\_E2\_1160. On the left the finding chart is plotted. The red marked objects are possible contamination sources. The right graph shows the light curve as taken with the TEST.

### 9.3. SRc02\_E2\_1160

The period observed for the CoRoT candidate SRc02\_E2\_1160 is 3.29 days, the transit depth is given with 4.0%, the transit length is about 4.1 hours. The target has a brightness of 13.2 magnitudes. I observed the object on ten nights. The transit event was observed in two nights, although only in one night a clear signal could be detected. This might be caused by errors in the period. The observations were conducted between the 24th of August 2009 and the 15th September of 2010. The transit event was observed on the 3rd July 2010.

The 2MASS catalogue lists up to ten possible contamination sources in a distance below 25 arc seconds. Only one of which is nearer the ten arc seconds to the target object, and can therefore not be separated by the TEST. The follow-up observations for this object are still ongoing as no final conclusions could be drawn.

### 9.4. Conclusion

Only for a small sample of CoRoT targets the needed precision can be reached to directly detect a transit event with the TEST. Using exposure times of 300 seconds, the magnitude range for possible follow-up measurements is limited to stars between 12.5 and 13.5 magnitudes. For fainter stars follow-up measurements using the TEST are nearly impossible. For brighter targets, shorter exposure times are possible. However, only a few CoRoT targets are brighter than 12th magnitude.

Even as the spatial resolution of the TEST is not always high enough to exclude all contamination sources, it can help to identify the most promising candidates for follow-up using larger telescopes, for example at the IAC.



## 10. TEST Candidates

In the course of the transit survey, three selected fields have been observed with the TEST. Two of these fields,  $F_2$  and  $F_{15}$  were previously observed with the *Berlin Exoplanet Search Telescope* (BEST) when it was stationed in Tautenburg (2002/2003) (Voss (2006), Rauer et al. (2004), Pasternacki et al. (2011)). These two fields have been selected for observation to allow for an increased orbital coverage by combining the datasets of the BEST and the TEST. Next to the two BEST fields another crowded field,  $P_1$  was selected for transit search observations. The field  $F_2$  was observed with highest priority, followed by  $F_{15}$  and field  $P_1$  with the lowest priority. In Table 10.1 the coordinates of the fields, as well as the observations conducted with the TEST in the years 2008 and 2009, are listed.

The exposure time for all fields was set to 120 seconds. Whereas shorter exposure times would have allowed us to observe brighter targets, which would be easier to follow-up, longer exposure times increase the number of observed stars, therefore increase the chance to find a transit. The exposure time of 120 seconds balances these two arguments.

The TEST transit survey led to the detection of seven candidates showing transit-like signals. For each candidate the VizieR database of astronomical catalogues (Ochsenbein et al. (2000)) was used to extract colour information of the candidate. In all cases J-, H- and K-magnitudes of the 2MASS catalogue (Cutri et al. (2003)) were identified. In addition for most cases B-, V-, and R-magnitudes could be found, unfortunately only with large errors. I used the colour information for a first stellar fit, applying the fitting tool by Robitaille et al. (2007). Although this tool is mainly designed for young stellar objects, it also allows to fit general stellar models computed by the ATLAS program of Kurucz (1970). This fit of a stellar model can be used only as a first estimate for stellar classification, for more reliable informations, a complete spectrum needs to be analysed. But even a first estimate can help to decide whether a candidate should be analysed further or whether the signal is probably not caused by a transiting planet.

**Table 10.1.:** *Fields observed in the course of the transit survey.  $F_2$  and  $F_{15}$  are fields previously observed with the BEST, whereas  $P_1$  is a newly selected field.*

Field Name	RA	DEC	Observing Nights (All / Good)	Observing Hours (All / Good)	Stars with $\sigma < 0.03$
$F_2$	02:40:00	+52:00:00	106 / 71	230 / 145	157
$F_{15}$	20:00:00	+48:00:00	93 / 73	152 / 100	505
$P_1$	06:00:00	+40:00:00	64 / 53	98 / 73	567

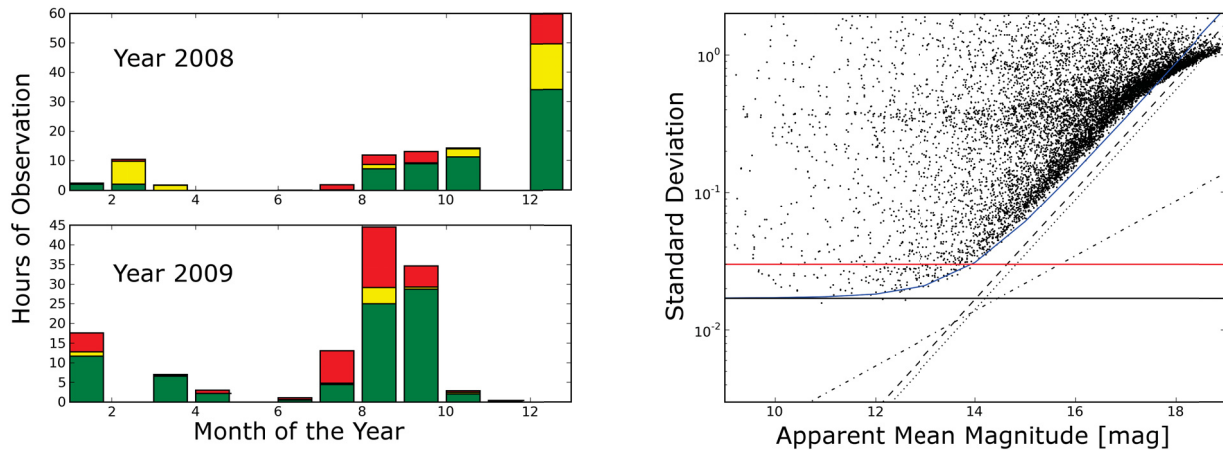


**Figure 10.1:** The observed field  $F_2$ , left the observing hours, coloured depending on the quality of the images. red: No astrometry possible as no stars at all or not enough stars are visible (also due to jumps of the mount). yellow: images of bad photometric quality, identified during the noise reduction step in light curve analysis. green: Actual images used in the final light curves. In the right figure the Standard deviation of all light curves is shown.

## 10.1. Candidates Field $F_2$

The field  $F_2$  is one of two BEST fields (Voss (2006), Pasternacki et al. (2011)) observed with the TEST. It is a crowded field near the Galactic plane. This field was observed with the TEST in the years of 2008 and 2009 during 106 nights<sup>1</sup> for over 230 hours (Figure 10.1 (left)).

As changing weather conditions as well as influences due to the Moon phases result in changing precision reached with the TEST, not all these observations could be used for transit search. In Figure 10.1 (left), the observed hours with bad photometric conditions are marked in red, whereas *good* observations are shown in green colour. Using only the observations marked in green, 157 light curves show a standard deviation below three percent, and 444 stars show a standard deviation below five percent (Figure 10.1 (right)).

The goodness of an observing night is determined by the number of stars showing a standard deviation lower than three percent in their light curve. For all nights the standard deviation of each light curve is calculated and the number of stars displaying such low standard deviation are counted (Figure 10.2). Observing nights displaying a high standard deviation in the light curves due to weather conditions or Moon-phase are deselected and not used in following analysis steps. Additionally, observing nights with observing time below 30 minutes were also deselected. Only during ten nights continuous observations of more than four hours have been conducted, thus making it difficult to observe a complete transit event.

When selecting nights for analysis two factors have to be recognised. On the one hand a higher number of observations increases the chance of observing a transit due to a higher orbital coverage. On the other hand, observations of bad quality might decrease the signal-to-noise ratio and therefore reduce the

<sup>1</sup>This only refers to nights where the field was observed at least half an hour.



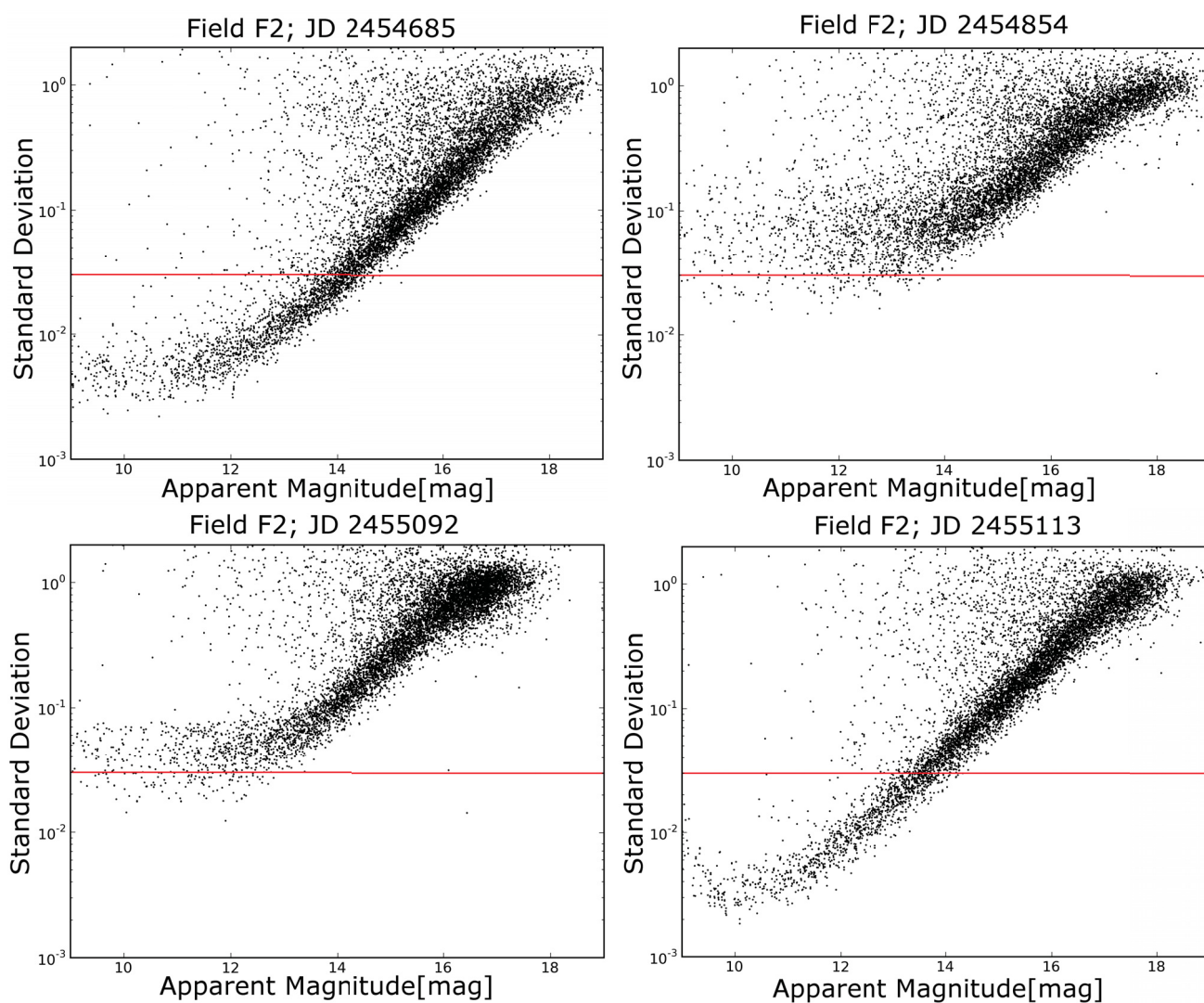


**Figure 10.2.:** The standard deviation of all light curves in field F2 for four different nights, representing the different photometric qualities of observing nights. The red line displays a standard deviation of three percent. A night was selected for further analysis, if over 750 stars show a standard deviation below this red line.

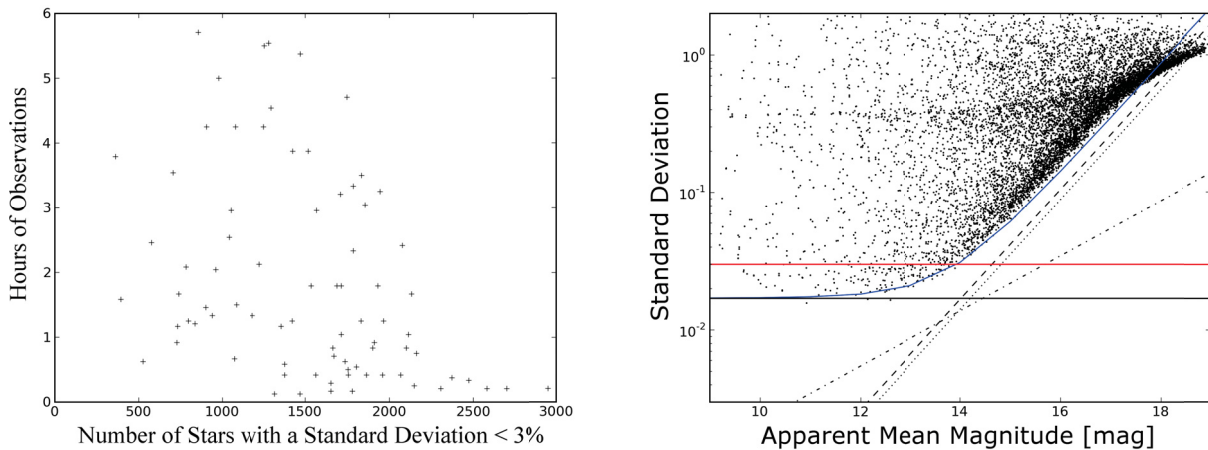


**Figure 10.3.:** Observations of field F2. For each night the photometric quality is evaluated based on the number of light curves below a standard deviation of three percent. The Y-axis displays the observing time for each night in hours. Observing nights with less than half an hour of observations were not used in the final search for transit events. In the right graph the Standard deviation for all light curves is shown. The different blueish straight lines represent the different noises, like photon noise and scintillation.

**Table 10.2.:** Parameters of the binary system F2\_7259

TEST-ID	RA	DEC	B-mag	V-mag	R-mag	J-mag	H-mag	K-mag
F2_07259	02:40:51.5	+52:45:06.6	12.5	12.2	11.9	10.77	10.62	10.56

chance to detect a periodic signal hidden by the noise of bad observing nights. The orbital coverage for both, all observations and only the used ones is shown in Figure 10.3 (right). For the final data analysis 165 of the conducted 230 observing hours distributed over 80 nights were used.

### Candidate F2\_7259

One transit event of the candidate F2\_7259 was previously observed with the BEST (Voss (2006)). Although a second partial drop was observed, no period could be determined at this point. In the TEST data a clear period of  $\sim 1.35$  days was found (Figure 10.4). Four single transit events have been observed with the TEST. The combination of these events gives a best fit with a transit depth of 3.5% (Figure 10.5).

The colour information found in catalogues is given in Table 10.2. A stellar model was fit to the colour information (Figure 10.6). The best fit used a stellar model with an effective temperature of 7750 K, a surface gravity (logg) of 4.5, and a metallicity ( $\text{Log}[Z/H]$ ) of 0.5. The primary would thus be a main-sequence star of a spectral type between F0 and A8.

In 2010 follow-up observations were made using the Échelle spectrograph of the 2-m Tautenburg telescope. Seven spectra of 30 minutes exposure were taken to determine accurate stellar parameters as well as the mass of the companion. These seven spectra were combined and for this combined spectrum a stellar classification was done by A. Tkachenko as described in Lehmann et al. (2010) (Figure 10.7). The spectral analysis allowed to determine the spectral type of the primary object to be a rapidly rotating A0 subgiant.



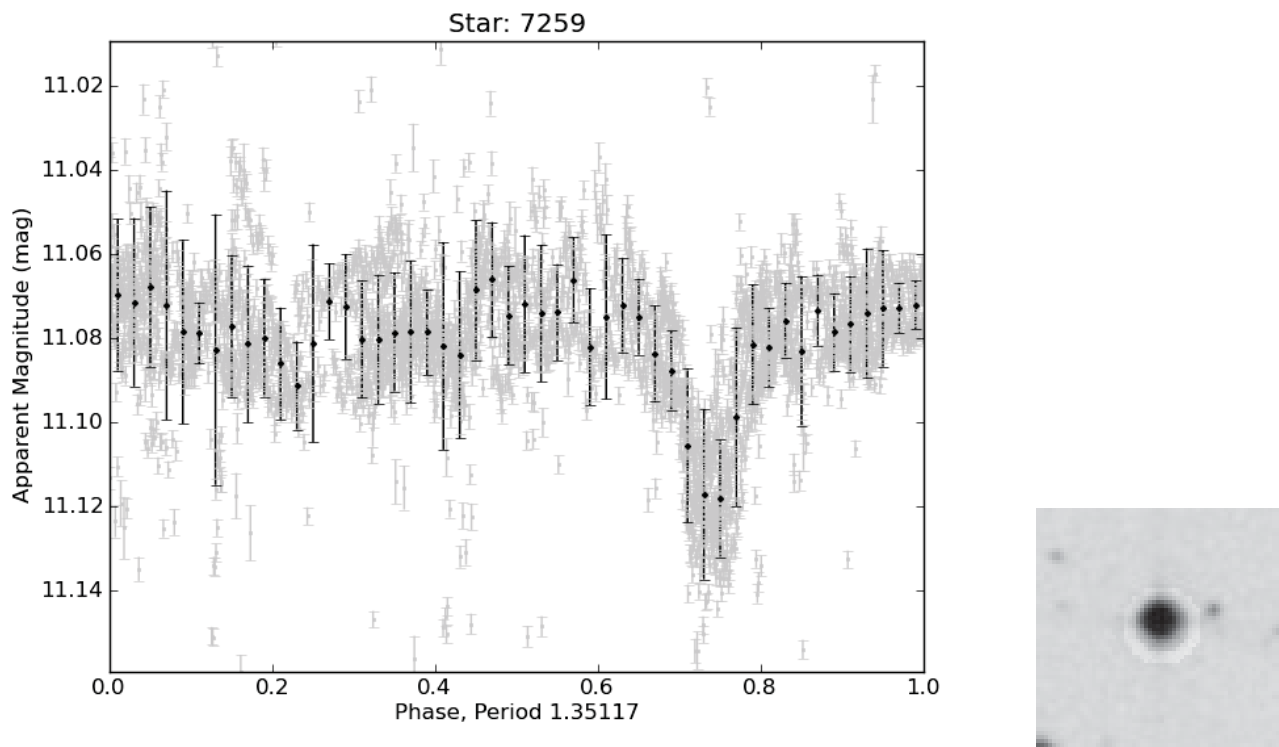


**Figure 10.4.:** The phase folded lightcurve of Candidate F2\_7259 (left) and the finding chart (right).

The radial velocity measurements show a clear signal caused by the companion (Figure 10.8). The amplitude of the radial velocity curve is  $\sim 25$  km/s. Combining the information of the transit and the radial velocity measurements, as well as the stellar classification of the primary, the companion is clearly a M-dwarf with a radius of 0.27 solar radii and a mass of 0.21 solar mass (Table 10.3). Only around a few dozen M-dwarfs in eclipsing systems are known so far. Only twelve of them have a mass below 0.4 solar masses (Figure 10.9 Irwin et al. (2009)). The mass-radius relation determined for the dwarf star shows a lower density than expected (Figure 10.9). As this is the only parameterized M-dwarf eclipsing a subgiant primary object, final conclusions cannot yet be made. But it is clear that the stellar evolution in this system, although it is a detached binary system, differs significantly from systems known so far. As the mass and radius of the dwarf is deduced from the mass and radius of the subgiant, it is at this point not possible to say whether the observed deviation from stellar evolution models results from the subgiant or the M-dwarf. Further observations of such detached eclipsing systems may be used to increase our understanding of the stellar evolution. This is needed not only for stellar physics, but also for the interpretation of observed planetary transits. Large uncertainties of planetary radius and mass are at the moment caused by insufficient knowledge of the physical parameters of the host star.

### Candidate F2\_35765

For object F2\_35765 colour information in six bands is available (Table 10.4). In the catalogues no contamination source (background binary) was found. Only one complete transit event was observed. No period was found so far. The shape, as well as the very low depth of only one percent, make this a promising candidate for further photometric observations (Figure 10.10). Unfortunately, the colour information from the catalogues suggest the host star to be a K-giant with an effective temperature of

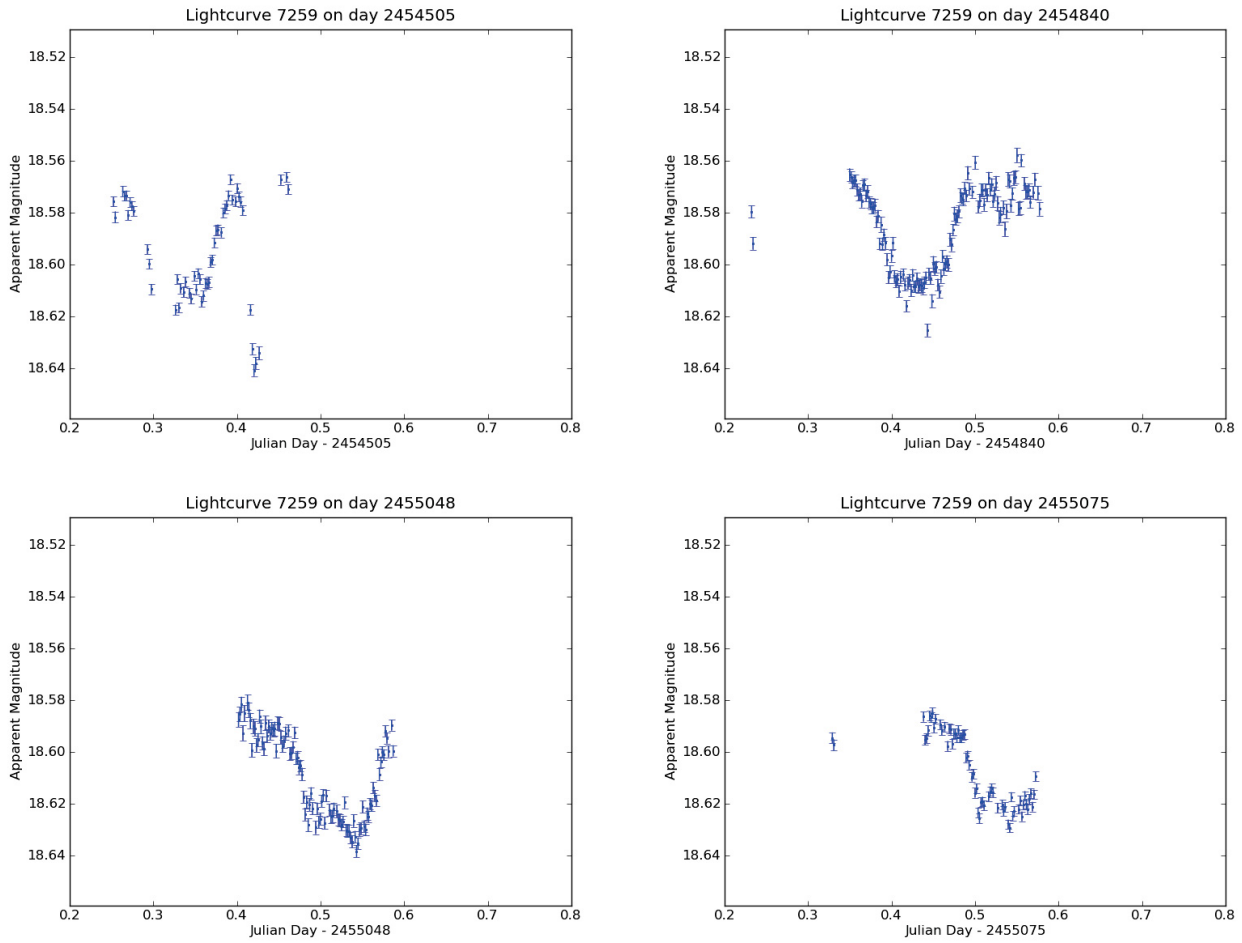


Figure 10.5.: Four single transit events of the candidate F2\_7259, as observed with the TEST.

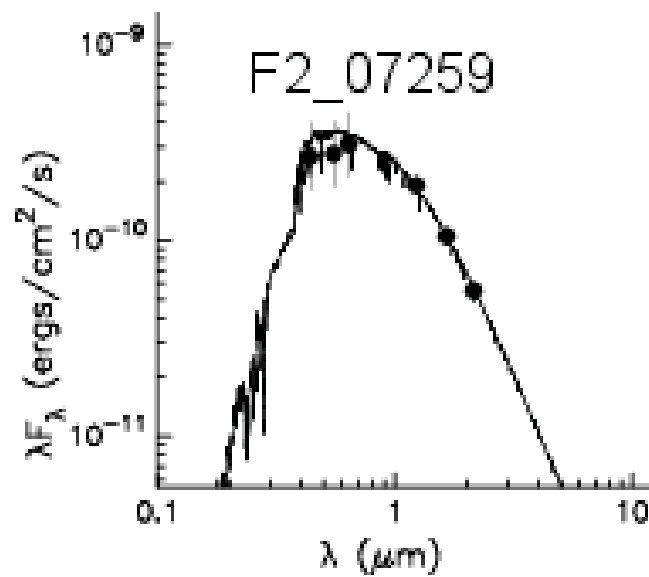


Figure 10.6.: The spectral fit of Candidate F2\_7259 (black line) to the data points as found in the catalogues (dots).

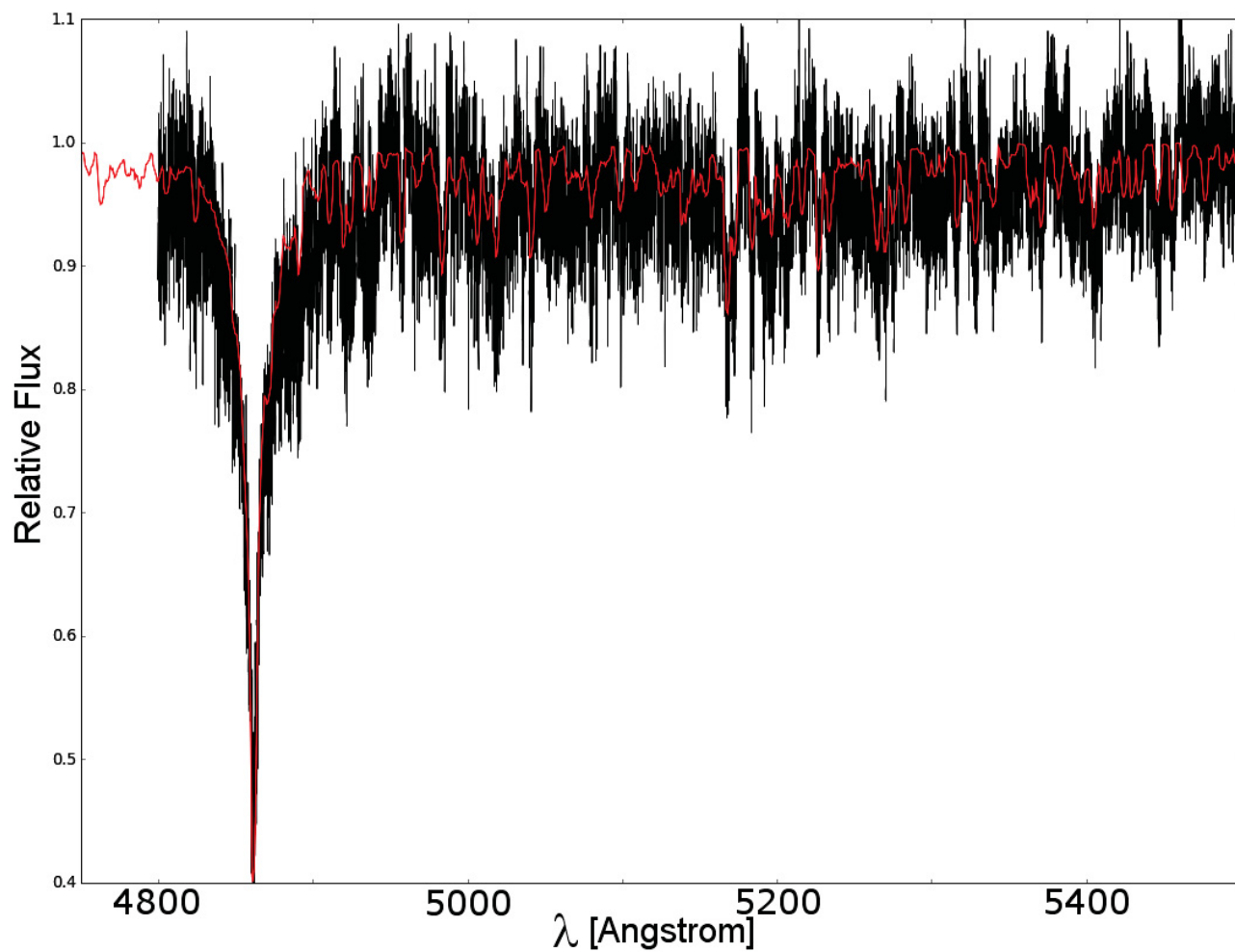


Figure 10.7.: The spectrum of Candidate F2\_7259 (black) and the best fit (red).

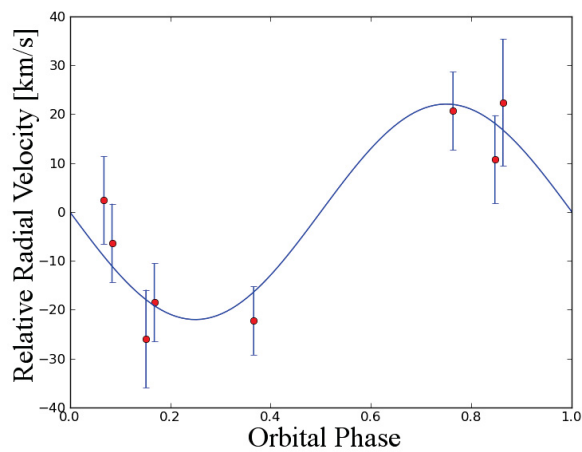


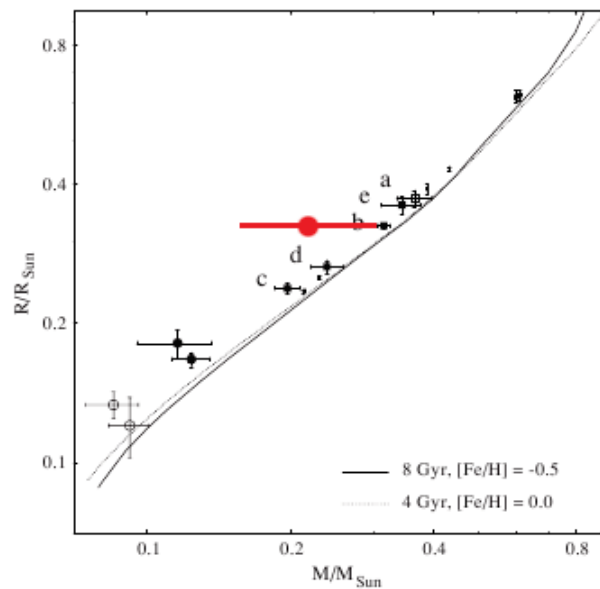
Figure 10.8.: The radial velocity measurements of Candidate F2\_7259, and the best orbital solution.

**Table 10.3.:** Parameters of the binary system F2\_7259

Primary	
Effective Temperature	$7245 \pm 125$
Logg	$3.43 \pm 0.2$
Log[Z/H]	$0.38 \pm 0.1$
Rotation	$116 \pm 15$
Mass	$1.98 \pm 0.18 M_{sol}$
Radius	$2.45 \pm 0.3 R_{sol}$
Spectral Type	Subgiant (III.7) A9.5

Secondary	
Effective Temperature	4000
Mass	$0.21 \pm 0.05 M_{sol}$
Radius	$0.27 \pm 0.02 R_{sol}$



**Figure 10.9.:** Candidate F2\_7259 - Mass-Radius diagram. The diagram is taken from Fernandez et al. (2009). The red dot shows the Candidate F2\_7259. The error bar is quite large due to the poor radial velocity measurements.

**Table 10.4.:** Parameters of the binary system F2\_35765

TEST-ID	RA	DEC	B-mag	V-mag	R-mag	J-mag	H-mag	K-mag
F2_35765	02:40:17.0	+51:25:17.1	12.6	11.7	11.1	8.79	7.84	7.61

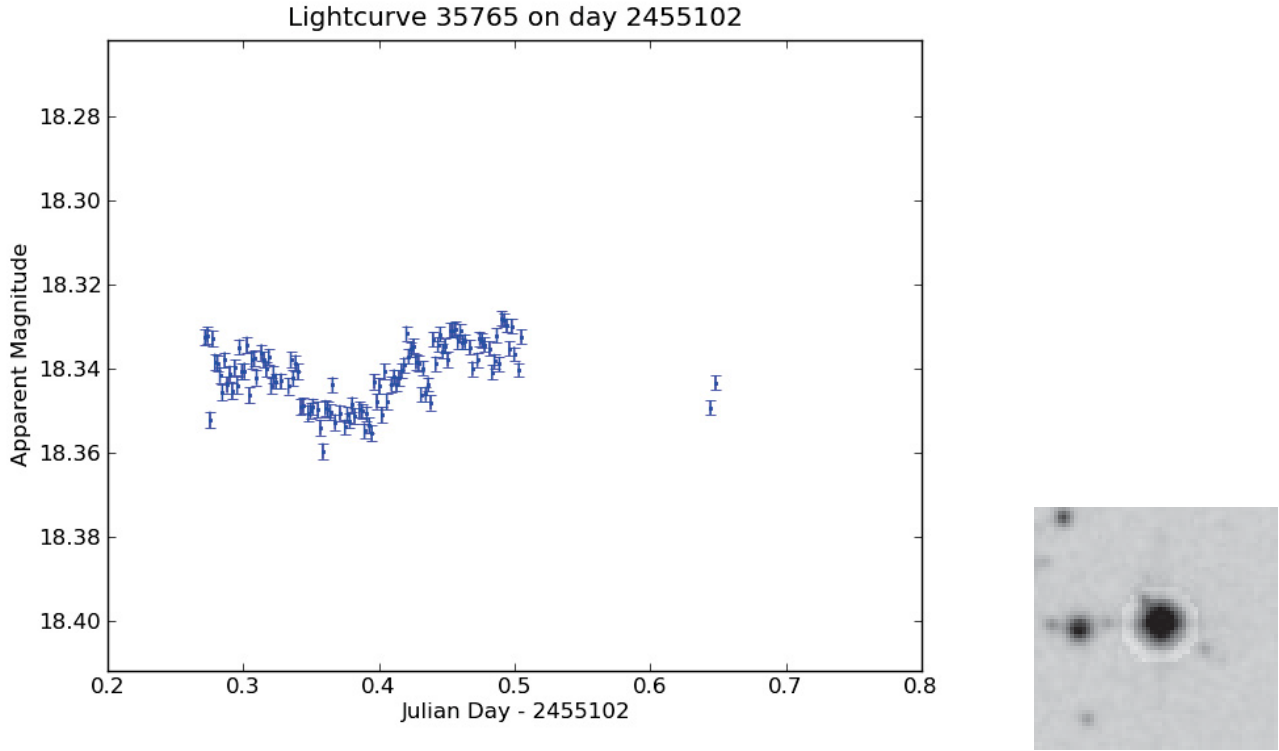


**Figure 10.10.:** The transit event of Candidate F2\_35765 (left) and the finding chart (right).

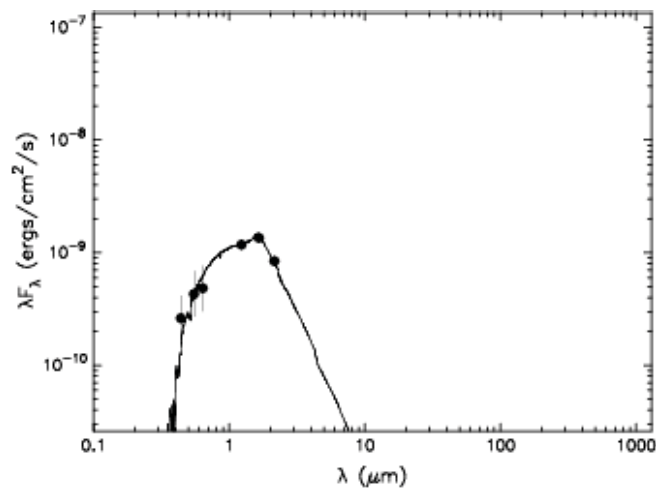


**Figure 10.11.:** The stellar fit for Candidate F2\_35765.

4000 K and a surface gravity of 2.0(Figure 10.11). This first estimate on the stellar classification renders a planetary transit as cause of the observed signal unlikely, instead it seems to be a binary system.

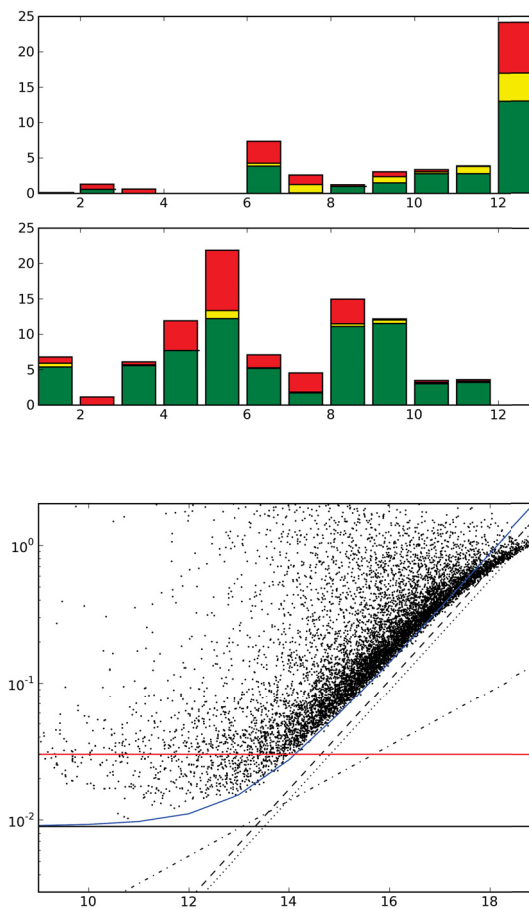


**Figure 10.12.:** Observations of the field F15, taken with the TEST. On the left, the observing hours per month are shown, where red displays not usable observations, yellow displays observations, deselected to increase the overall photometric accuracy, and green shows the analysed observations. The graph on the right shows the standard deviation of all light curves reached in these 100 hours.

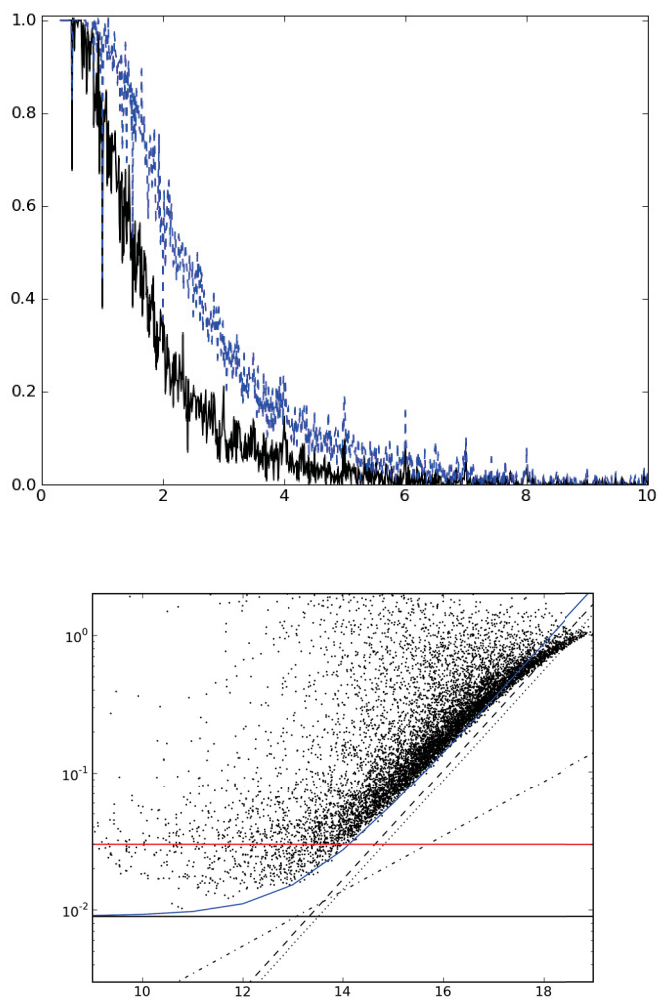
## 10.2. Candidates Field F15

The field F15 is the second BEST field (Voss (2006)) monitored with the TEST. The field is a crowded field near the Galactic plane. It has been observed during 93 nights. 73 of them show a sufficient photometric precision, giving 100 hours of observation (Figure 10.12 (left)). In this 100 hours of observation over 500 stars show in their light curves a standard deviation below 3 percent (Figure 10.12 (right)).

Included in these 100 hours of observations, only 11 nights with continuous observations longer than four hours were made (Figure 10.13 (left)). The observation of a complete transit, therefore is nearly impossible. The orbital coverage allows to detect transits with periods up to 3 days with a probability of 12% (Figure 10.13 (right)).

### Candidate F15\_33633

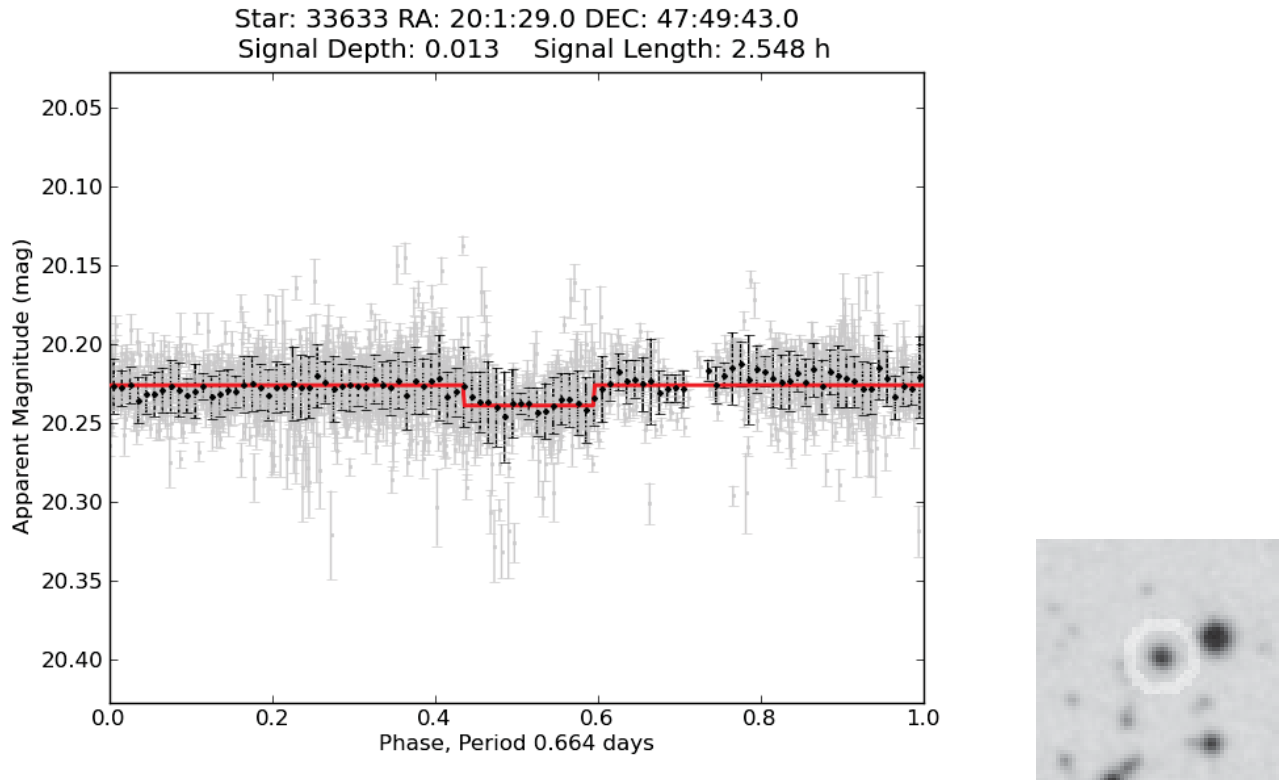
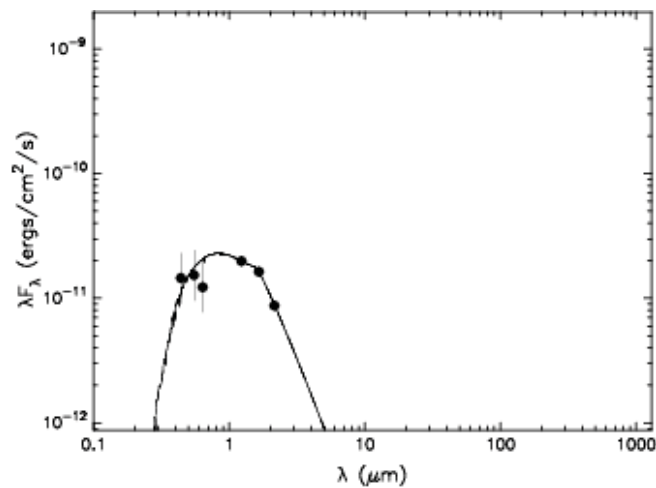
Candidate F15\_33633 shows a signal with a period of 0.664 days (10.14). In close proximity to the candidate, but well outside the aperture, a bright star is present. This star was excluded as source of the



**Figure 10.13.:** *This Figure shows the orbital coverage of the field F15. The blue dashed line displays the orbital coverage, reached when using all observations, the black continuous line shows the orbital coverage using only the “good” observations.*

**Table 10.5.:** Parameters of the binary system F15\_33633

TEST-ID	RA	DEC	B-mag	V-mag	R-mag	J-mag	H-mag	K-mag
F15_33633	20:01:29.0	+47:49:43.5	15.7	15.3	15.1	13.22	12.63	12.56

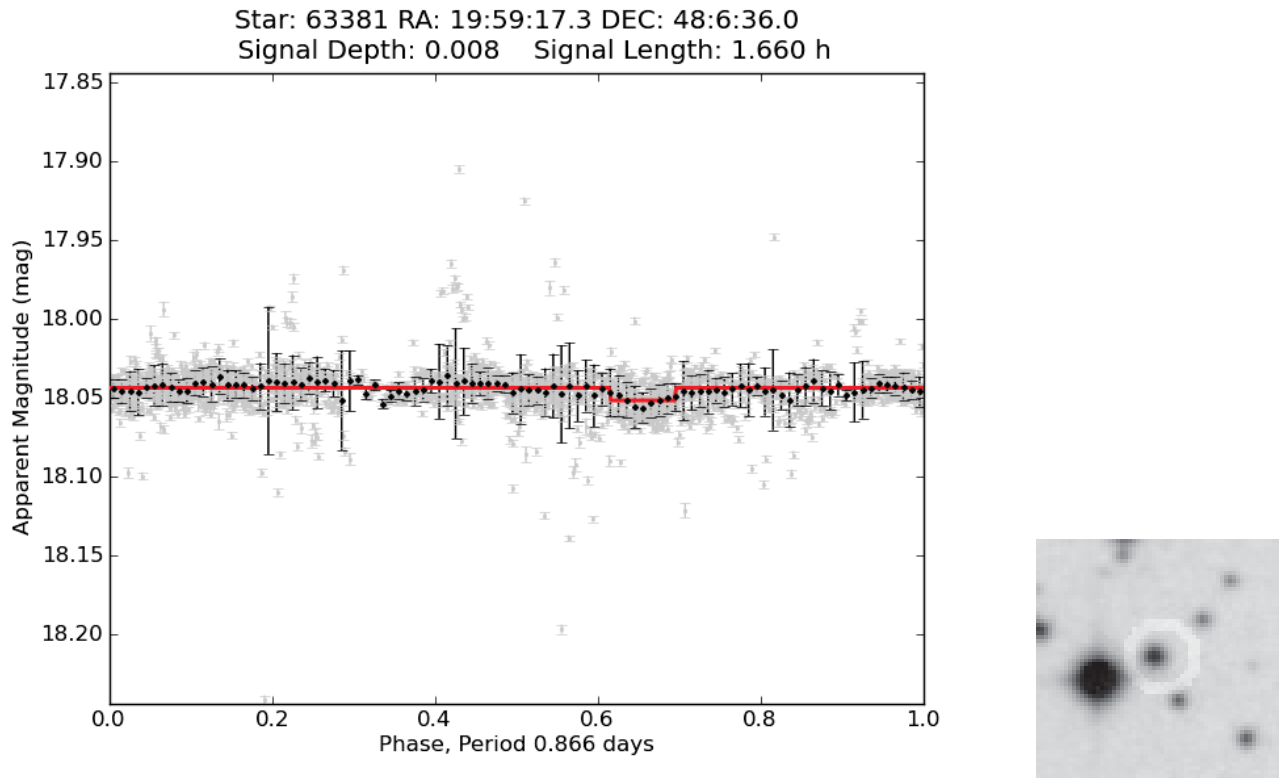
**Figure 10.14.:** The phase folded lightcurve of Candidate F15\_33633 (left) and the finding chart (right).**Figure 10.15.:** Fit of stellar models to the colour information of candidate F15\_33633.

signal. Colour information, as given in Table 10.5, allows to estimate the host star to be a K-subgiant, with a temperature of 5000K and a  $\log g$  of 2.0 (Figure 10.15). The transit depth of 1.5% can therefore only be caused by stellar objects of the M-dwarf class. Further investigations of this faint object therefore have not been committed.



**Table 10.6.:** Parameters of the binary system F15\_63381

TEST-ID	RA	DEC	B-mag	V-mag	R-mag	J-mag	H-mag	K-mag
F15_63381 (1)	19:59:17.3	+48:06:36.7	14.9	15.2	14.5	13.22	12.68	12.52
F15_63381 (2)	19:59:17.5	+48:06:35.5	15.2		14.5			

**Figure 10.16.:** The phase folded lightcurve of Candidate F15\_63381 (left) and the finding chart (right).

### Candidate F15\_63381

In the light curve of candidate F15\_63381 a transiting signal with a period of 0.866 days was detected (Figure 10.16). Although in the finding chart no contamination source inside the aperture is visible, two stars, separated only by one arc second are listed in the USNO-B1 catalogue (Monet et al. (2003)). In the 2MASS catalogue only one source is identified. The colour information therefore might be influenced by two sources and thus not allow for stellar classification. Nevertheless the colours as given in Table 10.6 were used for a stellar fit (Figure 10.17). Taking this stellar model the object F15\_63381 is a K-Main-Sequence star with a temperature of 4500K and a logg of 4.0. This supports the planet hypothesis for the companion.

For a detailed study, this object would need to be observed in more detail, unfortunately with a brightness of 15.2 magnitudes spectral analysis is not possible with the 2-m telescope.

### Candidate F15\_7387

The 2MASS catalogue lists two objects well inside the aperture of this candidate (Table 10.7). With the given colour information stellar model were fitted to the observed data. The best Kurucz model suggests

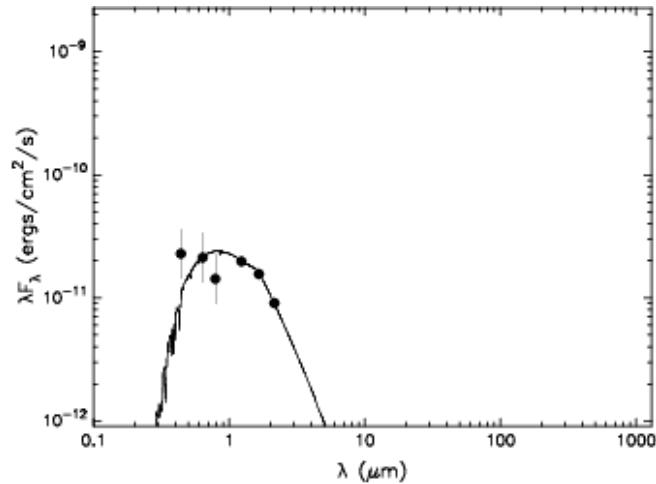


**Figure 10.17.:** Fit of a stellar model to the catalog colour informations of candidate F15\_63381.

**Table 10.7.:** Parameters of the binary system F15\_7387

TEST-ID	RA	DEC	B-mag	V-mag	R-mag	J-mag	H-mag	K-mag
F15_7387 (1)	19:55:36.2	+48:42:58.0	13.2	12.0		11.44	11.15	11.10
F15_7387 (2)	19:55:36.3	+48:42:51.6	12.8	13.1		13.18	12.96	12.88

for the object F15\_7387 (1) a effective temperature of 6000K and a logg of 2.0, which would present a FII star (see Figure 10.19). The second object is fitted best with a stellar model of an effective temperature of 6750K and a logg of 0.5. These parameters are well outside what can be plausible explained by standard models, suggesting a young stellar object (Figure 10.20). For this candidate no final conclusion can be drawn. If the signal is caused by a companion around F15\_7387 (1), this could be an exoplanet.

### 10.3. Candidates Field P1

The field P1 was not previously observed with the BEST. Variable stars found in this field have been compared with published data as found in different catalogues, especially the GCVS (Samus et al. (2004)). The P1 field has been observed in over 50 nights, 38 of which show a sufficient photometric precision. The data merged into light curves used observations of over 72 hours of observations. The precision of the data and the orbital coverage reached for the P1 field is shown in Figure 10.21. Information about this field can be found in Table 10.1.

#### Candidate P1\_10221

The colour information for object P1\_10221 as given in Table 10.8 leads to a stellar fit, suggesting an effective temperature of 7000K and a logg of only 0.5. That value would be well beyond supergiants. Instead it might be a young stellar object. As this object is also very faint, follow-up observations are not possible with the 2-m telescope in Tautenburg.

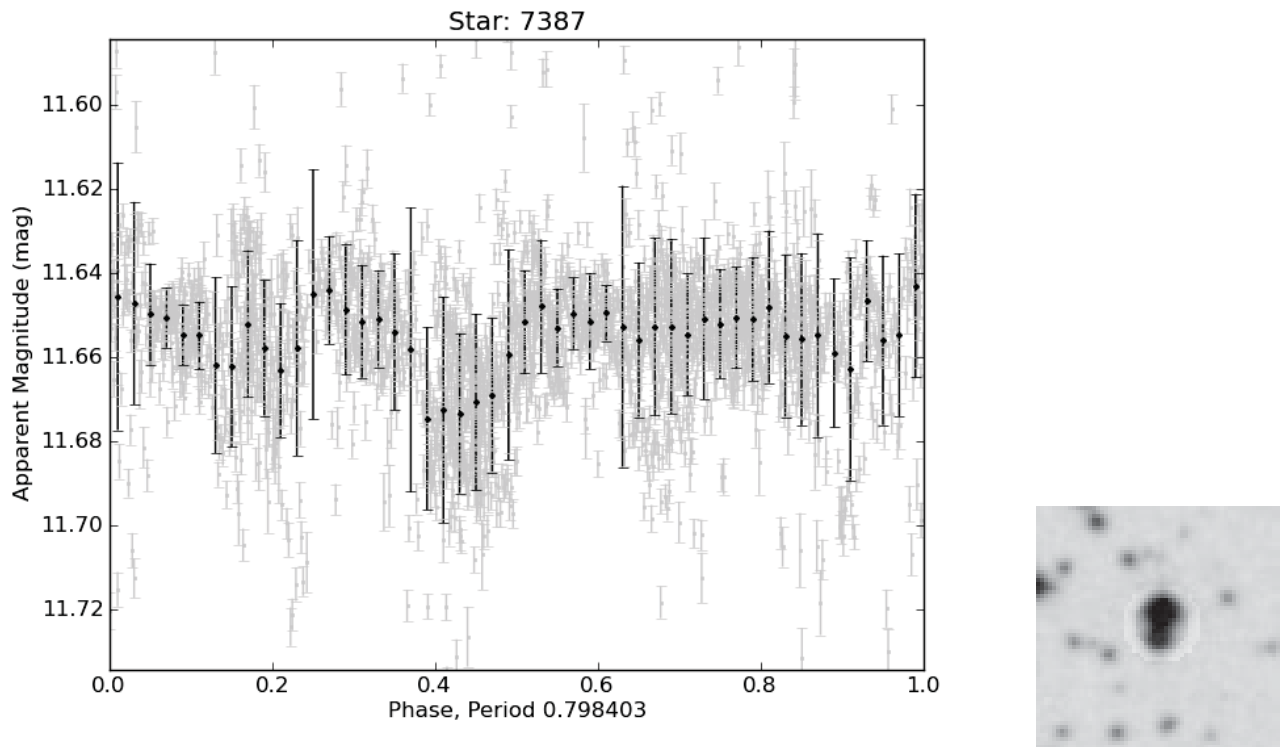


Figure 10.18.: The phase folded lightcurve of Candidate F15\_7387 (left) and the finding chart (right).

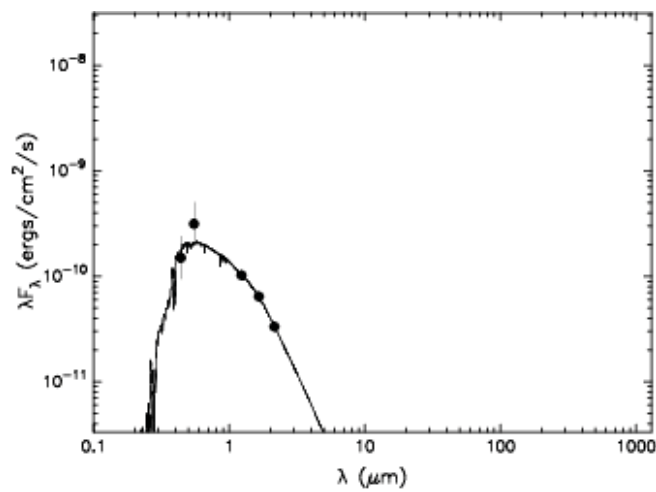


Figure 10.19.: Single transit events of the candidate F15\_7387, as observed with the TEST.

Table 10.8.: Parameters of the binary system P1\_10221

TEST-ID	RA	DEC	B-mag	V-mag	R-mag	J-mag	H-mag	K-mag
P1_10221	05:59:17.7	+40:28:53.7	16.2	15.9	15.8	15.15	14.96	14.85

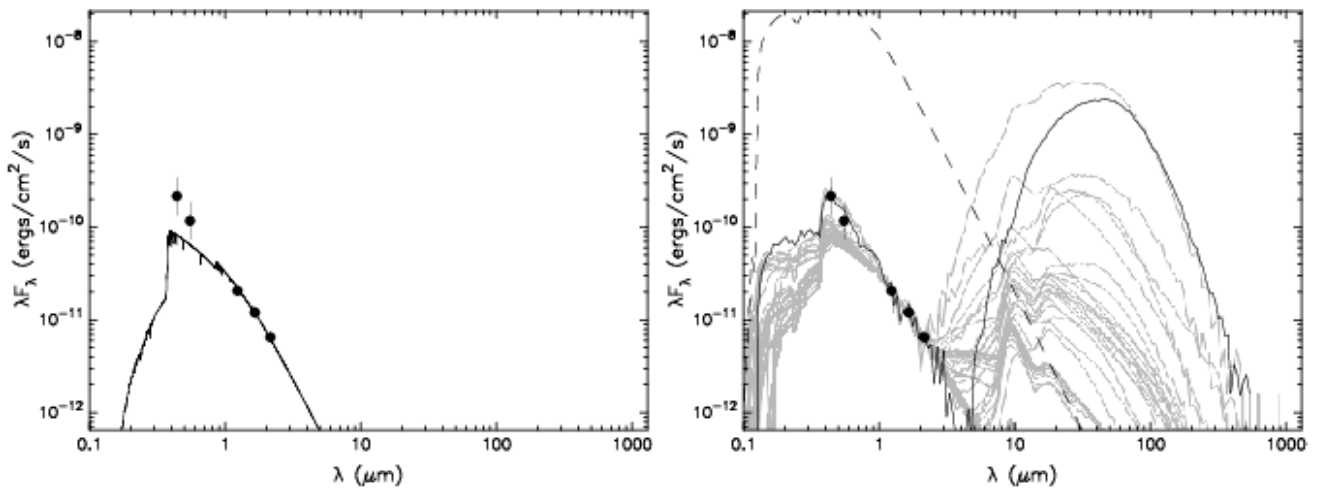


Figure 10.20.: Best stellar photosphere fit by the Kurucz models (left) and the set of best YSO SED fits (right).

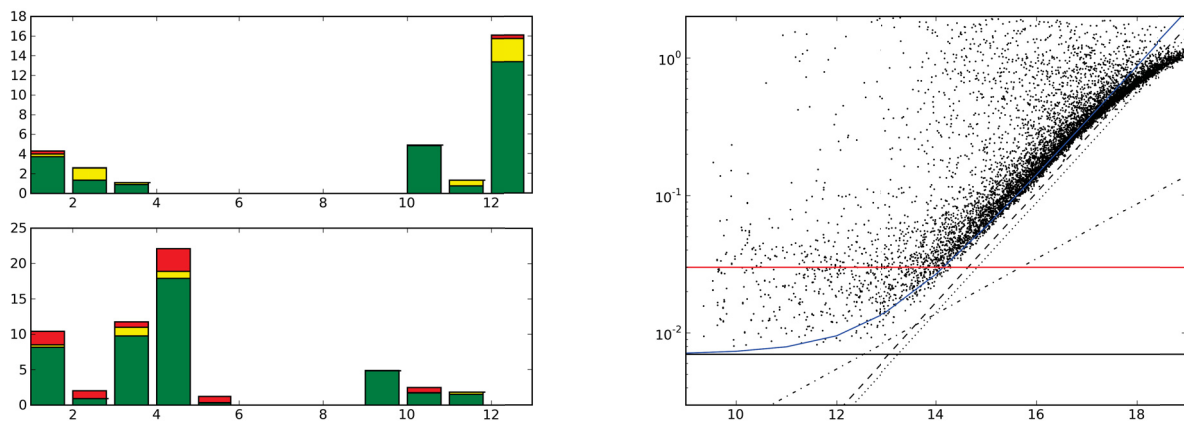


Figure 10.21.: Observations of the field P1, taken with the TEST. On the left, the observing hours per month are shown, where red displays not usable observations, yellow displays observations, deselected to increase the overall photometric accuracy, and green shows the analysed observations. The graph on the right shows the standard deviation of all light curves reached in these 72 hours.

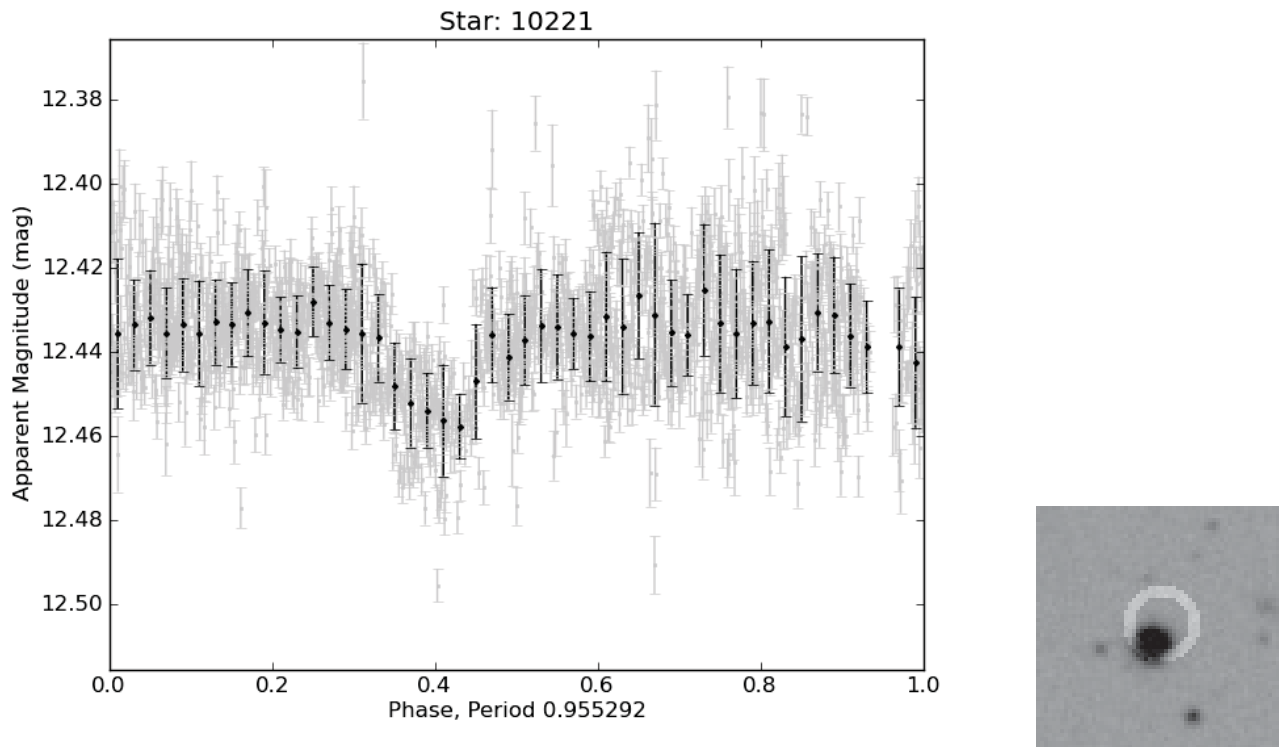


Figure 10.22.: The phase folded lightcurve of Candidate P1\_10221 (left) and the finding chart (right).

Table 10.9.: Parameters of the binary system P1\_40834

TEST-ID	RA	DEC	B-mag	V-mag	R-mag	J-mag	H-mag	K-mag
P1_40834 (1)	05:59:04.9	+38:51:12.8			19.0			
P1_40834 (2)	05:59:04.3	+38:51:13.2	16.9		13.6			
P1_40834 (3)	05:59:04.3	+38:51:14.4	14.4		14.1			
P1_40834 (4)	05:59:04.1	+38:51:11.9	16.4		15.0	14.63	14.32	14.27
P1_40834 (5)	05:59:04.5	+38:51:16.9	16.8		15.4	14.01	13.61	13.47

## Candidate P1\_40834

Inside the aperture of P1\_40834 USNO-B1.0 list 5 objects (cf. Table 10.9). The signal depth observed is 2.0%. Combining the flux in the R-Band of all these sources, the minimal actual depth would be over 4% even if it were caused by a transit around the brightest source. This makes it very unlikely to be the signal of a planetary transit.

## 10.4. Conclusion

Three field have been observed for over two years. The light curves have been analysed for transit like events. For one candidate radial velocity measurements have been taken. This candidate turned out to be a M-dwarf orbiting a Ao Subgiant. For two promising candidates, follow up observations are not possible due to brightness of the host star. For the other four candidates first estimates on the spectral type of the host star, render the planet hypothesis unlikely. These first estimates are based on photometric colour informations of the star. Three of these candidates are also faint and therefore will

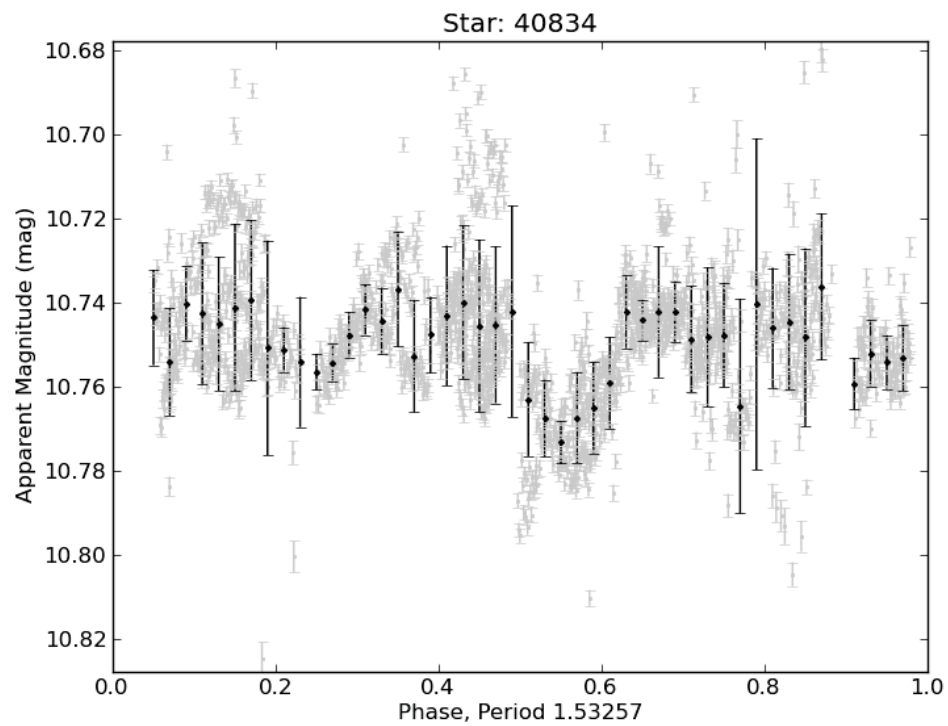


**Figure 10.23.:** *The phase folded lightcurve of Candidate P1\_40834.*

also not allow for radial velocity follow up, the only other bright candidate unfortunately shows only one transit event, thus no period is known.

## 11. Variable Stars identified with the TEST

Photometric surveys used for the search of transiting planets observe simultaneously many thousands of stars with a high photometric precision. In the obtained light curves of these stars, photometric variability not only caused by transiting planets, but by stellar variability (Chapter 2), can be observed. Such variable stars are often of special interest as they allow us a deeper insight into their physical parameters and chemical composition due to accurate observation and understanding of these variabilities.

Asteroseismology for example allows a very good estimation of the stellar age, the mass and the radius. Such physical parameters are of outer importance when searching for example for exoplanet transits. As discussed in previous chapters, the determination of the planets physical parameters are dependent on the knowledge about the star.

Another example are eclipsing binary systems, which allow to test stellar evolution models, as they allow us to get the ratio between the radii and masses of two stars. If one of them additionally is asteroseismic active, all these models can be brought together and tested and maybe even enhanced.

I therefore analysed all light curves in the TEST data sets for general variability as well as for periodic variabilities. Stars showing periodic variabilities have been analysed further. The list of the periodic stars will get published in catalogues, to allow people interested in special kind of stellar variability to find objects of interest and access the parameters determined in this work.

In all three observed fields over 15 percent of the stars showed general variability. For the determination two variability indices were used (Chapter 6.2). For the Stetson variability index the limit was set to 2.0, for the standard deviation based variability index, the variability limit was set to 1.0 (Figure 11.1).

All stars showing variability according to at least one of the indices were analysed for periodicity. Overall 334 periodic variable stars were identified. The 165 variable stars found in field F2 were compared to the results of the BEST data (Pasternacki et al. (2011)). Only 17 stars previously found to be variable with the BEST, could not be verified in the TEST data. In exchange 77 new periodic variables have been found (Figure 11.2). The differences in the detection can be explained by a different magnitude range. Additionally, the spatial resolution of the TEST is much higher than the spatial resolution of the BEST, and a much better orbital coverage was reached as more observations were conducted with the TEST than with the BEST. For the other field previously observed with the BEST (F15), no BEST analysis of variable stars is published so far.

For the following analysis of the stars showing periodic signals, the found period, amplitude, and shape of the signal have been used to characterize the variable star. In Table 11.1 the main types of variable stars showing clear periodic signals have been listed. A first categorization was made using the period and amplitude (Figure 11.3). In a next step the shape of the sinusoidal fit was analysed for a final categorization of the variability. For the types of identified variable stars see A.

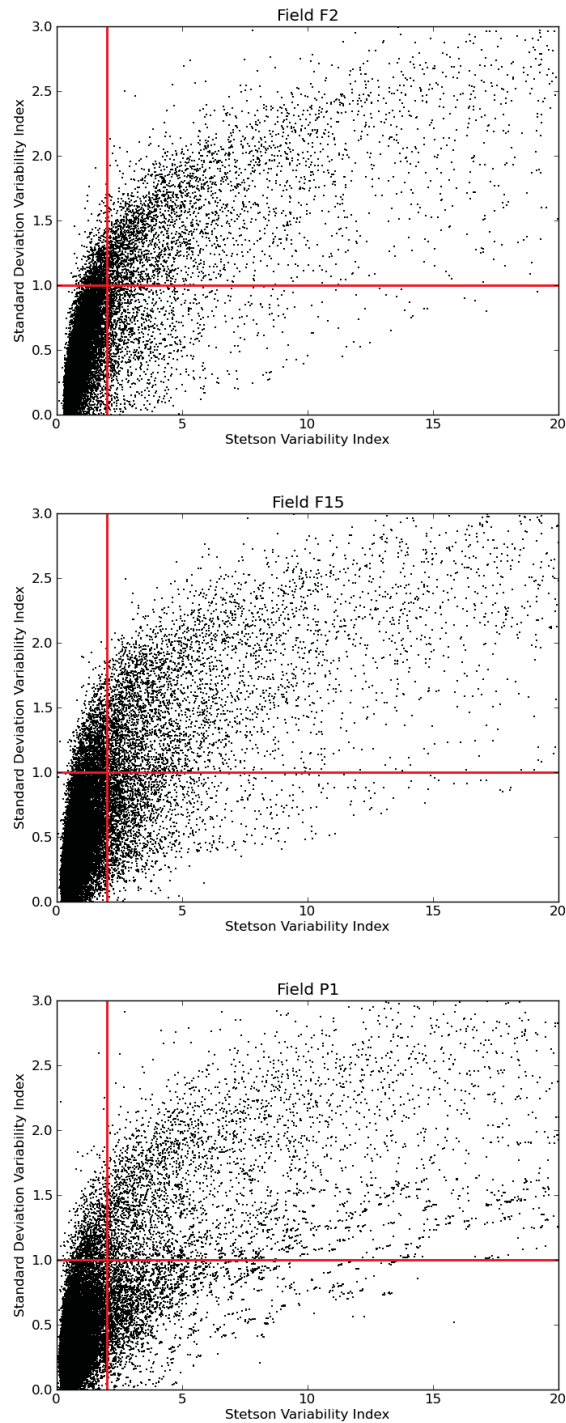


**Figure 11.1.:** General variability in field F2 (upper left), F15 (upper right), P1 (lower centre). For all stars the standard deviation based variability index is plotted over the Stetson variability index. The red lines indicate the selection limit for further analysis. Thus for each field, the lower left square shows the stars not variable at all, whereas the upper right corner shows the stars variable in both indices.



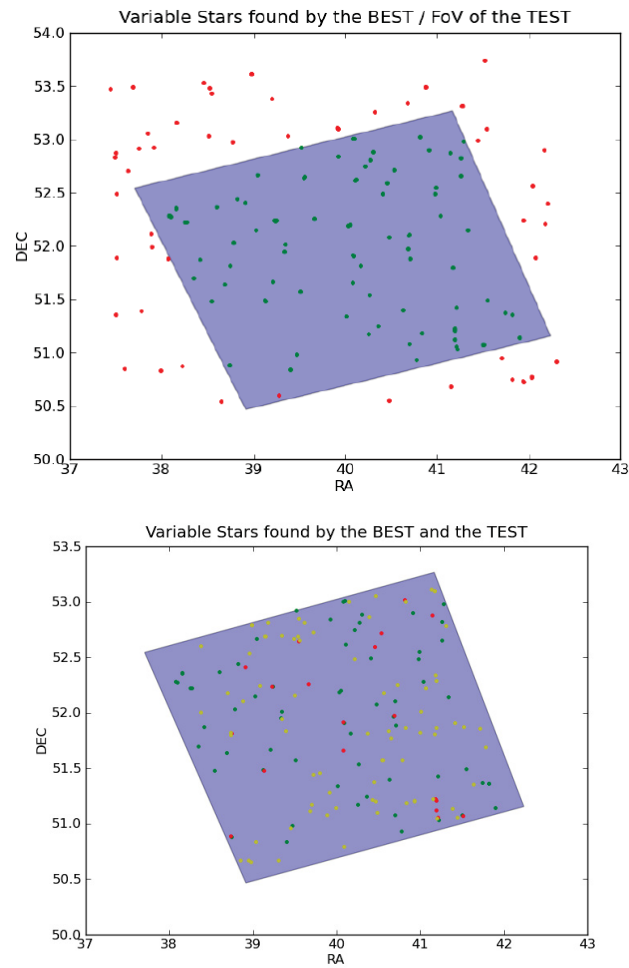


**Figure 11.2.:** The periodic variables found with the BEST and the TEST are shown in the field of view. The left image indicates the field of view of the TEST (blue) in comparison to field of view of the BEST (white). On the right side all periodic variables, identified with the BEST and TEST are shown. The green dots indicate the variables found with both telescopes, the yellow dots show stars only identified with the TEST, and the red dots show stars only found with the BEST.

**Table 11.1.:** The periodic variables found in the three different observed fields.

Type	F2	F15	P1
BCEP	6	2	
BCEPS	1	0	0
DCEP	20	1	0
DCEPS	15	1	7
DSCT	14	3	4
M	2	10	2
RRAB	2	5	1
RRC	26	18	7
EA	23	2	6
EB	4	9	3
EW	17	22	12

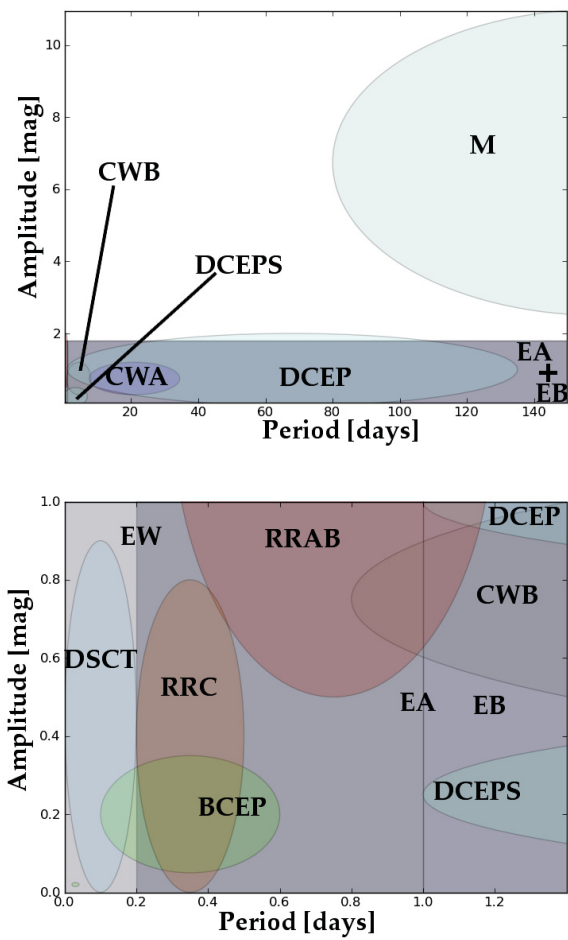


**Figure 11.3.:** The periods and amplitudes, as expected for the most common periodic variable stars as described in Samus et al. (2004). The expected amplitude is plotted over the period.

**Table 11.2.:** List of binaries, with classifications of the components (based on the light curve shape and 2MASS colour information.).

TEST-ID	$M_1 [M_{sol}]$	$M_2 [M_{sol}]$	Age [Gyr]
TEST-F2-43863	0.4	0.7	2.0
TEST-F2-53888	0.4	0.4	0.8
TEST-F2-8197	0.4	0.9	1.6
TEST-F2-54239	0.4	0.9	0.4
TEST-F2-25141	1.9	1.3	1.4
TEST-F2-14065	0.8	0.9	10.0
TEST-F2-9441	1.0	1.3	4.0
TEST-F2-12045	0.7	1.3	1.4
TEST-F2-45104	0.6	0.9	10.0
TEST-F2-39958	1.3	1.0	4.0
TEST-F2-9912	1.1	0.9	9.0
TEST-F2-55309	0.9	0.4	1.2
TEST-F2-10042	1.6	1.1	2.5
TEST-F2-6428	1.1	0.9	0.4
TEST-F2-61120	1.2	0.9	5.0
TEST-F2-27267	1.1	1.0	7.0
TEST-F2-42725	1.6	1.2	2.5
TEST-F2-33301	0.9	0.8	0.8
TEST-F2-26981	0.4	1.2	0.8
TEST-F2-29421	1.1	1.0	8.0
TEST-F2-39039	1.6	1.2	1.0
TEST-F2-10734	0.5	0.6	6.6
TEST-F2-19850	0.7	0.5	0.2
TEST-F2-22171	1.0	0.9	0.9
TEST-F2-44250	1.3	1.3	1.0
TEST-F2-28427	0.7	0.5	10.0
TEST-F2-62510	1.8	1.2	1.2
TEST-F2-29674	0.7	1.3	0.2
TEST-F2-28942	1.0	0.9	10.0
TEST-F2-44239	1.1	1.1	2.5
TEST-F2-2964	1.5	1.7	1.4
TEST-F2-41354	1.2	1.2	6.0
TEST-F2-15054	1.3	1.3	4.0
TEST-F2-39387	0.4	0.5	10.0
TEST-F2-37394	0.9	0.6	0.2
TEST-F2-21065	1.0	0.7	10.0
TEST-F2-3032	1.2	1.1	0.9
TEST-F2-31121	1.1	0.9	10.0

245 of the 343 periodic variable stars could thus be categorized (Table 11.1). In a last step the DEBil/MECI (6.5) program was used to get an even more detailed analysis of the detached binary systems. For 38 of 98 detached binaries a component analysis was successfully conducted (Table 11.2).

A complete list of all variable stars found, as well as the phase folded light curves are given in the appendix.



## 12. Conclusions

- The Tautenburg Exoplanet Search Telescope (TEST) system consisting of a telescope, a CCD camera, a filter wheel with the Kron filter system, a mount with a computer-controllable drive system, an autoguiding system, a dome, a weather control system, and a control PC was set up at the Thüringer Landessternwarte Tautenburg (TLS). The components were successfully implemented into a robotic observation mode. The TEST is capable of detecting transits of “hot-Jupiter” planets.
- I developed an automated data reduction and analysis program, connected to a database managing the TEST observations. The obtained light curves are also managed in a database. For the automated data reduction, an algorithm based on image convolution and deconvolution was developed to identify and dismiss flatfield images of bad quality.
- The TEST data reduction, photometry, and light curve analysis programs allows for a completely automated usage of the TEST, from observations to the identification of candidates for transiting planets and periodic variable stars.
- For the transit detection, I developed a new box-fit algorithm based on the statistical F-test (BFT). This algorithm was tested with original light curves which were superimposed with transiting signals. The newly developed algorithm performs better than other tested algorithms. Thus, using the newly developed algorithm, the detection rate could be enhanced significantly. The algorithm is computationally fast and allows to search for transiting signals without prior knowledge of system parameters. Although the newly developed algorithm shows improvements over the known algorithms, the best performance was achieved when combining the different algorithms.
- Using the programs I developed for the TEST, I analysed two years of observations. In the years 2008 and 2009, 200 observing nights with nearly 1000 hours of observations were taken. A tenth of the observing time was used in support of the CoRoT satellite mission. In the remaining time I conducted a transit survey. Approximately a third of the observations were taken during sufficiently good weather conditions, resulting in photometric accuracies that allow the detection of hot-Jupiter transit events.
- In support of the CoRoT mission six candidates have been observed successfully with the TEST. For these six candidates the source of the detected signal could be determined. One of these candidates was identified as a massive hot-Jupiter. With a planetary mass of  $M_p = 2.33 \pm 0.34 M_{Jup}$  and radius  $R_p = 1.43 \pm 0.03 R_{Jup}$ , the resulting mean density of CoRoT-11b is  $\rho_p = 0.99 \pm 0.15 \text{ g/cm}^3$ . The observed orbital period is  $P = 2.994329 \pm 0.000011$  days long. CoRoT-11b is orbiting a very rapidly rotating F6-type star. The planet is one of the most massive hot-Jupiters known so far. Models suggest CoRoT-11b to be an inflated hydrogen planet with high energy dissipation.

- In the three selected fields I found six candidates showing clear transit-like signals. These signals could have been caused by transiting planets. Four of these systems have a subgiant or even giant host star. The planetary character of the companion was therefore ruled out.
- For one of the candidates, the follow-up measurements led to the discovery of an M-dwarf orbiting an A0 subgiant. The radius and mass of both, the primary and secondary object could be determined. Although ~70% of all stars are M-dwarfs, only 14 M-dwarfs with masses below 0.4 solar masses are known to be in an eclipsing binary system. The detected object is the first one to be orbiting a subgiant. In addition this is the only known M-dwarf to be orbiting a rapidly rotating star in such a close orbit. Using stellar models and the photometric data as well as radial velocity measurements the basic physical parameters of the two objects of this binary system were determined. The density of the M-dwarf is slightly smaller than expected. It is unclear what the reason for this discrepancy between models and observations is. As several projects in search for transiting planets focus on M-dwarfs a better understanding of this type of stars is crucial to carry out these projects. M-dwarfs are interesting objects when looking for transiting planets in the habitable zone. The habitable zone of these stars is much closer to the star and therefore allows transits to be observed with a much higher probability compared to sun-like stars.
- The fields observed for the transit survey were also analysed for variable stars. The periodic variables were classified as far as possible. All together over 250 variable stars were classified.







# Bibliography

Alard, C. 2000, *A&APS*, 144, 363

Alard, C., & Lupton, R. H. 1998, *APJ*, 503, 325

Almenara, J. M., Deeg, H. J., Aigrain, S., Alonso, R., Auvergne, M., Baglin, A., Barbieri, M., Barge, P., Bordé, P., Bouchy, F., Bruntt, H., Cabrera, J., Carone, L., Carpano, S., Catala, C., Csizmadia, S., de La Reza, R., Deleuil, M., Dvorak, R., Erikson, A., Fridlund, M., Gandolfi, D., Gillon, M., Gondoin, P., Guenther, E., Guillot, T., Hatzes, A., Hébrard, G., Jorda, L., Lammer, H., Léger, A., Llebaria, A., Loeillet, B., Magain, P., Mayor, M., Mazeh, T., Moutou, C., Ollivier, M., Pätzold, M., Pont, F., Queloz, D., Rauer, H., Régulo, C., Renner, S., Rouan, D., Samuel, B., Schneider, J., Shporer, A., Wuchterl, G., & Zucker, S. 2009, *A&AP*, 506, 337

Alonso, R., Brown, T. M., Charbonneau, D., Dunham, E. W., Belmonte, J. A., Deeg, H. J., Fernández, J. M., Latham, D. W., Mandushev, G., O'Donovan, F. T., Rabus, M., & Torres, G. 2007, in *Astronomical Society of the Pacific Conference Series*, Vol. 366, *Transiting Extrapolar Planets Workshop*, ed. C. Afonso, D. Wel Drake, & T. Henning, 13–+

Baglin, A., Michel, E., Auvergne, M., & The COROT Team. 2006, in *ESA Special Publication*, Vol. 624, *Proceedings of SOHO 18/GONG 2006/HELAS I, Beyond the spherical Sun*

Bakos, G. Á., Noyes, R. W., Kovács, G., Latham, D. W., Sasselov, D. D., Torres, G., Fischer, D. A., Stefanik, R. P., Sato, B., Johnson, J. A., Pál, A., Marcy, G. W., Butler, R. P., Esquerdo, G. A., Stanek, K. Z., Lázár, J., Papp, I., Sári, P., & Sipőcz, B. 2007, *APJ*, 656, 552

Barge, P., Baglin, A., Auvergne, M., & the CoRoT team. 2008, in *IAU Symposium*, Vol. 249, *IAU Symposium*, ed. Y.-S. Sun, S. Ferraz-Mello, & J.-L. Zhou, 3–16

Bean, J. L., Miller-Ricci Kempton, E., & Homeier, D. 2010, *Nature*, 468, 669

Benz, W., Alibert, Y., Mordasini, C., & Naef, D. 2006, in *IAU Colloq. 200: Direct Imaging of Exoplanets: Science & Techniques*, ed. C. Aime & F. Vakili, 1–10

Bertin, E., & Arnouts, S. 1996, *A&APS*, 117, 393

Borucki, W. J., & Summers, A. L. 1984, *ICARUS*, 58, 121

Brown, T. M. 2003, *APJL*, 593, L125

Chelli, A. 2000, *A&AP*, 358, L59

Crouzet, N., Guillot, T., Agabi, A., Rivet, J.-P., Bondoux, E., Challita, Z., Fanteï-Caujolle, Y., Fressin, F., Mékarnia, D., Schmider, F.-X., Valbousquet, F., Blazit, A., Bonhomme, S., Abe, L., Daban, J.-B., Gouvret, C., Fruth, T., Rauer, H., Erikson, A., Barbieri, M., Aigrain, S., & Pont, F. 2010, *A&AP*, 511, A36+

- Cutri, R. M., Skrutskie, M. F., van Dyk, S., Beichman, C. A., Carpenter, J. M., Chester, T., Cambresy, L., Evans, T., Fowler, J., Gizis, J., Howard, E., Huchra, J., Jarrett, T., Kopan, E. L., Kirkpatrick, J. D., Light, R. M., Marsh, K. A., McCallon, H., Schneider, S., Stiening, R., Sykes, M., Weinberg, M., Wheaton, W. A., Wheelock, S., & Zacarias, N. 2003, 2MASS All Sky Catalog of point sources., ed. Cutri, R. M., Skrutskie, M. F., van Dyk, S., Beichman, C. A., Carpenter, J. M., Chester, T., Cambresy, L., Evans, T., Fowler, J., Gizis, J., Howard, E., Huchra, J., Jarrett, T., Kopan, E. L., Kirkpatrick, J. D., Light, R. M., Marsh, K. A., McCallon, H., Schneider, S., Stiening, R., Sykes, M., Weinberg, M., Wheaton, W. A., Wheelock, S., & Zacarias, N.
- Deeg, H. J., Gillon, M., Shporer, A., Rouan, D., Stecklum, B., Aigrain, S., Alapini, A., Almenara, J. M., Alonso, R., Barbieri, M., Bouchy, F., Eislöffel, J., Erikson, A., Fridlund, M., Eigmüller, P., Handler, G., Hatzes, A., Kabath, P., Lendl, M., Mazeh, T., Moutou, C., Queloz, D., Rauer, H., Rabus, M., Tingley, B., & Titz, R. 2009, *A&AP*, 506, 343
- Deeg, H. J., Moutou, C., Erikson, A., Csizmadia, S., Tingley, B., Barge, P., Bruntt, H., Havel, M., Aigrain, S., Almenara, J. M., Alonso, R., Auvergne, M., Baglin, A., Barbieri, M., Benz, W., Bonomo, A. S., Bordé, P., Bouchy, F., Cabrera, J., Carone, L., Carpano, S., Ciardi, D., Deleuil, M., Dvorak, R., Ferraz-Mello, S., Fridlund, M., Gandolfi, D., Gazzano, J.-C., Gillon, M., Gondoin, P., Guenther, E., Guillot, T., Hartog, R. D., Hatzes, A., Hidas, M., Hébrard, G., Jorda, L., Kabath, P., Lammer, H., Léger, A., Lister, T., Llebaria, A., Lovis, C., Mayor, M., Mazeh, T., Ollivier, M., Pätzold, M., Pepe, F., Pont, F., Queloz, D., Rabus, M., Rauer, H., Rouan, D., Samuel, B., Schneider, J., Shporer, A., Stecklum, B., Street, R., Udry, S., Weingrill, J., & Wuchterl, G. 2010, *Nature*, 464, 384
- Desort, M., Lagrange, A.-M., Galland, F., Udry, S., & Mayor, M. 2007, *A&AP*, 473, 983
- Devor, J. 2005, *APJ*, 628, 411
- Devor, J., & Charbonneau, D. 2006, *APJ*, 653, 647
- Doyle, L. R., Deeg, H. J., Kozhevnikov, V. P., Oetiker, B., Martín, E. L., Blue, J. E., Rottler, L., Stone, R. P. S., Ninkov, Z., Jenkins, J. M., Schneider, J., Dunham, E. W., Doyle, M. F., & Paleologou, E. 2000, *APJ*, 535, 338
- Eigmüller, P. 2006, Diploma thesis, Lehrstuhl für Nukleare Festkörperphysik, Fakultät für Physik und Geowissenschaften, Universität Leipzig, (Engl. translation: Automated identification of variable stars using the example of selected fields)
- Eislöffel, J., Hatzes, A. P., Rauer, H., Voss, H., Erikson, A., Eigmüller, P., & Guenther, E. 2007, in *Astronomical Society of the Pacific Conference Series*, Vol. 370, *Solar and Stellar Physics Through Eclipses*, ed. O. Demircan, S. O. Selam, & B. Albayrak, 91–+
- Fernandez, J. M., Latham, D. W., Torres, G., Everett, M. E., Mandushev, G., Charbonneau, D., O'Donovan, F. T., Alonso, R., Esquerdo, G. A., Hergenrother, C. W., & Stefanik, R. P. 2009, *APJ*, 701, 764
- Gandolfi, D., Hébrard, G., Alonso, R., Deleuil, M., Guenther, E. W., Fridlund, M., Endl, M., Eigmüller, P., Csizmadia, S., Havel, M., Aigrain, S., Auvergne, M., Baglin, A., Barge, P., Bonomo, A. S., Bordé, P., Bouchy, F., Bruntt, H., Cabrera, J., Carpano, S., Carone, L., Cochran, W. D., Deeg, H. J., Dvorak, R., Eislöffel, J., Erikson, A., Ferraz-Mello, S., Gazzano, J., Gibson, N. B., Gillon, M., Gondoin, P., Guillot, T., Hartmann, M., Hatzes, A., Jorda, L., Kabath, P., Léger, A., Llebaria, A., Lammer, H., MacQueen, P. J., Mayor, M., Mazeh, T., Moutou, C., Ollivier, M., Pätzold, M., Pepe, F., Queloz, D., Rauer, H., Rouan, D., Samuel, B., Schneider, J., Stecklum, B., Tingley, B., Udry, S., & Wuchterl, G. 2010, *A&AP*, 524, A55+
- Hatzes, A. P. 2002, *Astronomische Nachrichten*, 323, 392
- Hatzes, A. P., Fridlund, M., Nachmani, G., Mazeh, T., Valencia, D., Hebrard, G., Carone, L., Paetzold, M., Udry, S., Bouchy, F., Borde, P., Deeg, H., Tingley, B., Dvorak, R., Gandolfi, D., Ferraz-Mello, S., Wuchterl, G., Guenther, E., Rauer, H., Erikson, A., Cabrera, J., Csizmadia, S., Leger, A., Lammer, H., Weingrill, J., Queloz, D., Alonso, R., & Schneider, J. 2011, *ArXiv e-prints*

- Hatzes, A. P., Guenther, E., Kürster, M., & McArthur, B. 2003, in *ESA Special Publication*, Vol. 539, *Earths: DARWIN/TPF and the Search for Extrasolar Terrestrial Planets*, ed. M. Fridlund, T. Henning, & H. Lacoste, 441–445
- Hoffmeister, C., Richter, G., & Wenzel, W. 1984, *Veraenderliche Sterne* (Berlin: Springer, 1984, 2. ueberarb. Aufl.)
- Irwin, J., Charbonneau, D., Berta, Z. K., Quinn, S. N., Latham, D. W., Torres, G., Blake, C. H., Burke, C. J., Esquerdo, G. A., Fürész, G., Mink, D. J., Nutzman, P., Szentgyorgyi, A. H., Calkins, M. L., Falco, E. E., Bloom, J. S., & Starr, D. L. 2009, *APJ*, 701, 1436
- Kabath, P., Eigmüller, P., Erikson, A., Hedelt, P., Rauer, H., Titz, R., Wiese, T., & Karoff, C. 2007, *AJ*, 134, 1560
- Kabath, P., Erikson, A., Rauer, H., Pasternacki, T., Csizmadia, S., Chini, R., Lemke, R., Murphy, M., Fruth, T., Titz, R., & Eigmüller, P. 2009a, *VizieR Online Data Catalog*, 3506, 60569
- Kabath, P., Erikson, A., Rauer, H., Pasternacki, T., Csizmadia, S., Chini, R., Lemke, R., Murphy, M., Fruth, T., Titz, R., & Eigmüller, P. 2009b, *A&AP*, 506, 569
- Kabath, P., Fruth, T., Rauer, H., Erikson, A., Murphy, M. G., Chini, R., Lemke, R., Csizmadia, S., Eigmüller, P., Pasternacki, T., & Titz, R. 2009c, *AJ*, 137, 3911
- Kay, S. 1998, *Fundamentals of Statistical Signal Processing, Vol II - Detection Theory* (Prentice Hall)
- Kholopov, P. N., Samus, N. N., Frolov, M. S., Goranskij, V. P., Gorynya, N. A., Karitskaya, E. A., Kazarovets, E. V., Kireeva, N. N., Kukarkina, N. P., Kurochkin, N. E., Medvedeva, G. I., Pastukhova, E. N., Perova, N. B., Rastorguev, A. S., & Shugarov, S. Y. 1998, in *Combined General Catalogue of Variable Stars*, 4.1 Ed (II/214A). (1998), 0–+
- Kovács, G., Bakos, G., & Noyes, R. W. 2005, *MNRAS*, 356, 557
- Kovács, G., Zucker, S., & Mazeh, T. 2002, *A&AP*, 391, 369
- Kurucz, R. L. 1970, *SAO Special Report*, 309
- Lang, D., Hogg, D. W., Mierle, K., Blanton, M., & Roweis, S. 2010, *AJ*, 139, 1782
- Léger, A., Rouan, D., Schneider, J., Barge, P., Fridlund, M., Samuel, B., Ollivier, M., Guenther, E., Deleuil, M., Deeg, H. J., Auvergne, M., Alonso, R., Aigrain, S., Alapini, A., Almenara, J. M., Baglin, A., Barbieri, M., Bruntt, H., Bordé, P., Bouchy, F., Cabrera, J., Catala, C., Carone, L., Carpano, S., Csizmadia, S., Dvorak, R., Erikson, A., Ferraz-Mello, S., Foing, B., Fressin, F., Gandolfi, D., Gillon, M., Gondoin, P., Grasset, O., Guillot, T., Hatzes, A., Hébrard, G., Jorda, L., Lammer, H., Llebaria, A., Loeillet, B., Mayor, M., Mazeh, T., Moutou, C., Pätzold, M., Pont, F., Queloz, D., Rauer, H., Renner, S., Samadi, R., Shporer, A., Sotin, C., Tingley, B., Wuchterl, G., Adda, M., Agogu, P., Appourchaux, T., Ballans, H., Baron, P., Beaufort, T., Bellenger, R., Berlin, R., Bernardi, P., Blouin, D., Baudin, F., Bodin, P., Boisnard, L., Boit, L., Bonneau, F., Borzeix, S., Briet, R., Buey, J.-T., Butler, B., Cailleau, D., Cautain, R., Chabaud, P.-Y., Chaintreuil, S., Chiavassa, F., Costes, V., Cuna Parrho, V., de Oliveira Fialho, F., Decaudin, M., Defise, J.-M., Djalal, S., Epstein, G., Exil, G.-E., Fauré, C., Fenouillet, T., Gaboriaud, A., Gallic, A., Gamet, P., Gavalda, P., Grolleau, E., Gruneisen, R., Gueguen, L., Guis, V., Guivarc'h, V., Guterman, P., Hallouard, D., Hasiba, J., Heuripeau, F., Huntzinger, G., Hustaix, H., Imad, C., Imbert, C., Johlander, B., Joutet, M., Journoud, P., Karioty, F., Kerjean, L., Lafaille, V., Lafond, L., Lam-Trong, T., Landiech, P., Lapeyrere, V., Larqué, T., Laudet, P., Lautier, N., Lecann, H., Lefevre, L., Leruyet, B., Levacher, P., Magnan, A., Mazy, E., Mertens, F., Mesnager, J.-M., Meunier, J.-C., Michel, J.-P., Monjoin, W., Naudet, D., Nguyen-Kim, K., Orcesi, J.-L., Ottacher, H., Perez, R., Peter, G., Plasson, P., Plessier, J.-Y., Pontet, B., Pradines, A., Quentin, C., Reynaud, J.-L., Rolland, G., Rollenhagen, F., Romagnan, R., Russ, N., Schmidt, R., Schwartz, N., Sebbag, I., Sedes, G., Smit, H., Steller, M. B., Sunter, W., Surace, C., Tello, M., Tiphène, D., Toulouse, P., Ulmer, B., Vandermarcq, O., Vergnault, E., Vuillemin, A., & Zanatta, P. 2009, *A&AP*, 506, 287

- Lehmann, H., Tkachenko, A., Semaan, T., Gutiérrez, J., Smalley, B., Briquet, M., Shulyak, D., Tsymbal, V., & de Cat, P. 2010, ArXiv e-prints
- Mayor, M., & Queloz, D. 1995, *Nature*, 378, 355
- McCullough, P. R., Stys, J. E., Valenti, J. A., Fleming, S. W., Janes, K. A., & Heasley, J. N. 2005, *PASP*, 117, 783
- Monet, D. G., Levine, S. E., Canzian, B., Ables, H. D., Bird, A. R., Dahn, C. C., Guetter, H. H., Harris, H. C., Henden, A. A., Leggett, S. K., Levison, H. F., Luginbuhl, C. B., Martini, J., Monet, A. K. B., Munn, J. A., Pier, J. R., Rhodes, A. R., Riepe, B., Sell, S., Stone, R. C., Vrba, F. J., Walker, R. L., Westerhout, G., Brucato, R. J., Reid, I. N., Schoening, W., Hartley, M., Read, M. A., & Tritton, S. B. 2003, *AJ*, 125, 984
- Ochsenbein, F., Bauer, P., & Marcout, J. 2000, *A&APS*, 143, 23
- Pasternacki, T., Csizmadia, S., Cabrera, J., Eig Müller, P., Erikson, A., Fruth, T., von Paris, P., Rauer, H., Titz, R., Eislöffel, J., Hatzes, A., Boer, M., Tournois, G., Kabath, P., Hedelt, P., & Voss, H. 2011, *AJ*, 142, 114
- Perryman, M. A. C. 2000, *Reports on Progress in Physics*, 63, 1209
- Pollacco, D. L., Skillen, I., Collier Cameron, A., Christian, D. J., Hellier, C., Irwin, J., Lister, T. A., Street, R. A., West, R. G., Anderson, D., Clarkson, W. I., Deeg, H., Enoch, B., Evans, A., Fitzsimmons, A., Haswell, C. A., Hodgkin, S., Horne, K., Kane, S. R., Keenan, F. P., Maxted, P. F. L., Norton, A. J., Osborne, J., Parley, N. R., Ryans, R. S. I., Smalley, B., Wheatley, P. J., & Wilson, D. M. 2006, *PASP*, 118, 1407
- Pont, F., Knutson, H., Gilliland, R. L., Moutou, C., & Charbonneau, D. 2008, *MNRAS*, 385, 109
- Press, W., Teukolsky, S., Vetterling, W., & Flannery, B. 1992, *Numerical Recipes in C* (Cambridge University Press)
- Rabus, M., Alonso, R., Belmonte, J. A., Deeg, H. J., Gilliland, R. L., Almenara, J. M., Brown, T. M., Charbonneau, D., & Mandushev, G. 2009, *A&AP*, 494, 391
- Rauer, H., Eislöffel, J., Erikson, A., Guenther, E., Hatzes, A. P., Michaelis, H., & Voss, H. 2004, *PASP*, 116, 38
- Rauer, H., Erikson, A., Kabath, P., Hedelt, P., Boer, M., Carone, L., Csizmadia, S., Eig Müller, P., Paris, P. v., Renner, S., Tournois, G., Titz, R., & Voss, H. 2010, *AJ*, 139, 53
- Ridderstad, M. 2009, Orientation of the northern gate of the Goseck Neolithic rondel, <http://adsabs.harvard.edu/abs/2009arXiv0910.0560R>
- Roberts, D. H., Lehar, J., & Dreher, J. W. 1987, *AJ*, 93, 968
- Robitaille, T. P., Whitney, B. A., Indebetouw, R., & Wood, K. 2007, *ApJS*, 169, 328
- Samus, N. N., Durlevich, O. V., & et al. 2004, *VizieR Online Data Catalog*, 2250, 0
- Scholz, A., & Eislöffel, J. 2004, *A&AP*, 419, 249
- Serra, J. 1983, *Image Analysis and Mathematical Morphology* (Orlando, FL, USA: Academic Press, Inc.)
- Stetson, P. B. 1996, *PASP*, 108, 851
- Surma, P. 1993, *A&AP*, 278, 654
- Tamuz, O., Mazeh, T., & Zucker, S. 2005, *MNRAS*, 356, 1466
- Tingley, B. 2003, *A&AP*, 408, L5

- Tody, D. 1986, in Presented at the Society of Photo-Optical Instrumentation Engineers (SPIE) Conference, Vol. 627, Society of Photo-Optical Instrumentation Engineers (SPIE) Conference Series, ed. D. L. Crawford, 733–+
- Tody, D. 1993, in Astronomical Society of the Pacific Conference Series, Vol. 52, Astronomical Data Analysis Software and Systems II, ed. R. J. Hanisch, R. J. V. Brissenden, & J. Barnes, 173–+
- Tyson, N. D., & Gal, R. R. 1993, *AJ*, 105, 1206
- Voss, H. 2006, Ph.D. Thesis
- Welch, D. L., & Stetson, P. B. 1993, *AJ*, 105, 1813
- Wikipedia. 2010a, Extrasolar planet — Wikipedia, The Free Encyclopedia, [Online; accessed 6-September-2010]
- . 2010b, Extrasolarer Planet — Wikipedia, Die freie Enzyklopädie, [Online; Stand 6. September 2010]
- Wolszczan, A., & Frail, D. A. 1992, *Nature*, 355, 145
- Zhang, X., Deng, L., Xin, Y., & Zhou, X. 2003, *Chinese Journal of Astronomy and Astrophysics*, 3, 151









# Appendices



# A. Types of periodic Variable Stars

## Pulsating stars

- **BCEP:** Variables of the Beta Cephei type. Light curves have a sinusoidal shape. Periods between 0.1 and 0.6 days and amplitudes of up to 0.3 magnitudes can be observed
- **BCEPS:** Beta Cephei type variables, with short periods (0.02-0.04 days). The signal amplitude is between 0.015 and 0.025 magnitudes.
- **DCEP:** The classical cepheids have periods between 1 and 135 days. The tooth-shape signal has an amplitude between 0.02 and 2 magnitudes.
- **DCEPS:** These Delta Cephei type variables have almost symmetrical light curves. The period does not exceed 7 days.
- **DSCT:** Delta Scuti type variables with periods below 0.2 days. The light curve displays an amplitude of up to 0.9 magnitudes.
- **M:** Mira Variable stars, are long period variables (> 85 days) and large amplitudes (> 1 mag).
- **RRAB:** These RR Lyrae variables have asymmetric light curves with periods from 0.3 to 1.2 days, and amplitudes from 0.5 to 2 magnitudes.
- **RRC:** These RR Lyrae have symmetric light curves, sometimes sinusoidal, with periods below 0.5 days.

## Eclipsing Binaries

- **EA:** Algol type eclipsing systems with periods over 0.2 days. The eclipses have a clear start and end, in between an almost constant flux is observed.
- **EB:** Beta Lyrae-type eclipsing systems have periods over 1.0 day. In contrast to Algol type systems, no parts of constant magnitude are observed in the light curve.
- **EW:** W Ursae Majoris-type eclipsing variables have periods below 1.0 days. Similar to Beta Lyrae-type systems, no clear start and end of the eclipse can be identified.



## B. Periodic Variable Stars - Field F2

Table B.1.: Periodic Variables in the F2 field

TEST-ID	2MASS designation	Found with BEST	RA	DEC	Period[days]	Amplitude[mag]	Type
TEST-F2-22687	02441621+5213316		02:44:16.2	52:13:31.4	0.0700	0.007	dsct
TEST-F2-24645	02344329+5138219	X	02:34:43.4	51:38:21.5	0.0738	0.014	dsct
TEST-F2-6381	02410442+5248406	X	02:41:4.4	52:48:40.0	0.0826	0.022	dsct
TEST-F2-4704	02411195+5253077	X	02:41:11.9	52:53:7.1	0.0903	0.009	dsct
TEST-F2-48496	02445207+5101576	X	02:44:52.0	51:01:57.4	0.1080	0.010	dsct
TEST-F2-29878	02380238+5134284	X	02:38:2.4	51:34:28.2	0.1088	0.026	bcep
TEST-F2-824	02401944+5300258	X	02:40:19.4	53:00:24.5	0.1104	0.056	dsct
TEST-F2-41800	02375264+5059025	X	02:37:52.7	50:59:2.4	0.1185	0.020	bcep
TEST-F2-19528	02372302+5200476	X	02:37:23.2	52:00:46.8	0.1257	0.101	dsct
TEST-F2-23567	02424679+5206265	X	02:42:46.8	52:06:26.3	0.1285	0.011	dsct
TEST-F2-21488	02332305+5141598	X	02:33:23.4	51:42:1.1	0.1337	0.152	ew
TEST-F2-52644	02440757+5216593	X	02:44:7.5	52:17:1.7	0.1338	0.168	ew
TEST-F2-16376	02350717+5202048	X	02:35:7.2	52:02:4.6	0.1367	0.276	ew
TEST-F2-49272	02401946+5300125	X	02:40:19.6	53:00:12.6	0.1434	0.038	dsct
TEST-F2-23607	02415315+5204511	X	02:41:53.1	52:04:50.2	0.1508	0.043	dsct
TEST-F2-13839	02450091+5239216	X	02:45:1.0	52:39:24.1	0.1550	0.058	bcep
TEST-F2-39862	02461264+5129397	X	02:46:12.6	51:29:39.5	0.1602	0.210	bcep
TEST-F2-27126	02340930+5128519	X	02:34:9.4	51:28:52.0	0.1637	0.469	ew
TEST-F2-20927	02372113+5156519		02:37:21.3	51:56:49.2	0.1650	0.124	ew
TEST-F2-26431	02424312+5158184	X	02:42:43.1	51:58:17.8	0.1721	0.276	bcep,ew
TEST-F2-41290	02410134+5110360	X	02:41:1.3	51:10:35.8	0.1780	0.245	ew
TEST-F2-27611	02403838+5148493	X	02:40:38.4	51:48:48.2	0.1787	0.012	dsct
TEST-F2-31860	02444127+5148223		02:44:41.3	51:48:22.0	0.1805	0.407	ew
TEST-F2-50722	02342284+5222011	X	02:34:23.2	52:21:59.8	0.1821	0.225	dsct
TEST-F2-49797			02:38:27.9	52:48:41.4	0.1996	0.026	dsct
TEST-F2-55309	02471709+5121451		02:47:17.1	51:21:47.2	0.1996	0.072	ew
TEST-F2-49734	02360063+5241129		02:36:0.8	52:41:15.4	0.1997	0.024	dsct
TEST-F2-48713	02454617+5103142		02:45:46.1	51:03:14.4	0.2008	0.023	rrc
TEST-F2-36670	02470836+5141416		02:47:8.4	51:41:41.3	0.2012	0.017	rrc
TEST-F2-7646	02321719+5216501	X	02:32:17.4	52:16:49.8	0.2062	0.013	rrc
TEST-F2-8197	02322158+5216307	X	02:32:21.8	52:16:29.6	0.2108	0.138	ew
TEST-F2-41813	02374727+5057475		02:37:47.2	50:57:47.9	0.2170	0.129	bcep
TEST-F2-41266	02393145+5104576		02:39:31.5	51:04:57.7	0.2184	0.244	bcep,ew
TEST-F2-52602	02345639+5149085		02:34:56.4	51:49:9.5	0.2202	0.019	rrc
TEST-F2-26435	02365029+5140042	X	02:36:50.3	51:40:4.1	0.2272	0.049	
TEST-F2-39958	02444949+5125434	X	02:44:49.5	51:25:42.6	0.2417	0.270	rrc
TEST-F2-53888	02423515+5146073		02:42:35.2	51:46:7.0	0.2493	0.048	rrc
TEST-F2-50984	02325902+5213320	X	02:32:59.1	52:13:31.4	0.2505	0.023	rrc
TEST-F2-45970	02354677+5040036		02:35:46.8	50:40:4.4	0.2520	0.009	rrc
TEST-F2-29675	02362820+5129152	X	02:36:28.2	51:29:15.4	0.2931	0.303	rrc
TEST-F2-14913	02360649+5209043	X	02:36:6.5	52:09:4.3	0.2953	0.063	rrc
TEST-F2-14065	02365649+5214098	X	02:36:56.6	52:14:9.6	0.3028	0.137	rrc
TEST-F2-6050	02323549+5221425	X	02:32:35.7	52:21:41.4	0.3040	0.188	rrc
TEST-F2-98	02380356+5255401	X	02:38:3.6	52:55:39.4	0.3057	0.126	rrc
TEST-F2-43295	02465785+5122230	X	02:46:57.8	51:22:23.2	0.3128	0.363	rrc
TEST-F2-40382	02345511+5053139		02:34:55.2	50:53:14.3	0.3153	0.008	rrc
TEST-F2-20675	02371925+5157070	X	02:37:19.3	51:57:6.8	0.3299	0.071	rrc
TEST-F2-54239	02465043+5151499		02:46:50.3	51:51:45.4	0.3321	0.053	ew
TEST-F2-47155	02371233+5040182		02:37:12.4	50:40:18.5	0.3322	0.236	ea
TEST-F2-51000	02330363+5213210	X	02:33:3.6	52:13:19.2	0.3343	0.085	rrc
TEST-F2-46015	02355420+5039229		02:35:54.2	50:39:23.8	0.3622	0.539	rrab
TEST-F2-7469	02351758+5226382	X	02:35:17.6	52:26:37.7	0.3664	0.062	rrc
TEST-F2-6428	02450728+5258492	X	02:45:7.3	52:58:50.2	0.3744	0.281	rrc
TEST-F2-6365	02381212+5238543		02:38:12.1	52:38:53.5	0.3800	0.169	ew
TEST-F2-37956	02423165+5124050	X	02:42:32.0	51:24:6.8	0.3856	0.317	rrc
TEST-F2-47714	02473525+5108374	X	02:47:35.2	51:08:37.3	0.4021	0.215	
TEST-F2-6745	02433777+5254020	X	02:43:37.8	52:54:1.4	0.4070	0.058	rrc
TEST-F2-48846	02401995+5047418		02:40:20.0	50:47:42.4	0.4120	0.057	rrc
TEST-F2-5191	02413203+5251475		02:41:32.0	52:51:47.9	0.4270	0.023	
TEST-F2-3968	02431643+5300120		02:43:16.4	53:00:12.2	0.4370	0.092	ea
TEST-F2-43259	02431890+5111194		02:43:18.9	51:11:19.0	0.4377	1.324	rrab
TEST-F2-43362	02432088+5111070		02:43:20.9	51:11:6.7	0.4377	0.027	ea
TEST-F2-20379	02444375+5220273		02:44:43.7	52:20:26.9	0.4410	0.071	
TEST-F2-45104	02424804+5104481	X	02:42:48.0	51:04:48.0	0.4500	0.017	rrc

Continued on Next Page...

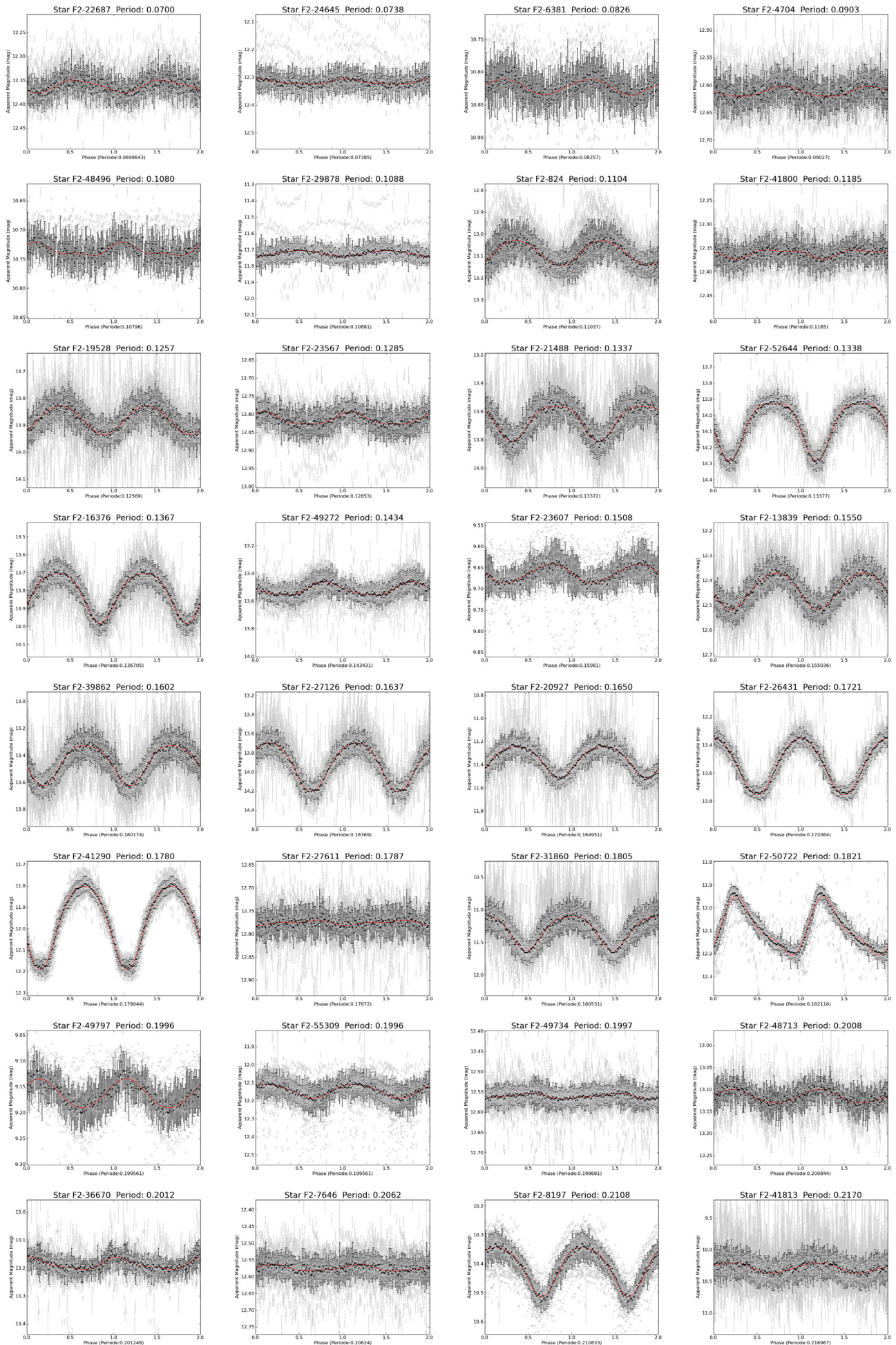
Table B.1 – Continued

TEST-ID	2MASS designation	Found with BEST	RA	DEC	Period[days]	Amplitude[mag]	Type
TEST-F2-48415	02455980+5104387	X	02:45:59.7	51:04:38.6	0.4519	0.206	rrc
TEST-F2-40469	02345700+5053005	X	02:34:57.1	50:53:1.0	0.4730	0.026	rrc
TEST-F2-44320	02373689+5050156	X	02:37:36.9	50:50:16.1	0.4733	0.351	bceps
TEST-F2-25141	02402065+5154387	X	02:40:20.7	51:54:38.5	0.4812	0.225	rrc
TEST-F2-12045	02415168+5235221		02:41:51.6	52:35:23.3	0.4920	0.061	
TEST-F2-43747	02443575+5113336		02:44:35.8	51:13:32.9	0.5310	0.056	ea
TEST-F2-10078	02450202+5249285	X	02:45:2.0	52:49:28.2	0.5360	0.064	ew
TEST-F2-41530	02415160+5112096		02:41:51.6	51:12:9.7	0.5376	0.033	dceps
TEST-F2-14043	02413839+5229342		02:41:38.4	52:29:34.1	0.5426	0.147	ea
TEST-F2-13771	02413675+5229427	X	02:41:36.7	52:29:42.4	0.5430	0.040	
TEST-F2-55908	02444921+5103026		02:44:49.3	51:02:59.6	0.5620	0.085	
TEST-F2-16342	02435549+5229214	X	02:43:55.5	52:29:21.1	0.5660	0.118	dceps
TEST-F2-16929	02375946+5209382		02:37:59.5	52:09:37.8	0.5690	0.043	
TEST-F2-33848	02410334+5132214	X	02:41:3.3	51:32:20.0	0.5770	0.024	ea
TEST-F2-36890	02400324+5120411	X	02:40:3.3	51:20:40.6	0.5842	0.067	bcep
TEST-F2-21079	02345591+5147525		02:34:55.9	51:47:52.8	0.5850	0.044	
TEST-F2-37552	02414645+5122523		02:41:46.5	51:22:52.3	0.6090	0.107	
TEST-F2-31050	02435866+5149142		02:43:58.8	51:49:16.3	0.6100	0.012	ea
TEST-F2-26068	02452012+5208475	X	02:45:20.1	52:08:46.7	0.6255	0.081	ew
TEST-F2-43348	02434306+5112342		02:43:43.0	51:12:33.8	0.6360	0.047	
TEST-F2-47447	02444882+5103094		02:44:48.8	51:03:8.6	0.6427	0.072	
TEST-F2-39962	02412699+5115012	X	02:41:27.0	51:15:1.1	0.6470	0.061	
TEST-F2-37399	02393868+5116522		02:39:38.7	51:16:51.2	0.6500	0.344	dceps
TEST-F2-40180	02384414+5106442		02:38:44.1	51:06:44.3	0.6909	0.040	
TEST-F2-19302	02333984+5152164	X	02:33:40.0	51:52:15.2	0.7010	0.026	
TEST-F2-46684	02453321+5108191		02:45:33.2	51:08:19.0	0.7370	0.029	
TEST-F2-3837	02394141+5250362	X	02:39:41.4	52:50:35.5	0.7879	0.054	
TEST-F2-15142	02353163+5206274		02:35:31.7	52:06:27.0	0.8130	0.167	ea
TEST-F2-55462			02:46:32.5	51:21:23.4	0.8270	0.062	
TEST-F2-43267	02463166+5121288		02:46:31.6	51:21:28.4	0.8271	0.060	
TEST-F2-42692	02360661+5050104		02:36:6.7	50:50:11.0	0.8510	0.145	ew
TEST-F2-50256			02:38:8.5	52:41:14.6	0.8591	0.081	
TEST-F2-1539	02415263+5302572		02:41:52.6	53:02:57.8	0.8890	0.168	ea
TEST-F2-30702	02453884+5154472		02:45:39.2	51:54:47.9	0.8900	0.085	ew
TEST-F2-1152	02403432+5300052		02:40:34.3	53:00:4.0	0.8930	0.043	ea
TEST-F2-49022	02460234+5104270		02:46:2.3	51:04:27.1	0.9040	0.064	
TEST-F2-33360	02385148+5126397		02:38:51.5	51:26:39.5	0.9268	0.040	ea
TEST-F2-4406	02372165+5242017		02:37:21.7	52:42:0.7	0.9671	0.060	ew
TEST-F2-50973			02:44:56.0	52:50:37.7	0.9770	0.116	
TEST-F2-10042	02443853+5248433		02:44:38.5	52:48:43.2	0.9801	0.164	dceps
TEST-F2-9912	02443738+5248352		02:44:37.4	52:48:35.3	0.9802	0.151	dceps
TEST-F2-50702	02321730+5215075		02:32:17.4	52:15:8.3	0.9825	0.033	ew
TEST-F2-11154	02430150+5240284		02:43:1.5	52:40:28.2	0.9843	0.087	dceps
TEST-F2-1795	02414197+5301216		02:41:41.9	53:01:21.0	0.9849	0.078	
TEST-F2-30424	02405866+5141115		02:40:58.7	51:41:11.0	0.9890	0.172	ea
TEST-F2-34527	02450576+5143025		02:45:5.7	51:43:1.9	0.9891	0.047	
TEST-F2-37197	02373010+5110562		02:37:30.1	51:10:55.9	0.9891	0.028	
TEST-F2-50362			02:39:25.7	52:43:31.4	0.9893	1.416	
TEST-F2-37473	02382665+5115476		02:38:26.7	51:15:47.2	0.9899	0.045	dcep
TEST-F2-9441	02363702+5225448		02:36:37.0	52:25:44.4	0.9924	0.111	
TEST-F2-33528	02401258+5130028		02:40:12.6	51:30:2.9	0.9926	0.049	
TEST-F2-12315	02324391+5205060		02:32:43.9	52:05:6.7	1.0071	0.123	dceps
TEST-F2-43863	02432863+5110380		02:43:28.6	51:10:37.6	1.0076	0.028	dcep
TEST-F2-54824			02:37:56.2	51:09:33.1	1.0104	0.023	dceps
TEST-F2-54909	02384896+5110196		02:38:48.9	51:10:19.6	1.0107	0.026	dcep
TEST-F2-7843	02420370+5247301		02:42:3.7	52:47:29.0	1.0108	0.019	dceps
TEST-F2-47667			02:44:59.7	51:00:36.7	1.0320	1.385	
TEST-F2-4002	02444019+5305461		02:44:40.2	53:05:45.6	1.0350	0.132	dceps
TEST-F2-35179	02430828+5134330		02:43:8.3	51:34:32.5	1.0660	0.085	dceps
TEST-F2-52301	02401239+5211554		02:40:12.3	52:11:55.3	1.1180	0.073	ea
TEST-F2-21134	02421422+5211013		02:42:14.2	52:11:1.3	1.2190	0.082	ea
TEST-F2-5203	02385197+5243434		02:38:52.0	52:43:43.3	1.3120	0.072	ea
TEST-F2-7259	02405152+5245066	X	02:40:51.5	52:45:5.8	1.3510	0.056	ea
TEST-F2-31019	02444553+5151524		02:44:45.5	51:51:54.7	1.4260	0.082	ea
TEST-F2-40772	02394225+5107204		02:39:42.3	51:07:20.3	1.6077	0.120	eb
TEST-F2-31893	02460447+5152342		02:46:4.5	51:52:33.6	1.7180	0.089	ea
TEST-F2-43252	02434232+5112187		02:43:42.3	51:12:18.7	1.7630	0.085	eb
TEST-F2-2926	02443140+5306407		02:44:31.3	53:06:40.7	1.8182	0.343	ea
TEST-F2-44492	02444505+5112566		02:44:45.0	51:12:56.2	1.9650	0.359	ea
TEST-F2-11107	02451366+5247016		02:45:13.7	52:47:1.0	2.2580	0.078	ea
TEST-F2-49275	02364329+5248463		02:36:43.2	52:48:46.4	2.8610	0.100	ea
TEST-F2-15107	02435636+5232593	X	02:43:56.4	52:32:58.9	4.1254	0.306	eb
TEST-F2-9727	02402729+5237154		02:40:27.3	52:37:14.9	4.9068	0.218	dceps
TEST-F2-9507	02402508+5237132	X	02:40:25.1	52:37:14.5	4.9081	0.099	dceps
TEST-F2-3629	02360907+5240069	X	02:36:9.1	52:40:6.2	5.2165	0.078	dceps
TEST-F2-1674	02332985+5236085		02:33:30.0	52:36:7.6	5.5190	0.100	dceps
TEST-F2-53609	02412860+5148579		02:41:28.8	51:48:53.6	7.6450	0.086	eb
TEST-F2-29459	02431722+5151571		02:43:17.2	51:51:56.5	8.6059	0.020	dcep

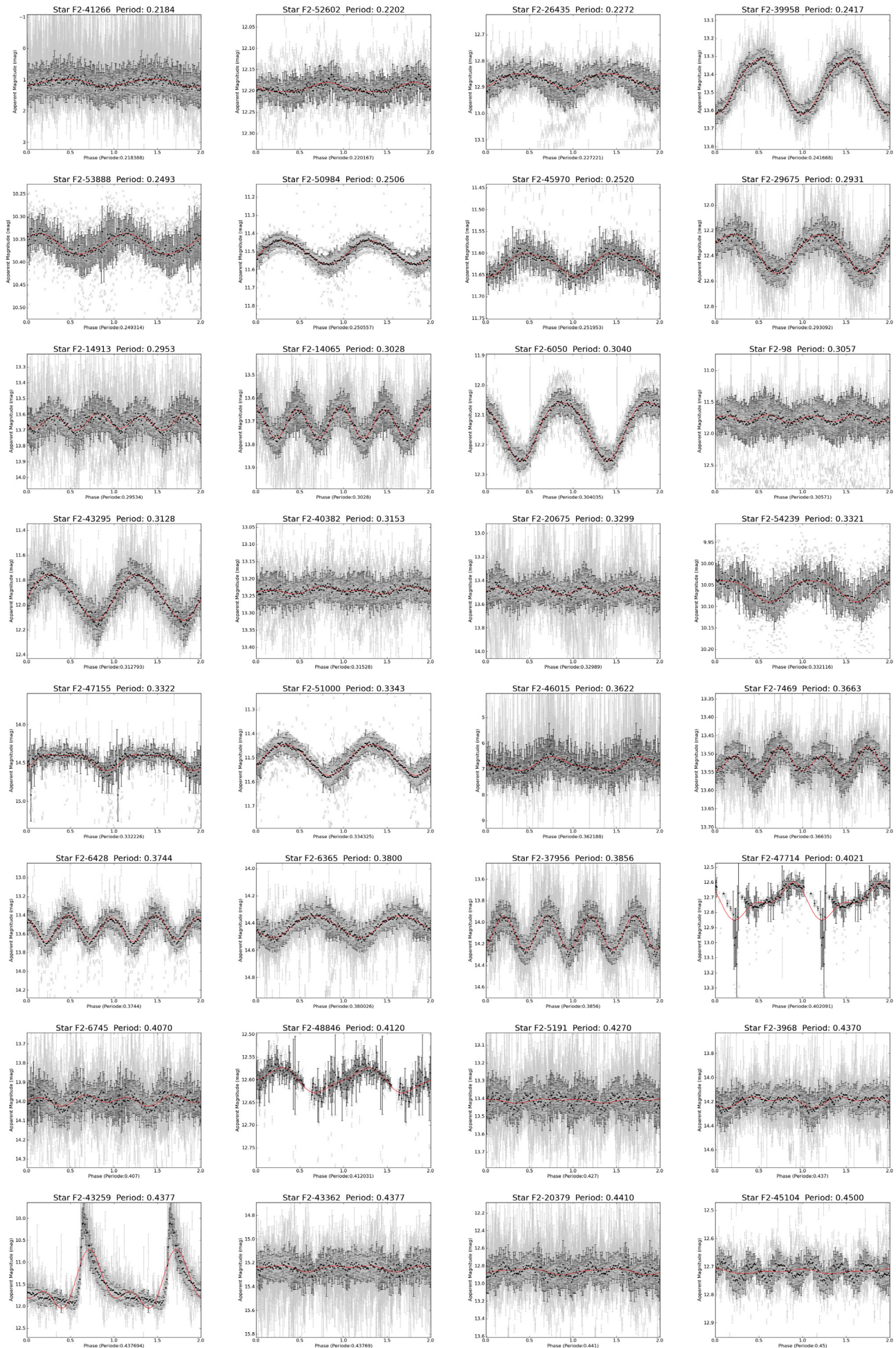
Continued on Next Page. . .

Table B.1 – Continued

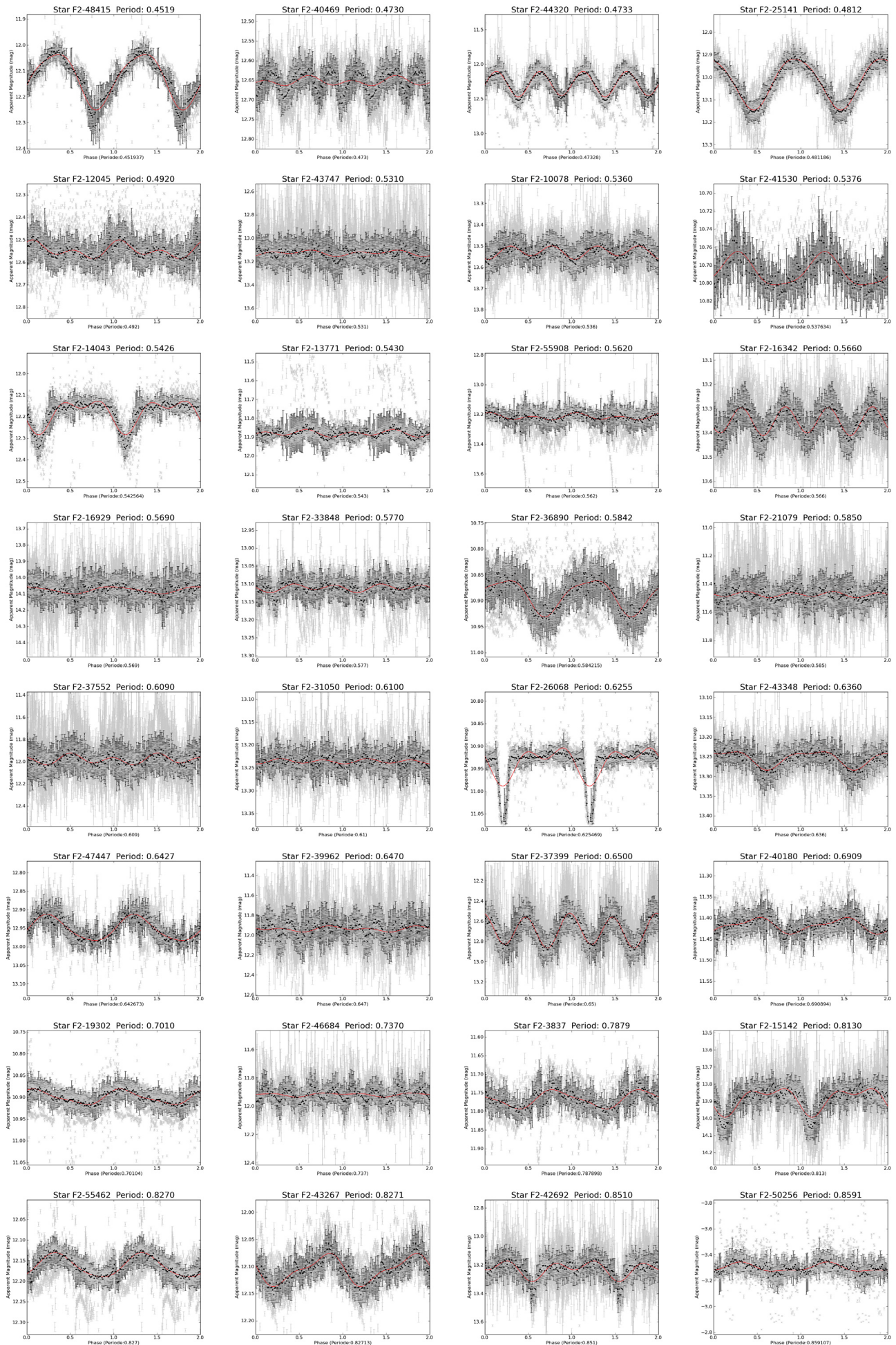
TEST-ID	2MASS designation	Found with BEST	RA	DEC	Period[days]	Amplitude[mag]	Type
TEST-F2-20320	02425518+5215180		02:42:55.2	52:15:17.6	9.4340	0.239	dcep
TEST-F2-55805	02415528+5106034		02:41:55.5	51:05:57.1	13.1579	0.056	
TEST-F2-13251	02405066+5229027		02:40:50.6	52:29:2.0	18.5185	0.055	dcep
TEST-F2-6328	02375742+5240057		02:37:57.4	52:40:4.8	29.0698	0.093	dcep
TEST-F2-49869	02444019+5305461		02:44:40.2	53:05:40.6	29.4118	0.118	dcep
TEST-F2-2580	02381081+5251132		02:38:10.8	52:51:12.2	30.3030	0.130	dcep
TEST-F2-21918	02444673+5217300		02:44:46.7	52:17:30.5	33.3333	0.049	dcep
TEST-F2-55685	02413995+5112532		02:41:39.9	51:12:52.9	34.8432	0.063	dcep
TEST-F2-50361	02355020+5232118		02:35:50.1	52:32:10.7	38.4615	0.013	
TEST-F2-49176	02355653+5247429		02:35:56.9	52:47:38.4	43.4783	0.130	dcep
TEST-F2-497	02355653+5247429		02:35:56.6	52:47:42.0	44.0529	0.128	dcep
TEST-F2-23695	02373455+5150106		02:37:34.6	51:50:10.7	52.0833	0.106	dcep
TEST-F2-51496			02:34:47.3	52:10:50.9	54.6448	0.564	dcep
TEST-F2-54324	02421035+5134402		02:42:10.1	51:34:42.6	60.9756	0.763	dcep
TEST-F2-34411	02421245+5134370		02:42:12.4	51:34:36.5	61.7284	0.132	dcep
TEST-F2-49697	02433654+5304387		02:43:36.6	53:04:40.1	68.0272	0.748	dcep
TEST-F2-40678	02395737+5108369		02:39:57.4	51:08:37.3	74.6269	0.039	dcep
TEST-F2-14839	02332866+5200101		02:33:28.7	52:00:10.4	79.3651	0.026	dcep
TEST-F2-46508	02450124+5107570		02:45:1.2	51:07:56.6	136.9860	0.030	
TEST-F2-49829			02:36:34.4	52:41:38.4	136.9860	0.862	m
TEST-F2-55190	02460816+5114454		02:46:8.2	51:14:44.9	136.9860	0.065	
TEST-F2-49868	02363314+5241231		02:36:33.1	52:41:22.9	138.8890	1.300	m
TEST-F2-13453	02361864+5214583		02:36:18.7	52:14:57.5	333.3330	3.783	ea



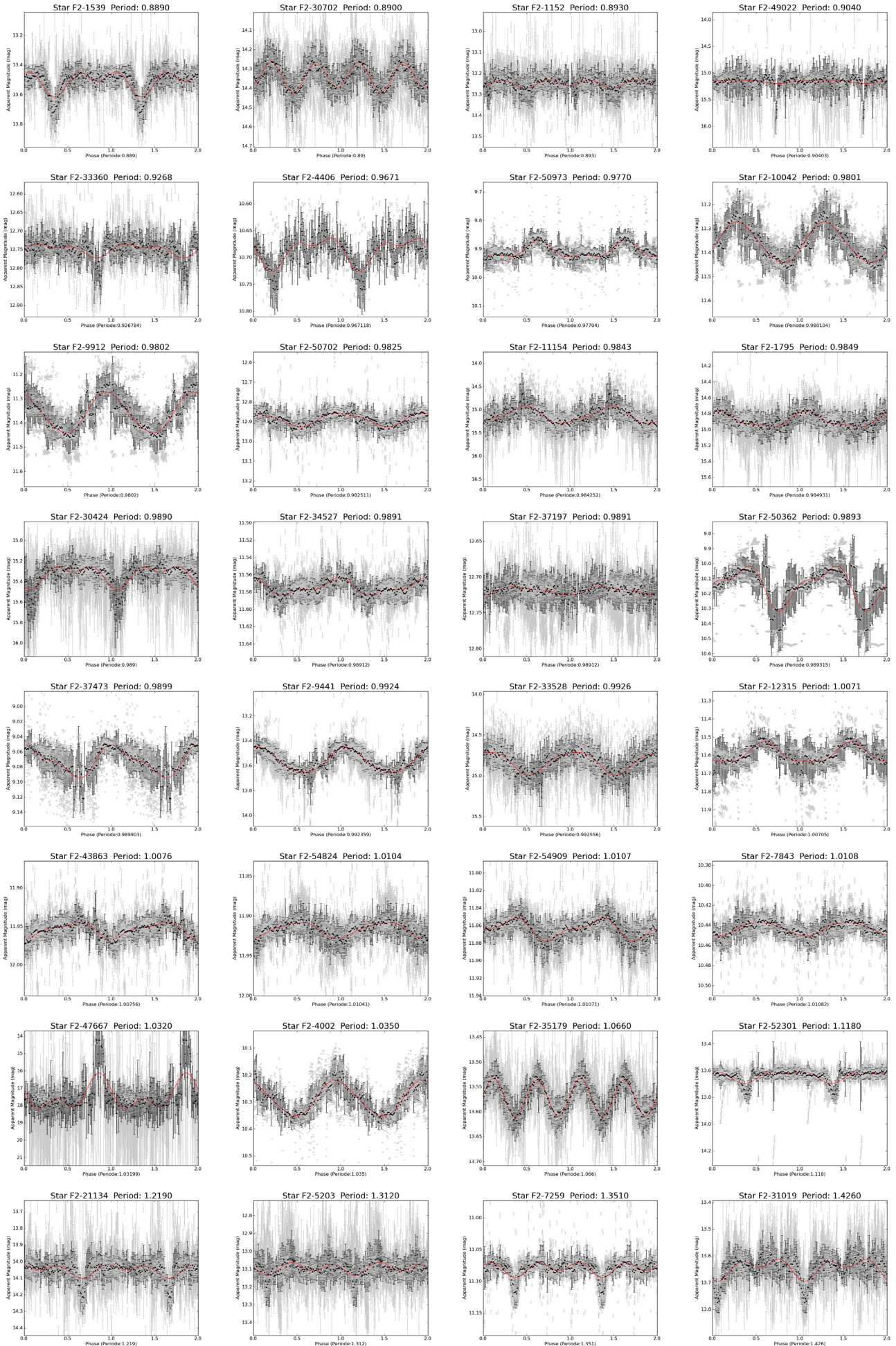


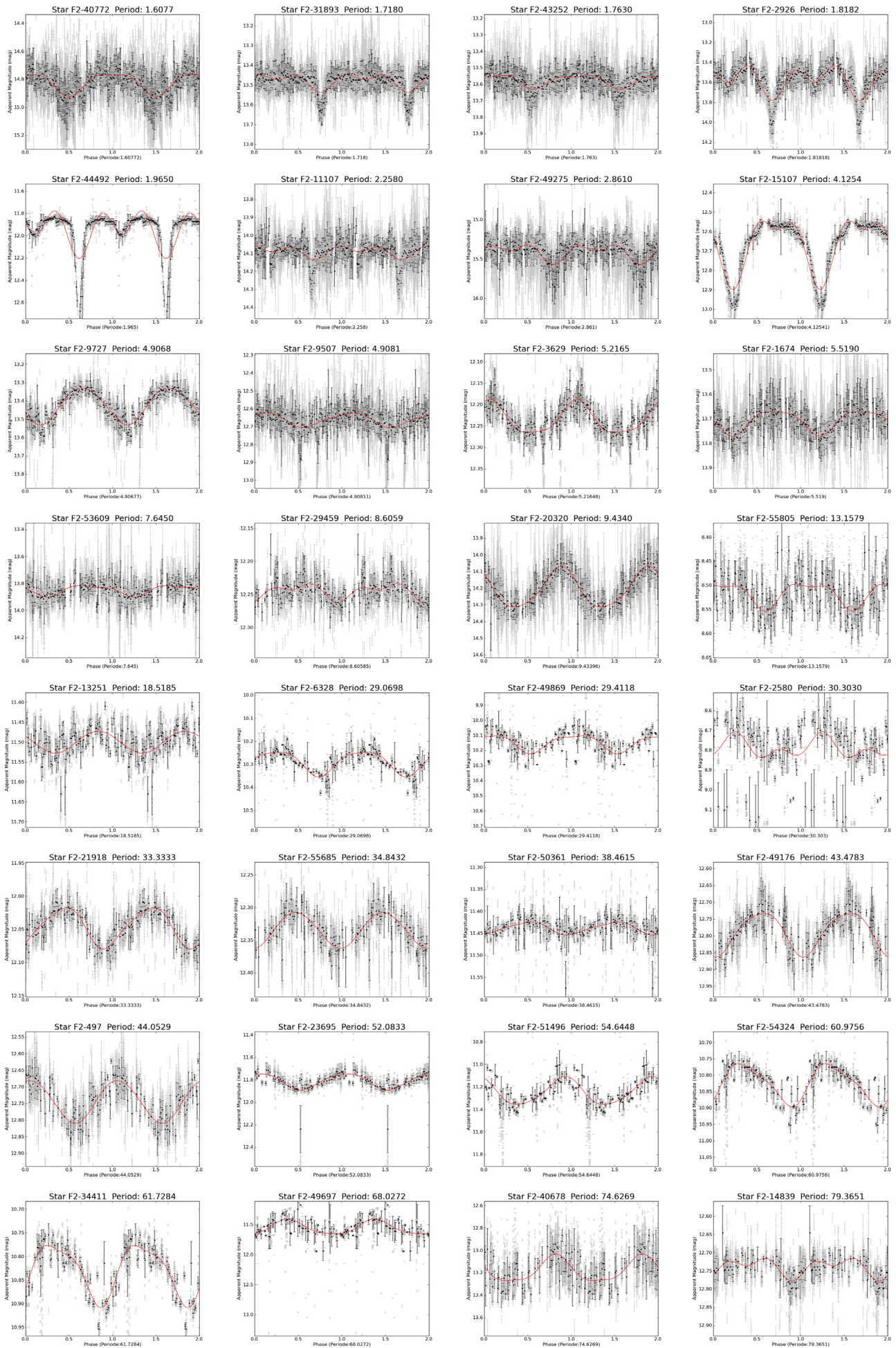




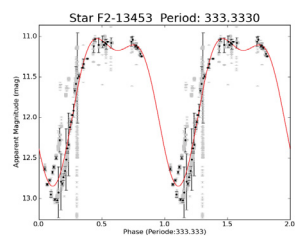
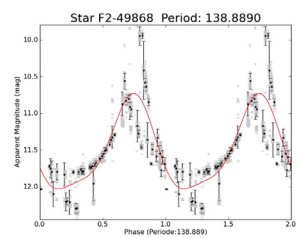
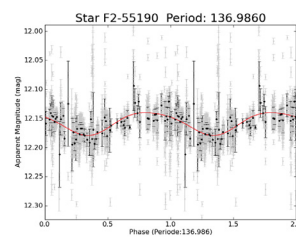
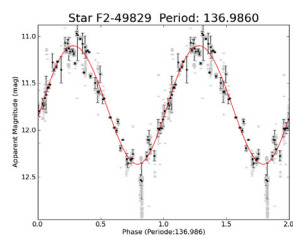
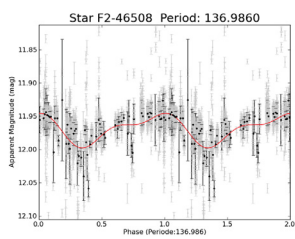














# C. Periodic Variable Stars - Field F15

Table C.1.: Periodic Variables in the F15 field

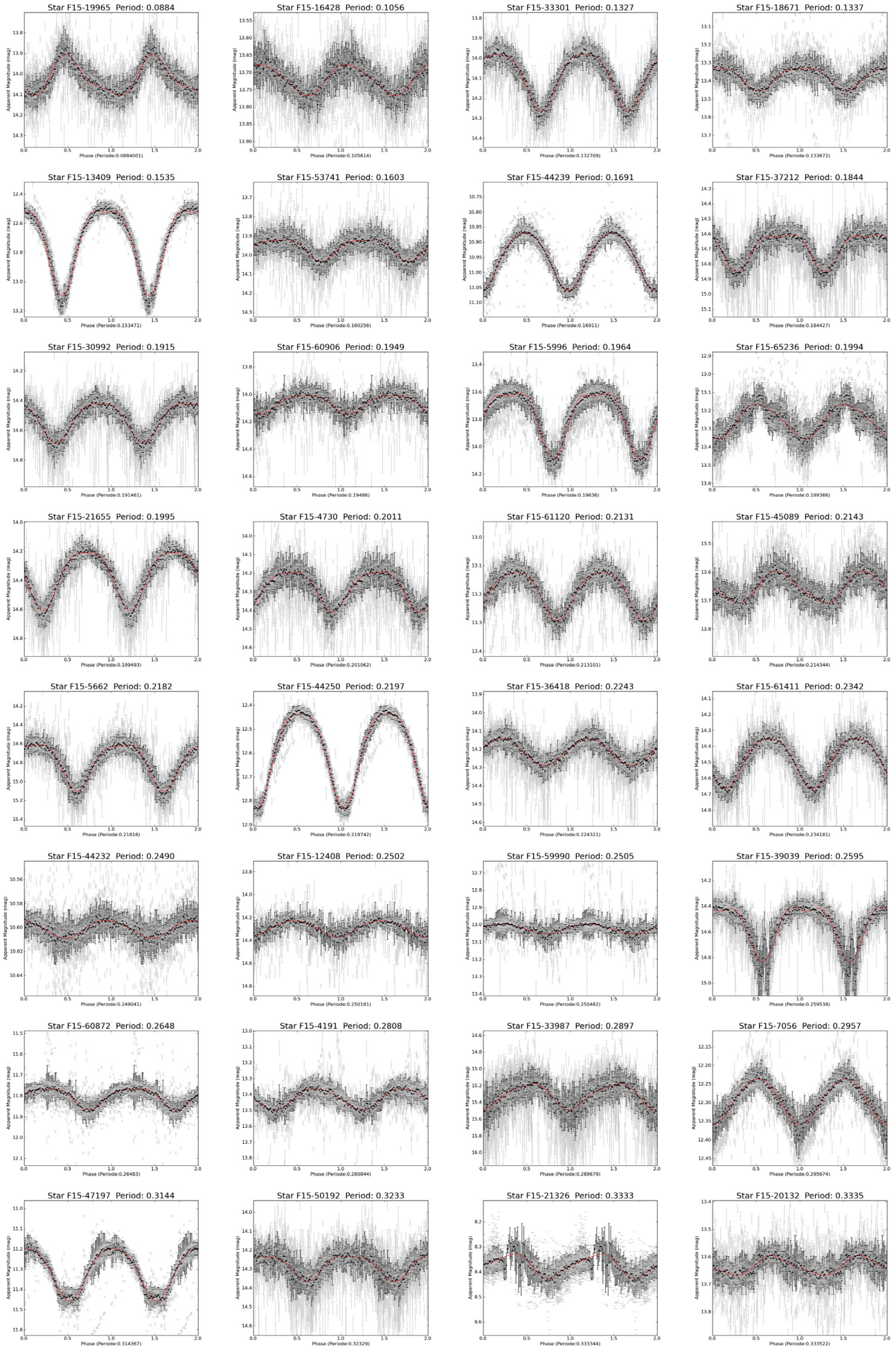
TEST-ID	2MASS designation	RA	DEC	Period[days]	Amplitude[mag]	Type
TEST-F15-19965	19542412+4810328	19:54:24.2	48:10:32.9	0.0884	0.199	dsct
TEST-F15-16428	19585651+4826163	19:58:56.4	48:26:15.0	0.1056	0.092	dsct
TEST-F15-33301	19565289+4743365	19:56:53.0	47:43:35.8	0.1327	0.282	ew
TEST-F15-18671		20:00:55.2	48:24:02.2	0.1337	0.126	ew
TEST-F15-13409	19581533+4832157	19:58:15.4	48:32:14.6	0.1535	0.584	ew
TEST-F15-53741	19563373+4659573	19:56:33.8	46:59:56.8	0.1603	0.114	ew
TEST-F15-44239	20052664+4733194	20:05:26.6	47:33:18.7	0.1691	0.190	bcep
TEST-F15-37212	20030471+4744113	20:03:04.8	47:44:11.0	0.1844	0.249	ew
TEST-F15-30992	19585264+4751358	19:58:52.6	47:51:36.0	0.1915	0.266	ew
TEST-F15-60906	20053432+4859550	20:05:34.3	48:59:54.2	0.1949	0.135	ew
TEST-F15-5996	19551530+4844020	19:55:15.4	48:44:01.7	0.1964	0.479	ew
TEST-F15-65236	19555382+4724272	19:55:53.8	47:24:26.6	0.1994	0.192	dsct
TEST-F15-21655	20042224+4821336	20:04:22.3	48:21:33.5	0.1995	0.400	ew
TEST-F15-4730	20000731+4854212	20:00:07.2	48:54:21.6	0.2011	0.212	rrc
TEST-F15-61120	20023521+4852353	20:02:35.3	48:52:35.8	0.2131	0.169	bcep
TEST-F15-45089	19565351+4718233	19:56:53.5	47:18:23.4	0.2143	0.114	rrc
TEST-F15-5662	19560180+4846150	19:56:01.9	48:46:14.2	0.2182	0.492	ew
TEST-F15-44250	19593564+4725172	19:59:35.5	47:25:16.3	0.2197	0.397	ew
TEST-F15-36418	20011832+4744000	20:01:18.5	47:43:56.3	0.2243	0.148	ew
TEST-F15-61411	20013025+4845464	20:01:30.2	48:45:45.4	0.2342	0.316	ew
TEST-F15-44232	20022502+4729069	20:02:25.0	47:29:06.4	0.2490	0.015	rrc
TEST-F15-12408	20060041+4844282	20:06:00.5	48:44:28.7	0.2502	0.141	rrc
TEST-F15-59990	19572141+4859527	19:57:21.4	48:59:53.2	0.2505	0.057	rrc
TEST-F15-39039	20023395+4739404	20:02:34.1	47:39:40.3	0.2595	0.427	ew
TEST-F15-60872	19543841+4844335	19:54:38.4	48:44:33.4	0.2648	0.102	ew
TEST-F15-4191	19535823+4846580	19:53:58.3	48:46:55.9	0.2808	0.137	rrc
TEST-F15-33987	20041635+4752449	20:04:16.3	47:52:44.8	0.2897	0.310	rrc
TEST-F15-7056	20011795+4851293	20:01:18.0	48:51:28.4	0.2957	0.122	rrc
TEST-F15-47197	19560480+4713138	19:56:04.8	47:13:13.4	0.3144	0.262	ew
TEST-F15-50192	20063502+4721216	20:06:35.0	47:21:23.4	0.3233	0.136	rrc
TEST-F15-21326	19594342+4818367	19:59:43.4	48:18:34.6	0.3333	0.099	rrc
TEST-F15-20132	19541680+4809471	19:54:16.8	48:09:47.2	0.3335	0.072	rrc
TEST-F15-61456	20055735+4850503	20:05:57.4	48:50:51.0	0.3371	0.222	rrc
TEST-F15-29421	20050312+4804149	20:05:03.1	48:04:14.2	0.3405	0.319	rrc
TEST-F15-22929	20052017+4820048	20:05:20.2	48:20:04.6	0.3448	0.172	rrc
TEST-F15-20344	19581927+4815549	19:58:19.2	48:15:55.1	0.3544	0.209	rrc
TEST-F15-48354	19560579+4710217	19:56:05.8	47:10:21.0	0.3560	0.321	rrc
TEST-F15-2964	20002685+4859375	20:00:26.9	48:59:36.6	0.3600	0.836	rrab
TEST-F15-62510	19581717+4821121	19:58:17.3	48:21:13.0	0.3645	0.159	ea
TEST-F15-42725	20050173+4735134	20:05:01.7	47:35:13.2	0.4048	0.381	rrab
TEST-F15-31537	20040304+4758086	20:04:03.1	47:58:08.0	0.4100	0.210	rrc
TEST-F15-27267	20015310+4805196	20:01:53.0	48:05:19.0	0.4418	0.339	ew
TEST-F15-65579		19:57:51.8	47:21:18.4	0.4892	0.141	ew
TEST-F15-38334	19555325+4730471	19:55:53.5	47:30:47.5	0.5133	0.471	rrab
TEST-F15-38608	19555564+4730285	19:55:55.7	47:30:28.4	0.5134	0.218	rrc
TEST-F15-28942	19593484+4758065	19:59:35.0	47:58:05.9	0.5170	0.232	ea
TEST-F15-29674	19543665+4747592	19:54:36.7	47:47:59.6	0.5274	0.724	rrab
TEST-F15-18713	19555802+4815585	19:55:58.1	48:15:58.3	0.6757	0.333	rrab
TEST-F15-28427	19545079+4751320	19:54:50.9	47:51:31.7	0.7048	0.219	ew
TEST-F15-9599	20015067+4845561	20:01:50.6	48:45:55.4	0.7185	0.108	ew
TEST-F15-21915	20003177+4818088	20:00:31.7	48:18:05.8	0.7191	0.065	ew
TEST-F15-2939	19592143+4858121	19:59:21.4	48:58:10.6	0.8329	0.159	ew
TEST-F15-31392	20025149+4758309	20:02:51.4	47:58:30.0	1.1265	0.021	dcep
TEST-F15-19850	20040249+4825380	20:04:02.4	48:25:37.6	1.9771	0.074	dcep
TEST-F15-26981	19592811+4803032	19:59:28.1	48:03:02.2	2.6589	0.033	eb
TEST-F15-10734	20001266+4841034	20:00:12.5	48:41:02.8	4.0683	0.073	dcep
TEST-F15-52031	20032997+4713513	20:03:30.0	47:13:50.9	4.7371	0.075	dceps
TEST-F15-49288	19585485+4713028	19:58:54.7	47:13:03.4	7.0522	0.295	eb
TEST-F15-22171	20031829+4818342	20:03:18.2	48:18:34.2	7.4405	0.249	eb
TEST-F15-22572	20031984+4818230	20:03:19.9	48:18:22.3	7.4460	0.239	dcep
TEST-F15-66875	19593813+4709551	19:59:38.2	47:09:56.2	8.7719	0.062	dcep
TEST-F15-62309		19:56:19.4	48:22:09.5	12.9366	0.041	dcep
TEST-F15-63104		19:58:20.4	48:10:56.6	19.2308	0.076	dcep
TEST-F15-46538	20041624+4726285	20:04:16.3	47:26:28.0	24.3902	0.088	dcep
TEST-F15-60994	20013119+4853033	20:01:31.2	48:53:03.5	36.6300	0.202	dcep
TEST-F15-33833	20011157+4749545	20:01:11.5	47:49:53.8	38.4615	0.210	dcep

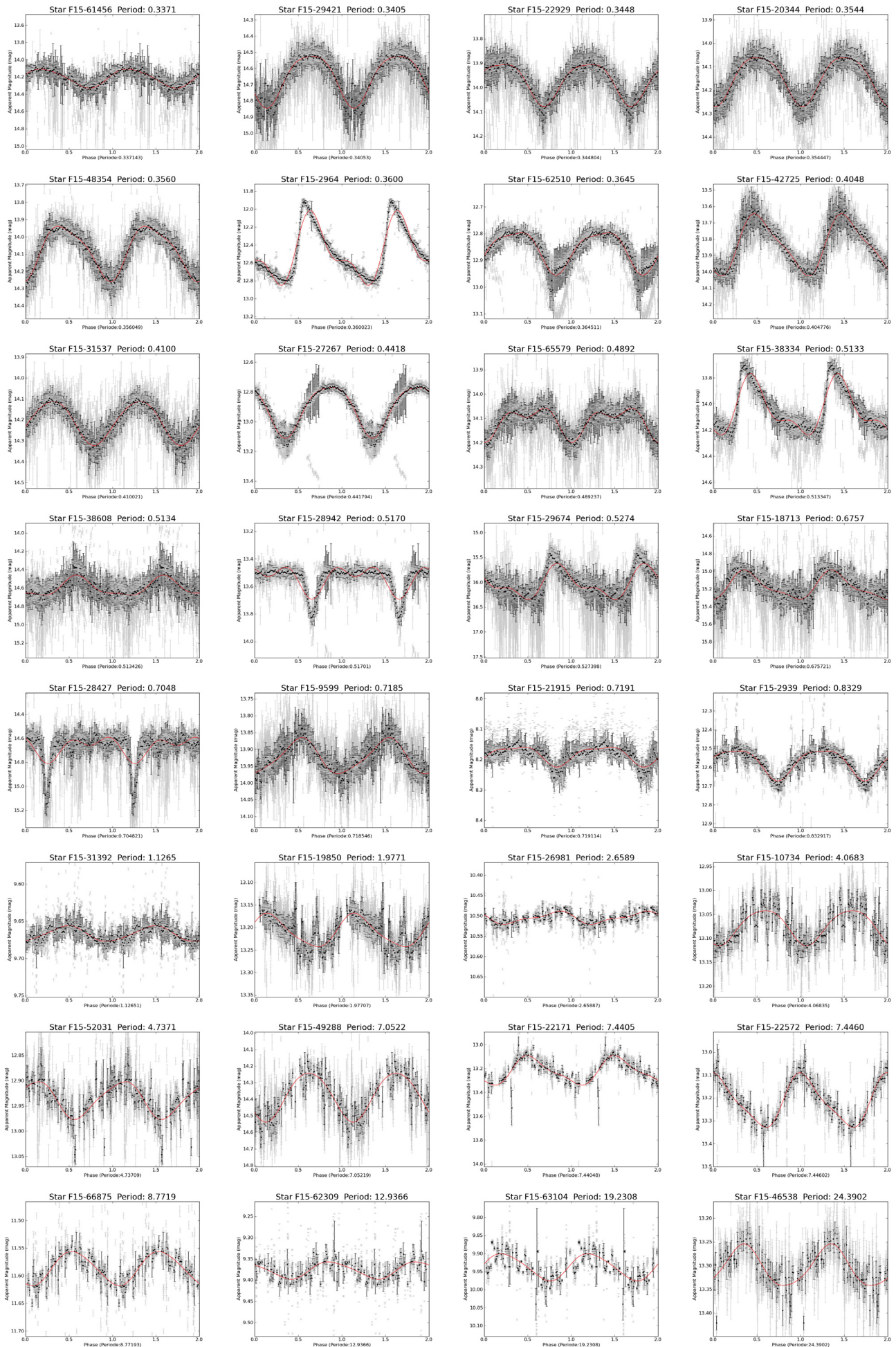
Continued on Next Page...

Table C.1 – Continued

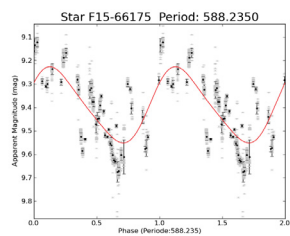
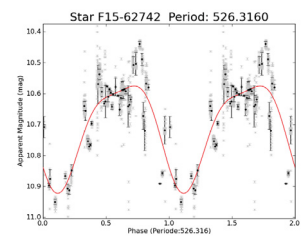
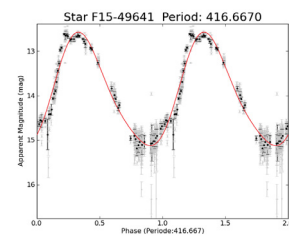
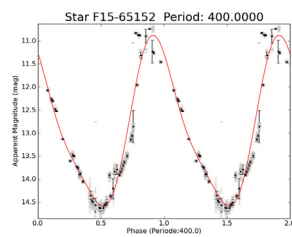
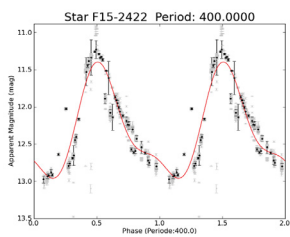
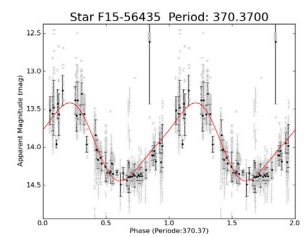
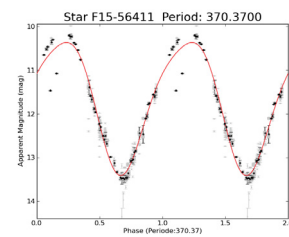
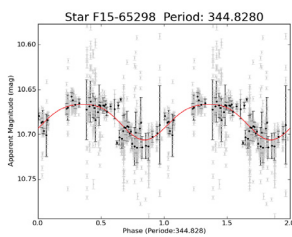
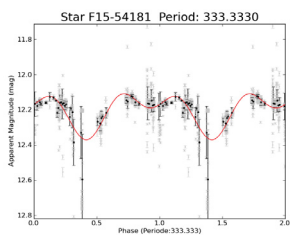
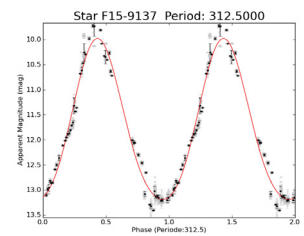
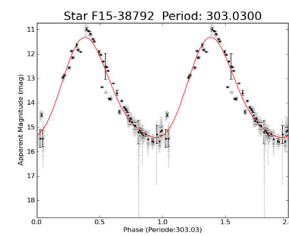
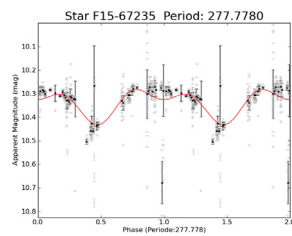
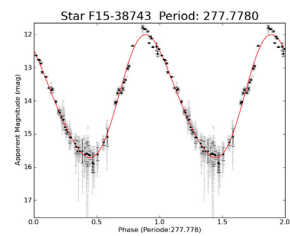
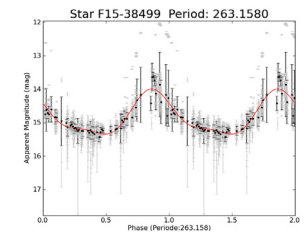
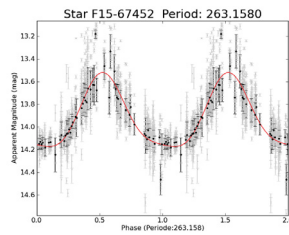
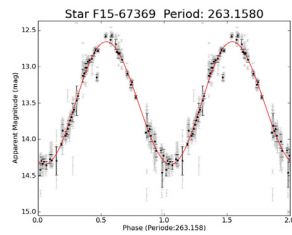
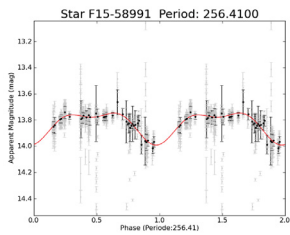
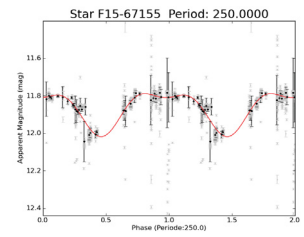
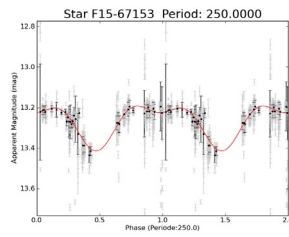
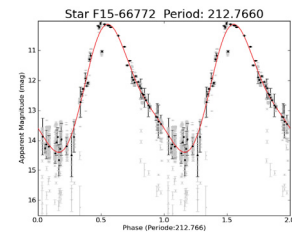
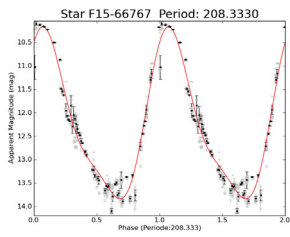
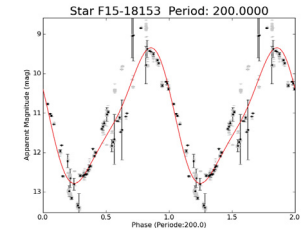
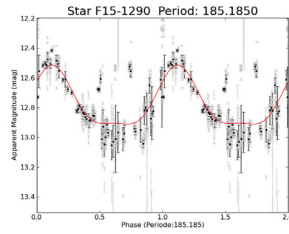
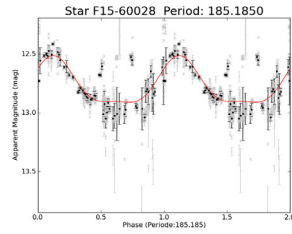
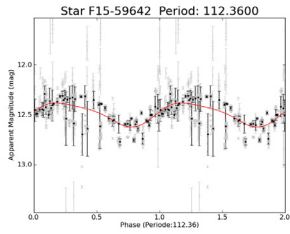
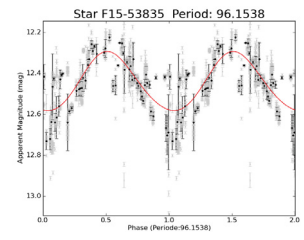
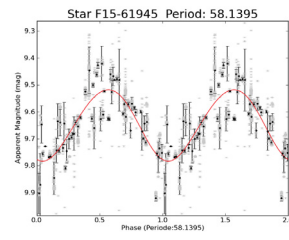
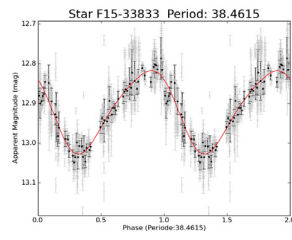
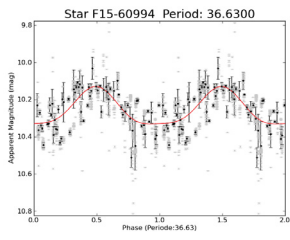
TEST-ID	2MASS designation	RA	DEC	Period[days]	Amplitude[mag]	Type
TEST-F15-61945		19:54:48.7	48:27:08.3	58.1395	0.265	dcep
TEST-F15-53835	20054642+4713262	20:05:46.3	47:13:26.0	96.1538	0.289	dcep
TEST-F15-59642	20014420+4658206	20:01:44.2	46:58:20.6	112.3600	0.242	dcep
TEST-F15-60028	19580053+4900164	19:58:00.5	49:00:17.6	185.1850	0.398	dcep
TEST-F15-1290	19580053+4900164	19:58:00.5	49:00:15.1	185.1850	0.396	dcep
TEST-F15-18153	20054415+4832091	20:05:44.2	48:32:08.2	200.0000	3.441	m
TEST-F15-66767		19:58:27.4	47:06:15.5	208.3330	3.669	m
TEST-F15-66772	19583029+4706176	19:58:30.2	47:06:18.0	212.7660	4.270	m
TEST-F15-67153	20061401+4704133	20:06:13.9	47:04:08.4	250.0000	0.220	eb
TEST-F15-67155		20:06:51.4	47:05:02.4	250.0000	0.229	eb
TEST-F15-58991	20063030+4703071	20:06:30.2	47:03:06.8	256.4100	0.244	eb
TEST-F15-67369	19580851+4655567	19:58:08.4	46:55:57.0	263.1580	1.686	m
TEST-F15-67452	19580581+4656204	19:58:05.8	46:56:20.8	263.1580	0.653	
TEST-F15-38499	20034355+4742191	20:03:43.7	47:42:19.1	263.1580	1.347	
TEST-F15-38743	20034559+4742166	20:03:45.6	47:42:16.2	277.7780	3.717	m
TEST-F15-67235		20:06:23.8	47:06:17.6	277.7780	0.149	eb
TEST-F15-38792	20054161+4745248	20:05:41.5	47:45:24.5	303.0300	4.109	m
TEST-F15-9137	19591195+4843335	19:59:12.0	48:43:32.2	312.5000	3.210	m
TEST-F15-54181	19550625+4656574	19:55:06.2	46:56:57.5	333.3330	0.261	eb
TEST-F15-65298		19:57:44.2	47:26:02.4	344.8280	0.040	eb
TEST-F15-56411	19575225+4656525	19:57:52.3	46:56:52.4	370.3700	3.042	m
TEST-F15-56435	19575170+4656300	19:57:51.8	46:56:30.8	370.3700	1.032	
TEST-F15-2422	20011068+4902147	20:01:10.6	49:02:14.6	400.0000	1.566	
TEST-F15-65152		19:59:37.9	47:31:35.4	400.0000	3.709	m
TEST-F15-49641		20:05:50.6	47:21:50.8	416.6670	2.550	m
TEST-F15-62742		19:55:48.5	48:13:23.2	526.3160	0.347	
TEST-F15-66175		20:00:40.3	47:16:53.0	588.2350	0.325	













# D. Periodic Variable Stars - Field P1

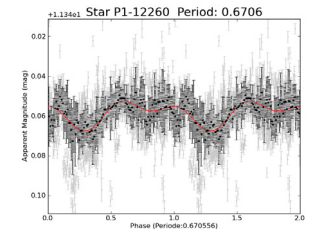
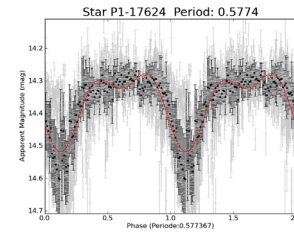
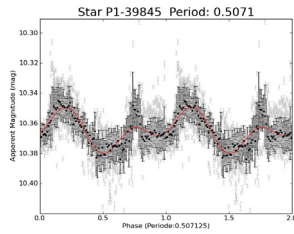
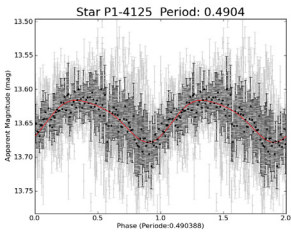
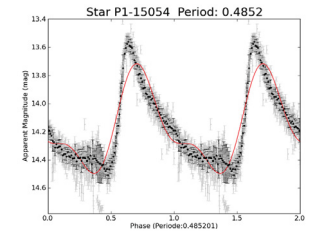
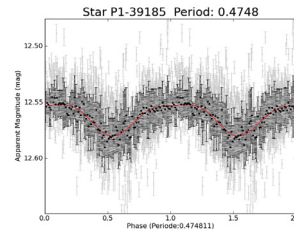
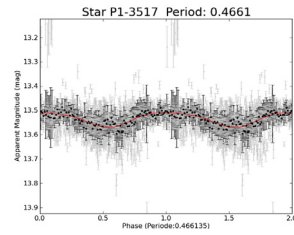
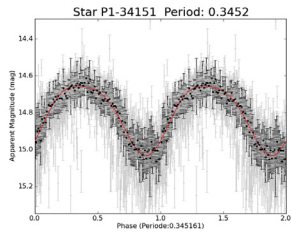
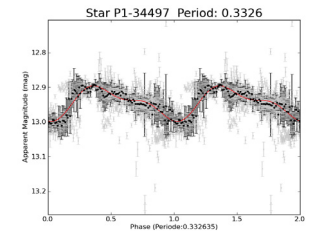
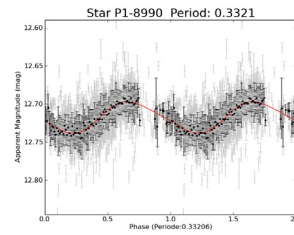
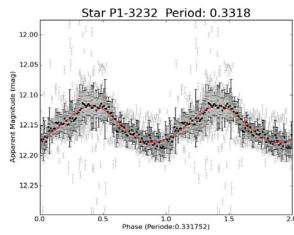
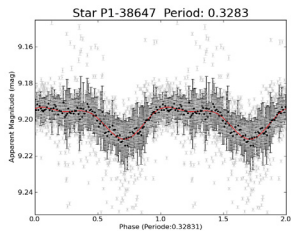
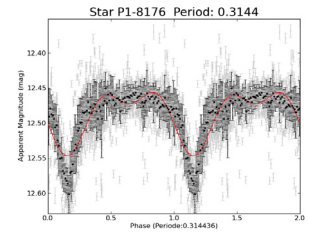
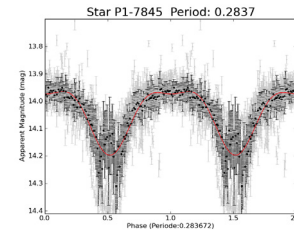
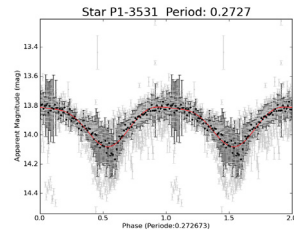
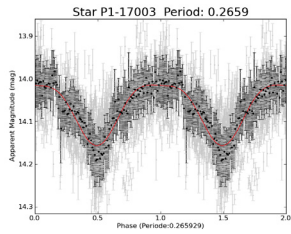
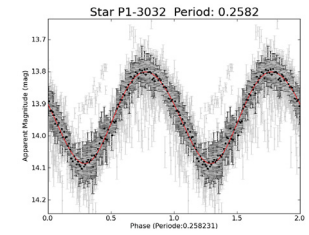
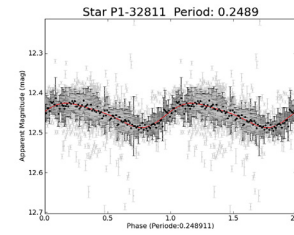
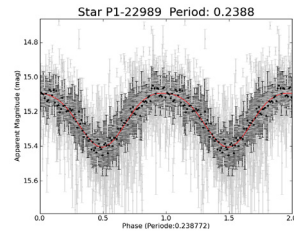
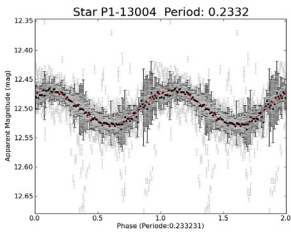
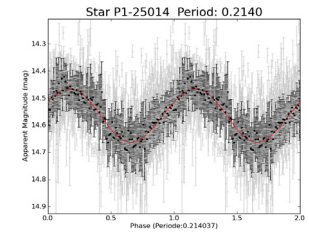
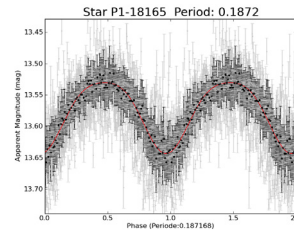
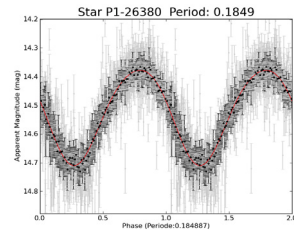
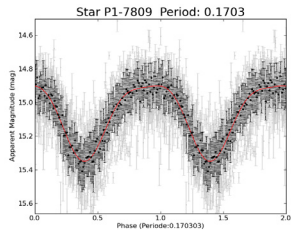
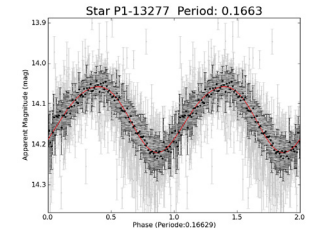
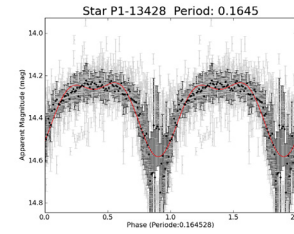
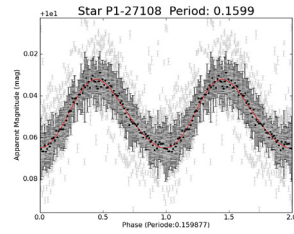
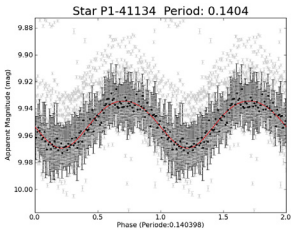
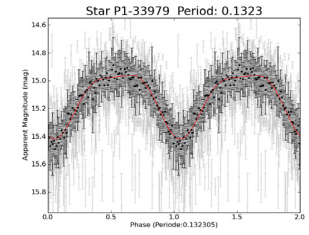
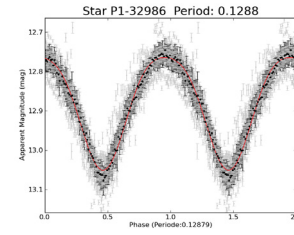
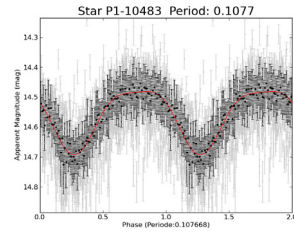
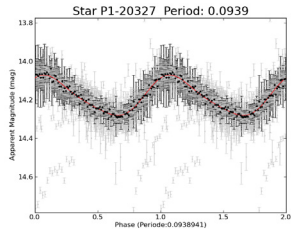
Table D.1.: Periodic Variables in the P1 field

TEST-ID	2MASS designation	RA	DEC	Period[days]	Amplitude[mag]	Type
TEST-P1-20327	05584349+3950165	05:58:43.1	39:50:30.5	0.0939	0.220	dsct
TEST-P1-10483	05585257+4026101	05:58:52.8	40:26:03.8	0.1077	0.210	ew
TEST-P1-32986		06:03:32.2	39:20:13.2	0.1288	0.286	ew
TEST-P1-33979		06:01:26.5	39:07:59.5	0.1323	0.459	ew
TEST-P1-41134	06013113+3922356	06:01:31.4	39:22:31.8	0.1404	0.034	dsct
TEST-P1-27108	06034321+3944468	06:03:43.4	39:44:52.4	0.1599	0.033	dsct
TEST-P1-13428	06025471+4030506	06:02:54.6	40:30:54.0	0.1645	0.349	ew
TEST-P1-13277	05571654+4009563	05:57:16.3	40:10:05.2	0.1663	0.163	dsct
TEST-P1-7809	05583868+4034043	05:58:38.6	40:34:08.0	0.1703	0.450	ew
TEST-P1-26380	06012694+3937523	06:01:26.8	39:37:48.7	0.1849	0.332	ew
TEST-P1-18185	06025192+4013416	06:02:51.7	40:13:51.6	0.1872	0.113	ew
TEST-P1-25014		06:05:39.7	39:58:56.6	0.2140	0.197	rrc
TEST-P1-13004	05581333+4014557	05:58:13.1	40:15:02.9	0.2332	0.059	bcep
TEST-P1-22989	06012951+3950459	06:01:29.0	39:51:02.5	0.2388	0.311	rrc
TEST-P1-32811		05:57:19.5	38:56:32.6	0.2489	0.061	rrc
TEST-P1-3032	05584689+4052096	05:58:46.9	40:52:10.2	0.2582	0.285	rrc
TEST-P1-17003	06034098+4022507	06:03:40.8	40:22:57.4	0.2659	0.142	ew
TEST-P1-3531	06035952+4109571	06:03:59.7	41:09:50.0	0.2727	0.272	ew
TEST-P1-7845	05564869+4026332	05:56:48.5	40:26:40.2	0.2837	0.232	ew
TEST-P1-8176	05560015+4023078	05:56:00.5	40:23:23.6	0.3144	0.090	ea
TEST-P1-38647		06:01:59.7	40:26:09.6	0.3283	0.018	ea
TEST-P1-3232	05543553+4035373	05:54:35.2	40:35:45.2	0.3318	0.060	rrc
TEST-P1-8990	06034888+4050338	06:03:48.9	40:50:31.2	0.3321	0.041	bcep
TEST-P1-34497	05581567+3854147	05:58:16.0	38:54:09.4	0.3326	0.103	rrc
TEST-P1-34151		06:03:42.9	39:16:19.2	0.3452	0.377	ew
TEST-P1-3517	06031659+4107249	06:03:16.8	41:07:35.4	0.4661	0.061	bcep
TEST-P1-39185	06043561+4017037	06:04:35.3	40:17:13.6	0.4748	0.028	ew
TEST-P1-15054	06042243+4031373	06:04:22.2	40:31:41.9	0.4852	0.780	rrab
TEST-P1-4125	06003492+4055306	06:00:35.0	40:55:28.9	0.4904	0.062	rrc
TEST-P1-39845		06:01:54.4	39:46:21.0	0.5071	0.031	
TEST-P1-17624	06020864+4013116	06:02:08.7	40:13:24.6	0.5774	0.240	ea
TEST-P1-12260	06010567+4028519	06:01:05.5	40:28:55.2	0.6706	0.015	ea
TEST-P1-31121	06010277+3917559	06:01:02.0	39:17:50.6	0.7026	0.137	dceps
TEST-P1-12501	06002010+4024310	06:00:20.0	40:24:36.0	0.8775	0.292	ea
TEST-P1-37394	05574912+4051550	05:57:49.0	40:51:59.0	1.1308	0.045	
TEST-P1-16448	06012968+4016034	06:01:29.4	40:16:10.6	1.5205	0.012	dceps
TEST-P1-41354	06061817+3945280	06:06:18.4	39:45:32.4	2.4826	0.128	dceps
TEST-P1-37735	06024513+4102109	06:02:45.3	41:02:06.0	2.9291	0.100	dceps
TEST-P1-25337		06:05:31.6	39:57:35.6	2.9647	0.218	ea
TEST-P1-23410		06:00:06.1	39:44:45.6	6.2578	0.075	bcep
TEST-P1-21065	06044516+4010551	06:04:44.7	40:11:07.8	6.6401	0.084	dceps
TEST-P1-39387	06044351+4010533	06:04:43.0	40:11:06.7	6.6401	0.083	dceps
TEST-P1-16059	05561915+3956331	05:56:18.8	39:56:44.9	8.0192	0.150	dceps
TEST-P1-21377	06042983+4008581	06:04:29.3	40:09:11.2	15.0602	0.018	
TEST-P1-9528	05593180+4032040	05:59:31.7	40:32:07.1	16.9205	0.153	dcep
TEST-P1-40426		06:00:40.1	39:25:40.1	18.8679	0.063	dcep
TEST-P1-24463		06:00:50.5	39:43:32.2	19.0476	0.313	eb
TEST-P1-21056	05555132+3936522	05:55:50.8	39:37:08.8	20.4499	0.048	dcep
TEST-P1-16204	05594608+4010037	05:59:45.8	40:10:12.0	28.9017	0.101	dcep
TEST-P1-41412		05:59:36.0	38:51:18.4	38.1679	0.110	dcep
TEST-P1-13974	06005315+4021390	06:00:53.0	40:21:44.6	38.6100	0.078	dcep
TEST-P1-22569	06040444+4003035	06:04:04.1	40:03:05.4	45.4545	0.104	eb
TEST-P1-23847		06:02:16.0	39:51:06.8	74.0741	0.112	dcep
TEST-P1-39933		06:01:06.1	39:40:16.0	92.5926	0.441	dcep
TEST-P1-33781		05:57:40.8	38:54:13.7	106.3830	0.078	dcep
TEST-P1-40667		05:57:16.3	38:53:12.5	107.5270	0.084	dcep
TEST-P1-34293		06:00:00.6	39:02:04.2	113.6360	0.071	dcep
TEST-P1-40616		05:59:09.4	39:00:20.5	114.9430	0.078	dcep
TEST-P1-40618		05:59:13.5	39:00:37.1	119.0480	0.073	dcep
TEST-P1-40889		06:04:47.8	39:33:52.2	128.2050	0.020	eb
TEST-P1-9262	06000918+4036382	06:00:09.1	40:36:40.0	129.8700	0.027	
TEST-P1-41041		06:06:04.2	39:16:40.1	131.5790	0.059	
TEST-P1-40148	06051530+3950317	06:05:14.9	39:50:44.2	131.5790	0.035	dcep
TEST-P1-41087		06:06:02.8	39:16:43.3	133.3330	0.063	
TEST-P1-23107		05:55:11.5	39:27:01.4	172.4140	0.084	
TEST-P1-38563	05570485+4009228	05:57:04.9	40:09:33.5	178.5710	0.647	

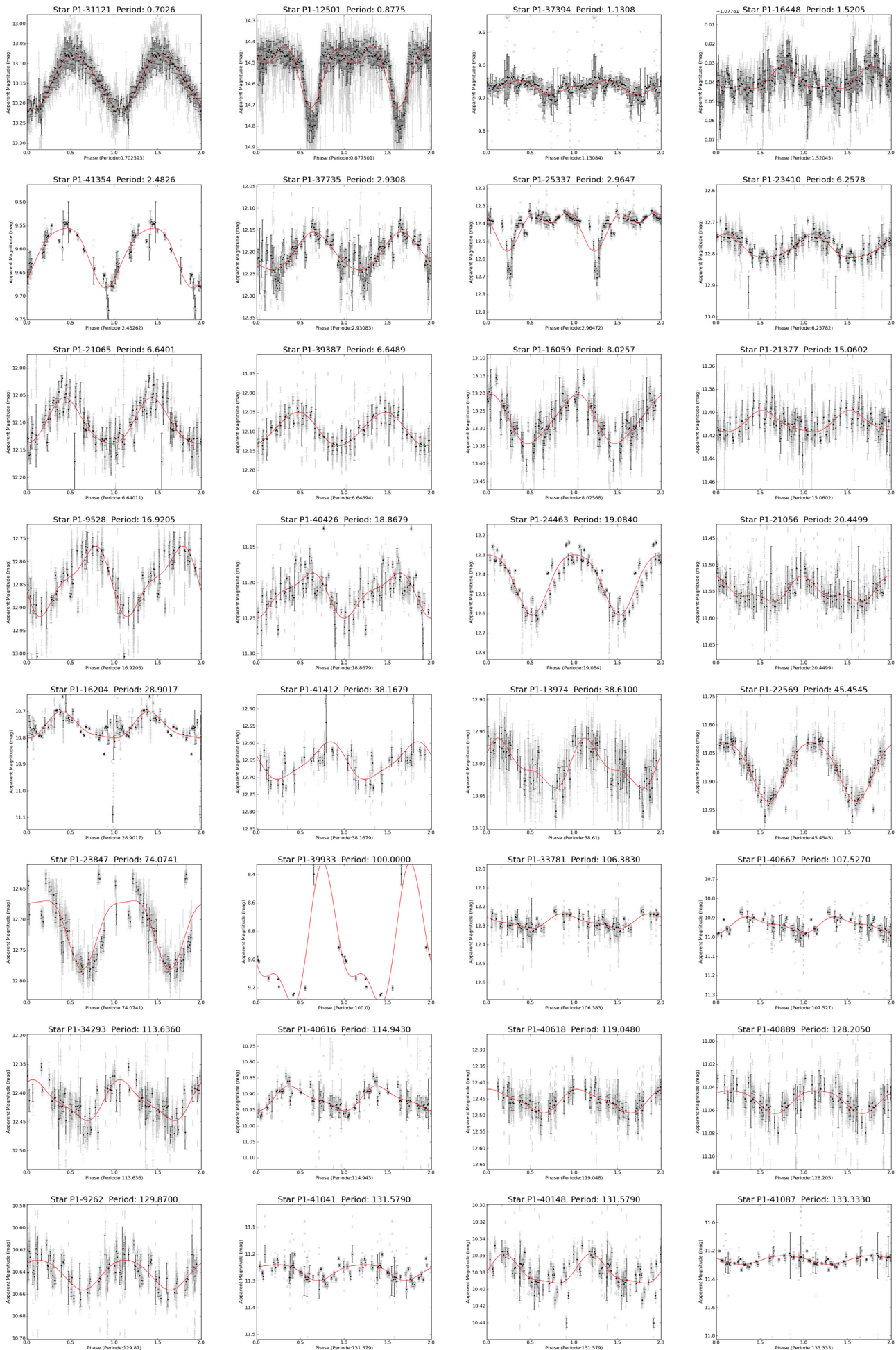
Continued on Next Page...

Table D.1 – Continued

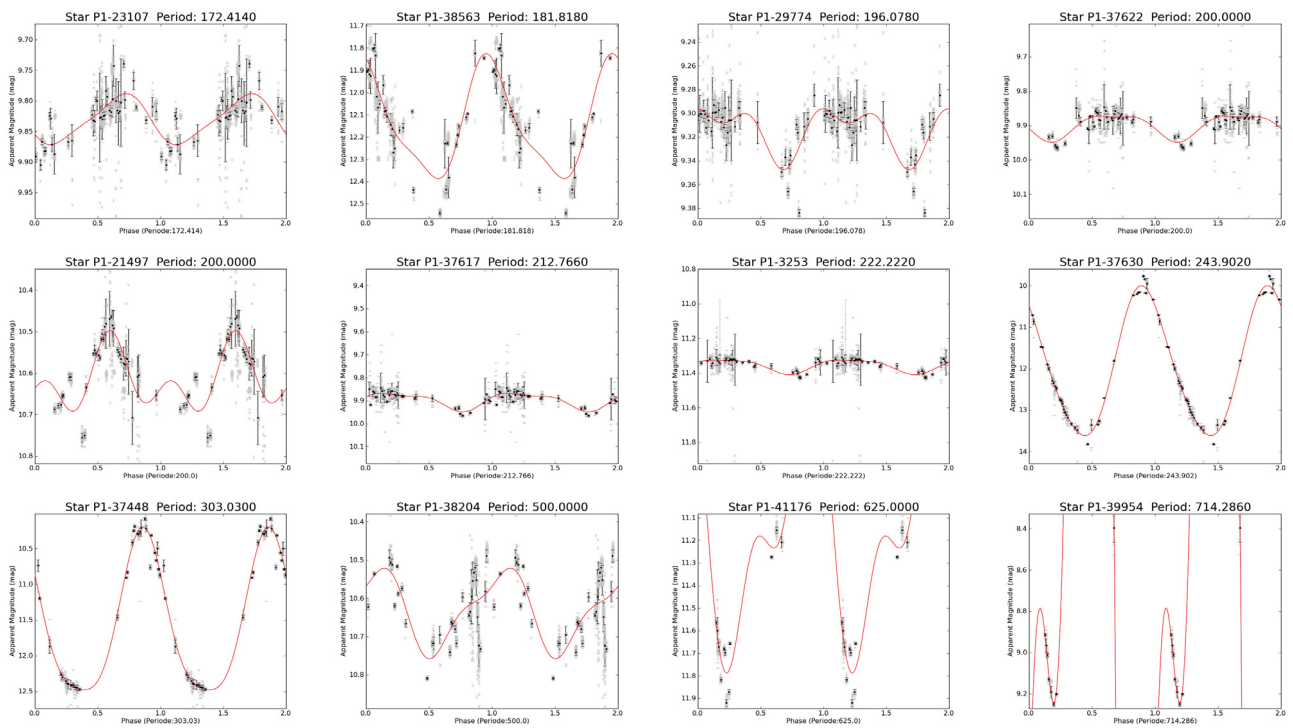
TEST-ID	zMASS designation	RA	DEC	Period[days]	Amplitude[mag]	Type
TEST-P1-29774		06:05:08.6	39:40:26.4	196.0780	0.051	
TEST-P1-37622		06:03:36.5	41:08:08.2	200.0000	0.076	
TEST-P1-21497	05572199+3942229	05:57:21.5	39:42:39.2	200.0000	0.194	
TEST-P1-37617	06033802+4108215	06:03:38.1	41:08:20.8	212.7660	0.081	
TEST-P1-3253	06031811+4108029	06:03:18.3	41:07:57.0	222.2220	0.085	
TEST-P1-37630	05543933+4033266	05:54:38.6	40:33:31.7	238.0950	3.580	m
TEST-P1-37448	06014901+4106278	06:01:49.1	41:06:22.3	303.0300	2.280	m
TEST-P1-38204	05553345+4015431	05:55:33.5	40:15:54.7	500.0000	0.236	
TEST-P1-41176	06064811+3918082	06:06:47.6	39:18:00.7	625.0000	1.483	
TEST-P1-39954		06:01:06.2	39:40:33.2	714.2860	13.782	











# Curriculum Vitae

Eigmüller, Philipp

Geboren in Berlin, Wilmersdorf

## Educations

Physik Diplom at the Universität Leipzig (2000-2006).

Referee: Prof. Dr. T. Butz (Universität Leipzig) and  
Dr. Jochen Eislöffel (Thüringer Landessternwarte Tautenburg).  
Titel: Automatisierte Identifikation veränderlicher Sterne am Beispiel  
ausgesuchter Himmelsfelder (gut 1,9)

Ev. Gymnasium zum Grauen Kloster (1990-1999) (secondary school)

Ev. Schule Steglitz (1987-1990) (primary school)

## Work Experience

since Dezember 2010

Research fellow at the Deutschen Zentrum für Luft- und Raumfahrt, Berlin-Adlershof.

*Scientific preparations for the PLATO mission (study phase)*

Januar 2007 – November 2010

Research fellow at the Thüringer Landessternwarte, Tautenburg.

*Programming of the robotic observation mode for the TEST, photometric transit survey, photometric follow up for the CoRoT mission, implementation of the data analysis software for the TEST*

Juni 2006 - Dezember 2006

Research assistant at the Deutschen Zentrum für Luft- und Raumfahrt, Berlin-Adlershof.

*Development of the reductions pipeline of the BESTII, programming parts of the light curve analysis software.*

April 2006 - Mai 2006

Student assistant at the Thüringer Landessternwarte, Tautenburg.

November 2003 - März 2005

Student assistant at the Leibniz-Institut für Troposphärenforschung e.V., Leipzig.

*Aerosol measurements, Assisting in the development of particle size spectrometers.*

August 2001 - Dezember 2001,

Student assistant at the Leibniz-Institut für Troposphärenforschung e.V., Leipzig.

1999 - 2000

Zivildienst, Übernachtungheim, Berlin

## Qualification

15. August - 28. August 2010

Participation at the Sino-German summer school in Weihai, China. Topic: "Observational Techniques and Data Analysis for Spectroscopy and Photometry"

21. Juli - 30. Juli 2009

Participation at the ESA summer school in Alpbach, Austria. Topic: "Exoplanets: Discovering and characterizing Earth type planets"

18. Mai - 20. Mai 2009

2nd Scientific Writing for Young Astronomers, by Astronomy & Astrophysics, Blankenberge, Belgien

## Computer Skills

Programming Languages: Python, C, Fortran, IDL, VBScript, Bash, Labview

Database: PostgreSQL, MySQL

Astrophysical software: Iraf, Pyraf, PyEphem, Midas, CCDSoft5, TheSky6, SAO DS9, AE

Others: LaTeX, Gimp, Office, Corel Draw

OS: Extended knowledge in Linux, basic knowledge in MS Windows

## Languages

German (native tongue), English (fluent)

## Poster

The Tautenburg Exoplanet Search Telescope, Big Science with small Telescopes October, 2010, Dornburg, Germany

TEST, The Tautenburg Exoplanet Search Telescope, IAU Symposium 253, Transiting Exoplanets May, 2008, Boston, USA

ELAP - Easy to use Lightcurve Analysis Program, 5th Planet Formation Workshop, September 2007, Braunschweig, Germany

## Popular science articles

Die Jets von RW Aurigae

Sterne und Weltraum, April 2007

## Publications

[1] L. Carone, D. Gandolfi, J. Cabrera, A. P. Hatzes, H. J. Deeg, S. Csizmadia, M. Paetzold, J. Weingrill, S. Aigrain, R. Alonso, A. Alapini, J. Almenara, M. Auvergne, A. Baglin, P. Barge, A. S. Bonomo, P. Bordé, F. Bouchy, H. Bruntt, S. Carpano, W. D. Cochran, M. Deleuil, R. F. Díaz, S. Dreizler, R. Dvorak, J. Eisloffel, **Eigmüller, P.**, M. Endl, A. Erikson, S. Ferraz-Mello, M. Fridlund, J. . Gazzano, N. Gibson, M. Gillon, P. Gondoin, S. Grziwa, E. W. Guenther, T. Guillot, M. Hartmann, M. Havel, G. Hébrard, L. Jorda, P. Kabath, A. Léger, A. Llebaria, H. Lammer, C. Lovis, P. J. MacQueen, M. Mayor, T. Mazeh, C. Moutou, L. Nortmann, A. Ofir, M. Ollivier, H. Parviainen, F. Pepe, F. Pont, D. Queloz, M. Rabus, H. Rauer, C. Régulo, S. Renner, R. de la Reza, D. Rouan, A. Santerne, B. Samuel, J. Schneider, A. Shporer, B. Stecklum, L. Tal-Or, B. Tingley, S. Udry, and G. Wuchterl. Planetary transit candidates in the CoRoT LRA01 field. ArXiv e-prints, October 2011.

[2] T. Pasternacki, S. Csizmadia, J. Cabrera, **Eigmüller, P.**, A. Erikson, T. Fruth, P. von Paris, H. Rauer, R. Titz, J. Eisloffel, A. Hatzes, M. Boer, G. Tournois, P. Kabath, P. Hedelt, and H. Voss. A Variable Star Census in a Perseus Field. AJ, 142:114, October 2011.

[3] D. Gandolfi, G. Hébrard, R. Alonso, M. Deleuil, E. W. Guenther, M. Fridlund, M. Endl, **Eigmüller, P.**, S. Csizmadia, M. Havel, S. Aigrain, M. Auvergne, A. Baglin, P. Barge, A. S. Bonomo, P. Bordé, F. Bouchy, H. Bruntt, J. Cabrera, S. Carpano, L. Carone, W. D. Cochran, H. J. Deeg, R. Dvorak, J. Eisloffel, A. Erikson, S. Ferraz-Mello, J.-C. Gazzano, N. B. Gibson, M. Gillon, P. Gondoin, T. Guillot, M. Hartmann, A. Hatzes, L. Jorda, P. Kabath, A. Léger, A. Llebaria, H. Lammer, P. J. MacQueen, M. Mayor, T. Mazeh, C. Moutou, M. Ollivier, M. Pätzold, F. Pepe, D. Queloz, H. Rauer, D. Rouan, B. Samuel, J. Schneider, B. Stecklum, B. Tingley, S. Udry, and

G. Wuchterl. Transiting exoplanets from the CoRoT space mission. XIV. CoRoT-11b: a transiting massive “hot-Jupiter” in a prograde orbit around a rapidly rotating F-type star. *A&AP*, 524:A55, December 2010.

[4] H. Rauer, A. Erikson, P. Kabath, P. Hedelt, M. Boer, L. Carone, S. Csizmadia, **Eigmüller, P.**, P. v. Paris, S. Renner, G. Tournois, R. Titz, and H. Voss. Pre-Discovery Observations of CoRoT-1b and CoRoT-2b with the BEST Survey. *AJ*, 139:53–58, January 2010.

[5] P. Kabath, A. Erikson, H. Rauer, T. Pasternacki, S. Csizmadia, R. Chini, R. Lemke, M. Murphy, T. Fruth, R. Titz, and **Eigmüller, P.** Periodic variable stars in CoRoT field LRa02 observed with BEST II. *A&AP*, 506:569–587, October 2009.

[6] H. J. Deeg, M. Gillon, A. Shporer, D. Rouan, B. Stecklum, S. Aigrain, A. Alapini, J. M. Almenara, R. Alonso, M. Barbieri, F. Bouchy, J. Eislöffel, A. Erikson, M. Fridlund, **Eigmüller, P.**, G. Handler, A. Hatzes, P. Kabath, M. Lendl, T. Mazeh, C. Moutou, D. Queloz, H. Rauer, M. Rabus, B. Tingley, and R. Titz. Ground-based photometry of space-based transit detections: photometric follow-up of the CoRoT mission. *A&AP*, 506:343–352, October 2009.

[7] P. Kabath, A. Erikson, H. Rauer, T. Pasternacki, S. Csizmadia, R. Chini, R. Lemke, M. Murphy, T. Fruth, R. Titz, and **Eigmüller, P.** BEST II CoRoT LRa02 field periodic variables (Kabath+, 2009). *VizieR Online Data Catalog*, 3506:60569, July 2009.

[8] P. Kabath, T. Fruth, H. Rauer, A. Erikson, M. G. Murphy, R. Chini, R. Lemke, S. Csizmadia, **Eigmüller, P.**, T. Pasternacki, and R. Titz. Characterization of CoRoT Target Fields With Berlin Exoplanet Search Telescope. II. Identification of Periodic Variable Stars in the LRc2 Field. *AJ*, 137:3911–3919, April 2009.

[9] Eigmüller, P. and J. Eislöffel. TEST The Tautenburg Exoplanet Search Telescope. In *IAU Symposium*, volume 253 of *IAU Symposium*, pages 340–342, February 2009.

[10] P. Kabath, **Eigmüller, P.**, A. Erikson, P. Hedelt, P. von Paris, H. Rauer, S. Renner, R. Titz, and C. Karoff. Characterization of CoRoT Target Fields with the Berlin Exoplanet Search Telescope: Identification of Periodic Variable Stars in the LRa1 Field. *AJ*, 136:654–661, August 2008.

[11] P. Kabath, **Eigmüller, P.**, A. Erikson, P. Hedelt, H. Rauer, R. Titz, T. Wiese, and C. Karoff. Characterization of COROT Target Fields with BEST: Identification of Periodic Variable Stars in the IR01 Field. *AJ*, 134:1560–1569, October 2007.

[12] J. Eislöffel, A. P. Hatzes, H. Rauer, H. Voss, A. Erikson, **Eigmüller, P.**, and E. Guenther. Results from the Exoplanet Search Programmes with BEST and TEST. In O. Demircan, S. O. Selam, and B. Albayrak, editor, *Solar and Stellar Physics Through Eclipses*, volume 370 of *Astronomical Society of the Pacific Conference Series*, page 91, May 2007.

[13] H. Rauer, A. Erikson, A. P. Hatzes, M. Pätzold, G. Wuchterl, R. Berlin, L. Carone, **Eigmüller, P.**, J. Eislöffel, A. Gahr, E. Guenther, P. Kabath, D. Kurtz, H. Lehmann, G. Peter, U. Rohbeck, N. Russ, B. Ulmer, H. Voss, and T. Zecha. The German Contribution to the CoRoT Mission. In M. Fridlund, A. Baglin, J. Lochard, and L. Conroy, editor, *ESA Special Publication*, volume 1306 of *ESA Special Publication*, page 123, November 2006.

## **Ehrenwörtliche Erklärung**

Ich erkläre hiermit ehrenwörtlich, dass ich die vorliegende Arbeit selbstständig, ohne unzulässige Hilfe Dritter und ohne Benutzung anderer als der angegebenen Hilfsmittel und Literatur angefertigt habe. Die aus anderen Quellen direkt oder indirekt übernommenen Daten und Konzepte sind unter Angabe der Quelle gekennzeichnet.

Bei der Auswahl und Auswertung folgenden Materials haben mir die nachstehend aufgeführten Personen in der jeweils beschriebenen Weise unentgeltlich geholfen:

1. A. Tkachenko modellierte ein stellares Spektrum zur Klassifikation des Hauptsternes eines Transit Kandidaten. Dies ist in Kapitel 10.1 entsprechend beschrieben.

Weitere Personen waren an der inhaltlich-materiellen Erstellung der vorliegenden Arbeit nicht beteiligt. Insbesondere habe ich hierfür nicht die entgeltliche Hilfe von Vermittlungs- bzw. Beratungsdiensten (Promotionsberater oder anderer Personen) in Anspruch genommen. Niemand hat von mir unmittelbar oder mittelbar geldwerte Leistungen für Arbeiten erhalten, die im Zusammenhang mit dem Inhalt der vorgelegten Dissertation stehen.

Die Arbeit wurde bisher weder im In- noch im Ausland in gleicher oder ähnlicher Form einer anderen Prüfungsbehörde vorgelegt.

Die geltende Promotionsordnung der Physikalisch-Astronomischen Fakultät ist mir bekannt.

Ich versichere ehrenwörtlich, dass ich nach bestem Wissen und die reine Wahrheit gesagt und nichts verschwiegen habe.